HIGH-SOLIDS, MIXED-MATRIX HOLLOW FIBER SORBENTS FOR CO_2 CAPTURE

A Dissertation
Presented to
The Academic Faculty

By

Vinod Babu Pandian Babu

In Partial Fulfillment
Of the Requirements for the Degree
Doctor of Philosophy in the
School of Chemical & Biomolecular Engineering

Georgia Institute of Technology

May 2014

HIGH-SOLIDS, MIXED-MATRIX HOLLOW FIBER SORBENTS FOR CO_2 CAPTURE

Approved by:

Dr. William J. Koros, Advisor
School of Chemical & Biomolecular Engineering
Georgia Institute of Technology

Dr. Ronald R. Chance, Advisor
School of Chemical & Biomolecular Engineering
Georgia Institute of Technology

Dr. Srinivas Garimella
George W. Woodruff School of Mechanical Engineering
Georgia Institute of Technology

Dr. Matthew J. Realff
School of Chemical & Biomolecular Engineering
Georgia Institute of Technology

Dr. David S. Sholl
School of Chemical & Biomolecular Engineering
Georgia Institute of Technology

Dr. Krista S. Walton
School of Chemical & Biomolecular Engineering
Georgia Institute of Technology

Date approved: February 3rd, 2014

DEDICATION

This dissertation is dedicated to my dear parents and to my sister Vandu for their constant love and support.

ACKNOWLEDGEMENTS

My experience at Georgia Tech has come to be an important part of my life, both academically and personally. I am truly fortunate to be part of the academic community at ChBE - Gatech and my gratitude goes first to my advisors Dr. Bill Koros and Dr. Ronald Chance for guiding me through this period and to ExxonMobil for providing the material and technical resources to support my research. Dr. Koros has provided an incredible amount of support, and where necessary, exhortation, that has been of great value to me. Right at the outset, he readily accommodated me as a full member of the Koros group; despite the fact that I was working on a co-advised project. He continued to be an unwavering source of encouragement and expertise throughout my graduate experience at Georgia Tech. His utter dedication to research, positive outlook, consideration of others' concerns while resolving issues and enthusiasm for good ideas have all been qualities to emulate. I would also like to thank Dr. Ronald Chance for guiding me throughout the project and sharing his invaluable technical insights.

I would not be where I am now if it weren't for the huge sacrifices my father Pandian Babu and my mother Anbukkarasi made in raising and educating me. Starting from kindergarten, they have provided me the best education available, often at great expense and against the opinion of others. Without their constant support, guidance and love, I would not have had many of the opportunities that I have been able to utilize. I thank my sister and partner in crime Vandana for always finding my jokes funny and also my large and loving family of cousins, aunts and uncles; and lately, nieces and nephews.

I would like to thank my thesis committee members Dr. Srinivas Garimella, Dr. Matthew J. Realff, Dr. David S. Sholl and Dr. Krista S. Walton for their guidance and evaluation of my research. I am grateful to the personnel at ExxonMobil, especially Dan Leta, Rusty Kelley, Harry Deckman, Hans Thomann and Bruce DeRites for supporting my research and providing us valuable sorbent samples as well as technical expertise.

A big part of my years at Georgia Tech has been the shared experiences with my fellow students and colleagues in the ChBE department. Starting my first semester late owing to a delayed visa, it helped that Mahalakshmi Ganesh, Anil Goteti, Carlos Espinoza, Swetha Sivaswamy, Meha Rungta, and Praveen Bollini were there to help me get up to speed. In meeting Manolis Haldoupis, I was glad to find someone who shared much of my worldview and interests, which was comforting in an initially unfamiliar city. These friends continued to show remarkable patience with my bad attempts at humor and for that alone they should be commended.

In the Koros group, I had the good fortune to meet people who have been so much more than just colleagues. I would like to thank Dr. Ryan Lively for being my mentor during my initial years at Georgia Tech and for giving me the opportunity to observe his remarkable knowledge and willingness to tackle problems head on. In particular, the ease with which he sets up and troubleshoots equipment is something I hope to achieve. As a new student occasionally needing help, I could not have managed without Dr. JR Johnson and Dr. Oguz Karvan, who were always ready to lend their technical knowledge and incredible physical strength, whether it was to repair an ISCO pump or to crack open a stubborn gas cylinder cap. Many thanks to Michelle Harden and

Rod Sefton for being incredibly patient and accommodating of our various research needs.

My thanks go out to my seniors in the Koros group: Dr. Dhaval Bhandari, Dr. Mita Das, Dr. Shan Wickramanayake, Dr. Mayumi Kiyono, Dr. Nayoki Bessho and especially Dr. Jong Suk Lee, for having served as role models and confidants. Speaking of confidants, Dr. Justin Vaughn has been that and more during our long stint as officemates. Whether it is airing out frustrations in research or sharing the results of our daring culinary forays, he has always been game. Stephanie Li and Graham Wenz have always lent a ear to my research ideas as well as general musings.

I have been equally lucky in having a circle of friends and mentors who have always supported me. In particular I would like to thank Dr. Renganathan, Dr. Lima Rose Miranda, Dr. Muthukumar, Suresh Babu and my friends at Anna University; past roommates Saurabh Kothari and Zimple Kurlawala; and not the least: Jamie Vidich, Dhana Sekar, Gus Kaufman, Praveen Rajendaran, Aman Altaf, Sandeep Mora and the guys at Trikone. There are more people than I can enumerate, who have helped me emotionally, financially and academically, and I wish to thank them all.

TABLE OF CONTENTS

LIST OF TABLES

LIST OF FIGURES

SUMMARY

Since the advent of the industrial era, the anthropogenic contribution to the carbon dioxide concentration in the atmosphere has been significant, and this has been linked to a similar rise in atmospheric temperatures. This phenomenon, called global warming, is likely to lead to large-scale climate change and cause economic and ecological disruption. Electricity generated from coal-fired power plants constitutes the single largest source of anthropogenic CO_2 emissions in many countries and any strategy to reduce CO_2 emissions must tackle these large point sources of CO_2 that are likely to persist into the foreseeable future. Post-combustion carbon capture, wherein the CO_2 produced as a result of coal combustion is trapped at the power plant exhaust, is seen as a bridging technology to reduce CO_2 emissions until more carbon-neutral electricity sources may be developed. This capture process will however impose a parasitic load on the power plant and technologies need to be developed to minimize this energy penalty.

This research focuses on a carbon capture platform which uses solid sorbents incorporated into a hollow fiber form that allows water-moderated thermal cycling as a means of trapping CO_2 from flue gas. While hollow fiber technology has intrinsic advantages over competing liquid amine and packed bed technologies, the materials used to fabricate hollow fibers and the fabrication process itself need to be optimized in order to result in competitive, robust hollow fiber sorbents. This dissertation focuses on the material selection process for each component of the hollow fiber platform and discusses ways to optimize the fiber and barrier layer formation. Different materials were evaluated to function as the solid sorbent, the matrix polymer and the barrier layer;

and eventually their performance was measured against past work in this area. Torlon®, a polyamide-imide was found to be a robust matrix polymer. High silica MFI was found to be a stable, hydrophobic sorbent material. PAN, a barrier polymer was targeted for the inner barrier, and methods were developed to lay down a PAN barrier on a previously spun Torlon® fiber. The technique to produce high-permeance sorbents with a good capacity for CO_2 sorption and a low-permeance inner barrier has also been described in this research.

CHAPTER 1

INTRODUCTION AND MOTIVATION

1.1 Motivation

The goal of this research is to identify materials and fabricate them into hollow fiber adsorbents usable in a rapid thermal swing adsorption system (RTSA) for flue gas CO_2 capture. This research is motivated by the need to address climate change by developing working technologies to mitigate emissions from the largest and most widespread point sources of CO_2 today and in the foreseeable future: coal-fired power plants. The challenge lies in achieving specific performance objectives that would render hollow fiber sorbents operable in an industrial flue gas setting, able to withstand temperatures over 100 °C and a moisture-saturated gas feed [1].

1.1.1 Anthropogenic Climate Change, its Causes and Impact

There has been a drastic increase in the emissions and atmospheric concentrations of long-lived greenhouse gases (LLGHGs) such as CO_2, methane, halocarbons and nitrous oxide (N_2O) since the start of the industrial era, resulting from combustion of fossil fuels, industrial activity and land use changes [2]. Greenhouse gases are responsible for absorbing thermal radiation from the earth's surface and radiating it in all directions, thereby warming the earth's surface more than if the heat were simply lost

to space. Hence, their concentration in the atmosphere directly affects the surface temperature, as well as the local and regional climate of the earth.

Of these LLGHGs, CO_2 is of particular importance because of its high concentration relative to the others. Among all greenhouse gases, only water vapor has a higher atmospheric concentration and a higher warming potential [2]. However, human activities have not directly affected the amount of atmospheric water vapor and only contribute about 0.18% of the total atmospheric concentration [3]. On the other hand, human activity has increased the atmospheric concentration of CO_2 by 36% to over 380 ppm in the last 250 years [4]. At the same time, historical temperature records have indicated an upward trend in both land and sea temperatures, as shown in Figure 1.1 [5].

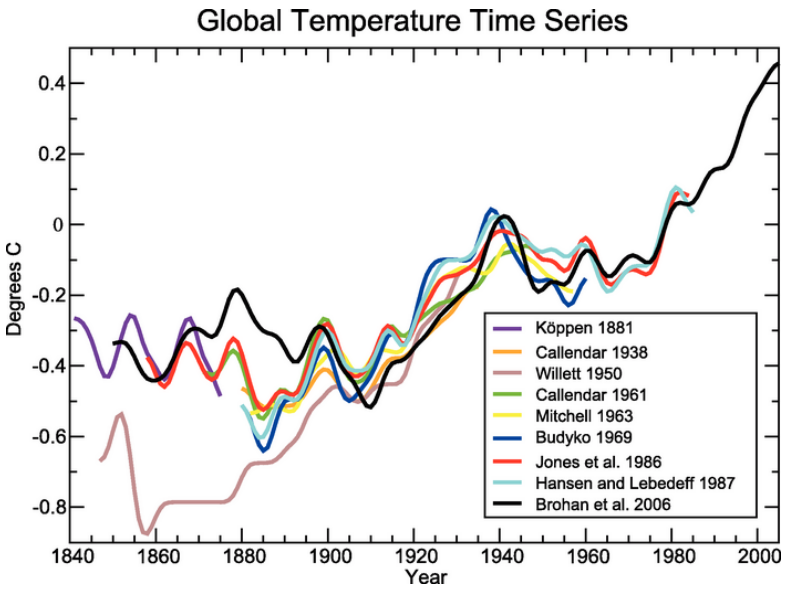

Figure 1.1: Land and ocean temperature records over large areas showing increases in temperature relative to a base temperature. Source: Intergovernmental Panel on Climate Change, 2007

Anthropogenic CO_2 emissions and the increase in radiative forcing attributable to it have been identified as a likely cause of this increase in global temperatures [6]. Such an increase could have serious environmental and economic consequences through changes in local and regional weather patterns and through increase in the sea level caused by melting polar ice sheets [7] - a phenomenon referred to as anthropogenic or man-made climate change. The fact that global CO_2 emissions have been increasing steeply during this period [8], and are projected to increase even further in the coming decades [9, 10] suggests that strategies should be developed to mitigate CO_2 emissions.

1.1.2 The Rise of Anthropogenic CO_2 Sources

The increase in anthropogenic CO_2 emissions is associated with the Industrial Revolution starting during the late 18^{th} century. This period saw a widespread adoption of industrial technologies and manufacturing processes that brought about profound and irreversible changes to the lifestyle and economic conditions of people, starting in Western Europe[11, 12]. In particular, coal and petroleum were widely exploited as energy sources that powered both the Industrial Revolution and the subsequent rise of chemical, electric power and automotive industries[8]. However, as a result of the changes in living standards that resulted, the major use of fossil fuels today has shifted to electricity production and transport. In fact nearly 69% of the energy produced in the United States today goes towards power generation and transportation [13].

Of these sources of energy, coal provides between 42% and 50% of US electricity and over 40% of electricity worldwide [9]. Power generation from coal hence contributed to 33% of anthropogenic CO_2 emission in the US in 2008 [14]: the single largest source of CO_2 emissions. Worldwide, coal power is an even more significant CO_2 source because of the large coal reserves of large, rapidly expanding economies such as China and India: the CO_2 emissions of such countries has already surpassed emissions from the developed or OECD nations, and is projected to grow much more steeply (Figure 1.2) [9]. Coal-fired power plants are and will be a major source of anthropogenic CO_2 emissions in the conceivable future.

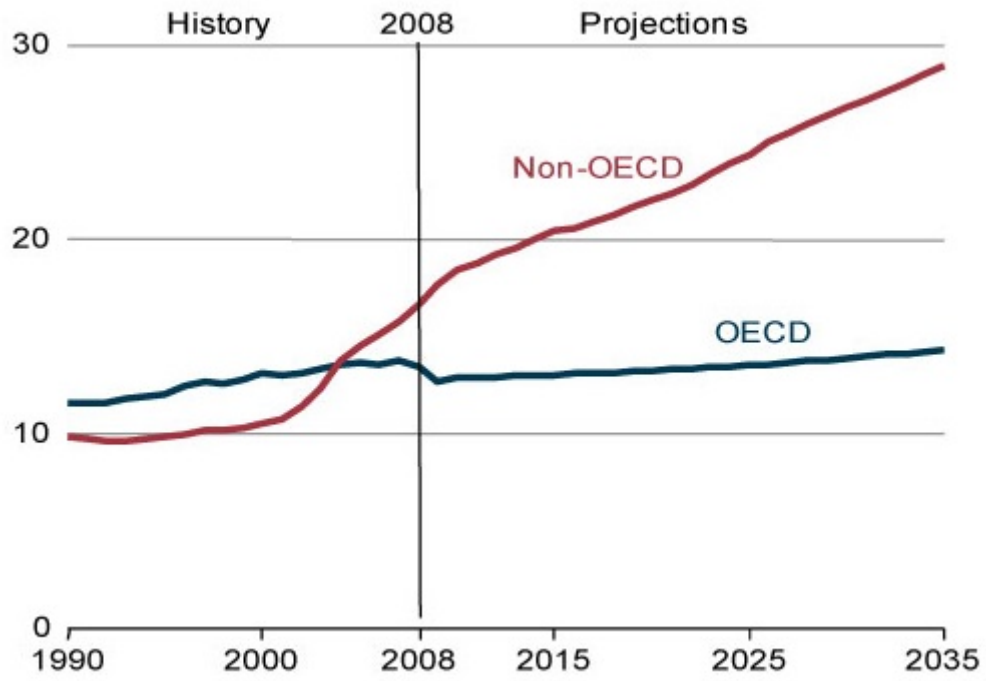

Figure 1.2: World Energy-related CO_2 emissions 1990-2035 (billion metric tons) Source: U.S. Energy Information Administration, 2011

1.1.3 Framing of the CO_2 Mitigation Issue in Relation to Capture from Pulverized Coal-Fired Power Plants

The previous sections provided a background into the global climate change problem, its origins and present and future CO_2 emission trends. It is important to note that though climate change is an issue on the global scale, it will manifest itself in a number of as-yet poorly predicted ways at the regional and local levels. Conversely, there is no single solution yet to the issue that can be prudently implemented on a global scale. Proposals such as geoengineering the earth to change the amount of solar insolation could mitigate climate change but possibly with disastrous unintended consequences [15]. Solutions to climate change should instead begin at the source - namely, manmade CO_2 sources, and should incorporate mitigation, substitution and recapture of emitted CO_2.

Pacala and Socolow [16] provide an intuitive way to visualize the CO_2 mitigation challenge through their stabilization wedges pictured in Figure 1.3 (b). Here the uppermost curve represents no effort to reduce CO_2 emissions (business-as-usual). The curve shaded in blue represents the emissions that would have to be permitted to stabilize the atmospheric CO_2 concentration at 500 ppm by 2125. The area between the curves, representing the magnitude of the mitigation effort required to achieve this limit, has been divided into seven (subsequently revised to nine) wedges, each representing 25 billion tons of carbon reduced. Each wedge may be achieved by one of several means such as fuel efficiency, transitioning to carbon-neutral energy and through carbon capture.

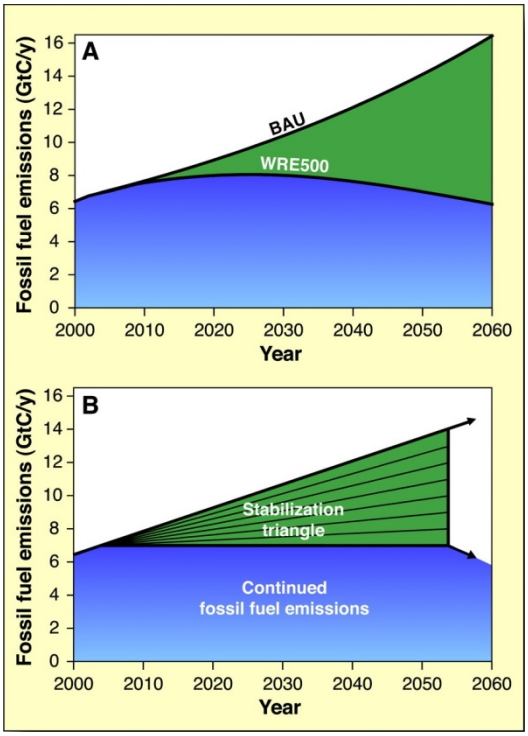

Figure 1.3: Stabilization triangle divided into 7 wedges between business-as-usual (BAU) and reduction required to limit atmospheric CO_2 concentration at 500 ppm by 2125 (accounting for CO_2 absorption into oceans) Source: S. Pacala and R. Socolow, 2004

Carbon capture from pulverized coal (PC)-fired power plants has been an issue of great debate centered on the cost and risks involved [17]. PC power plants produce over 90% of coal-based electricity [18]. The energetic cost of carbon capture reduces the power output of a plant and is described as a "parasitic load". A distinction may be made between carbon capture from a power plant and other industrial purification processes, most of which either add value to the end product or reduce operating costs by removing corrosive material or diluents. Carbon capture on the other hand, adds no such value; furthermore, CO_2 is not considered an air pollutant by the EPA. The closest analogue to power plant carbon capture is SO_x removal from power plant flue gas, which was successfully implemented under the U.S. EPA's Acid Rain Program [19]. Still, SO_x

emissions are much smaller than those of CO_2, and SO_2 has immediate adverse effects on health and environment, which made SO_x mitigation much more achievable than CO_2 mitigation is likely to be. In addition, the huge volumes of CO_2 captured must also be safely transported and stored or utilized, and unlike SO_2, cannot easily be turned into a benign solid form.

The incentive for power plant carbon capture only emerges when considering the fact that power plants are the only large point sources of CO_2. The next biggest CO_2 source, vehicle emissions, comes from distributed sources, which are much more expensive capture targets. Essentially, this means that if CO_2 mitigation is to be implemented as a realistic climate change avoidance strategy, PC power plants will explicitly have to be targeted. This necessitates the enforcement of policy tools such as the carbon caps or taxes to stimulate carbon capture from currently operational as well as planned power plants. This strategy will have to address utilization as well as storage of the captured CO_2 and is called Carbon Capture, Utilization and Storage (CCUS).

In such a scenario, it falls on power plant operators to reduce the energetic cost of carbon capture as much as possible. House et al [20] have estimated that at the thermodynamic limit, carbon capture and storage would require 19% of the power plant output for pressure-swing processes and 11% of the plant output for temperature-swing based processes. In reality, using existing technology, 50-80% of power plant output is likely to be consumed for carbon capture and storage [21]. This research studies ways to bring this cost closer to the thermodynamic limit by selecting and applying materials that would enable efficient and low-cost Rapid Thermal-Swing Adsorption (RTSA) systems.

1.2 Introduction to Power Plant Carbon Capture

The separation problem in power plant carbon capture can be described as the removal of CO_2 produced by coal combustion from N_2 diluent in the air used for combustion. Other products of combustion, such as ash, water vapor, sulfur and nitrogen oxides are removed for environment protection reasons unrelated to carbon capture and provide less of a challenge than the CO_2/N_2 separation. This separation can be performed at different points during the power generation process [22].

The CO_2 may be separated prior to fuel combustion by first oxidizing the fuel to a CO_2/H_2 mixture, removing and storing the CO_2 and then combusting the hydrogen to produce a CO_2-free exhaust (pre-combustion capture). It can also be separated from flue gas produced at the end of the process (post-combustion capture). Alternatively, the coal may be burned in O_2 instead of air, thereby making CO_2/N_2 separation unnecessary (oxy-fuel combustion).

1.2.1 Pre-combustion Capture

Pre-combustion capture is achieved through the Integrated Gasification Combined Cycle (IGCC). Here, the carbonaceous fuel is partly oxidized by steam to produce a mixture of CO and hydrogen called syngas. This process is called gasification as the solid fuel has been converted to a gas.

In the next step, the CO is further oxidized to CO_2 in the presence of more steam through the water-gas shift reaction shown below, resulting in a mixture of hydrogen, CO_2 and water vapor.

$$CO_{(g)} + H_2O_{(v)} \leftrightarrow CO_{2\,(g)} + H_{2\,(g)} \qquad (2.1)$$

The CO_2 is removed from hydrogen by amine scrubbing or pressure swing adsorption and the pure hydrogen is used as boiler fuel. Hence, the carbon capture has been performed before the fuel has been combusted. The process is called *combined cycle* because excess heat produced during the syngas process can be passed on to the steam cycle, improving efficiency. Figure 1.4 is a representation of a typical IGCC process.

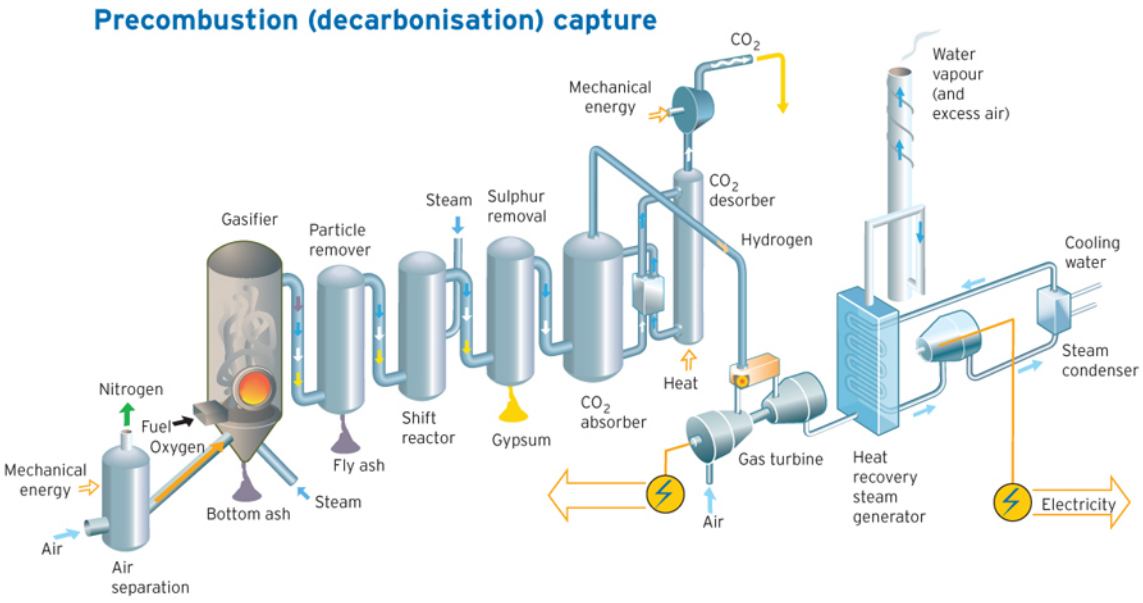

Figure 1.4: Process diagram of an IGCC plant with pre-combustion capture. Source: http://www.vattenfall.com/en/ccs/precombustion.htm

1.2.2 Oxy-fuel Combustion

CO_2/N_2 separation is made irrelevant if the coal is burned in O_2 instead of in air. The resultant flue gas is very CO_2-rich and can be sent to be compressed and stored. The process schematic is shown in Figure 1.5.

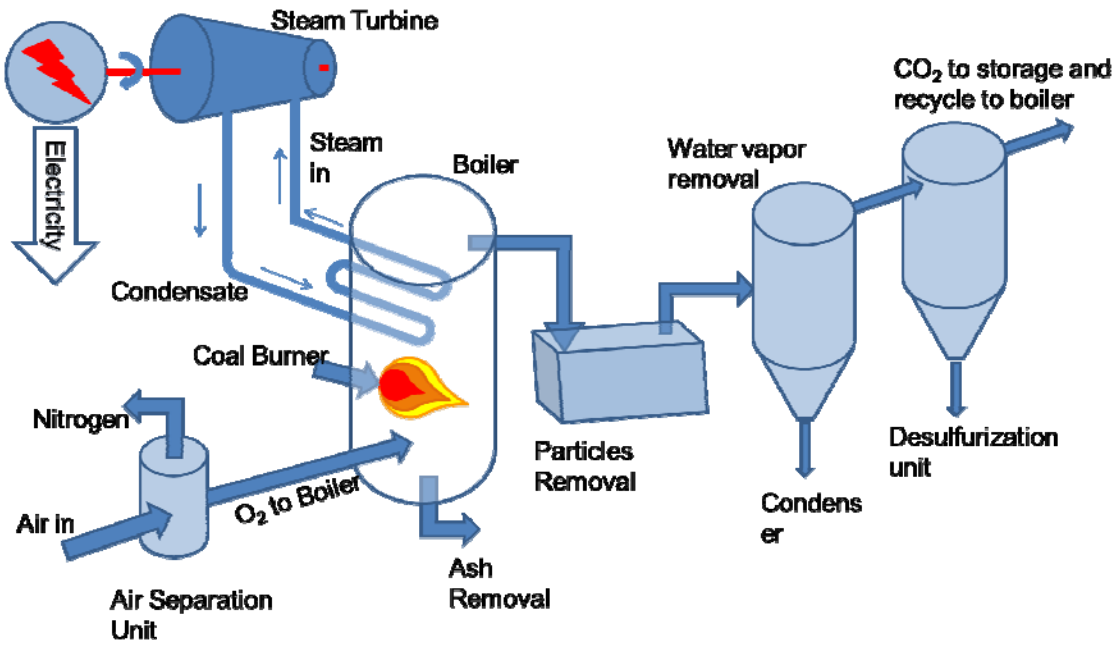

Figure 1.5: Process schematic of an oxy-fuel plant with Air separation unit. A portion of the CO_2 flue gas has to be recycled back to the boiler to reduce flame temperature in the boiler.

The chief challenges in implementing oxy-fuel combustion are the air separation units that have to be installed to supply oxygen to the boiler and the need for recycling part of the flue gas in order to reduce the flame temperature. Considerable retro-fitting is required before power plants can employ oxy-fuel combustion successfully.

1.2.3 Post-combustion Capture:

Alternatively, CO_2 can be captured from power plant flue gas, where it is called post-combustion capture. However, it requires installing a capture plant between the power plant and the stack. Post-combustion capture is, in fact, the most suitable capture method for currently operational power plants because of the smaller retrofit effort involved and the fact that power generation would not be contingent on efficient operation of the capture unit as it would be in the previous two cases. Figure 1.6 describes how such a process would work. Another advantage of post-combustion capture is that it provides the freedom to apply a wide range of separation processes for capture.

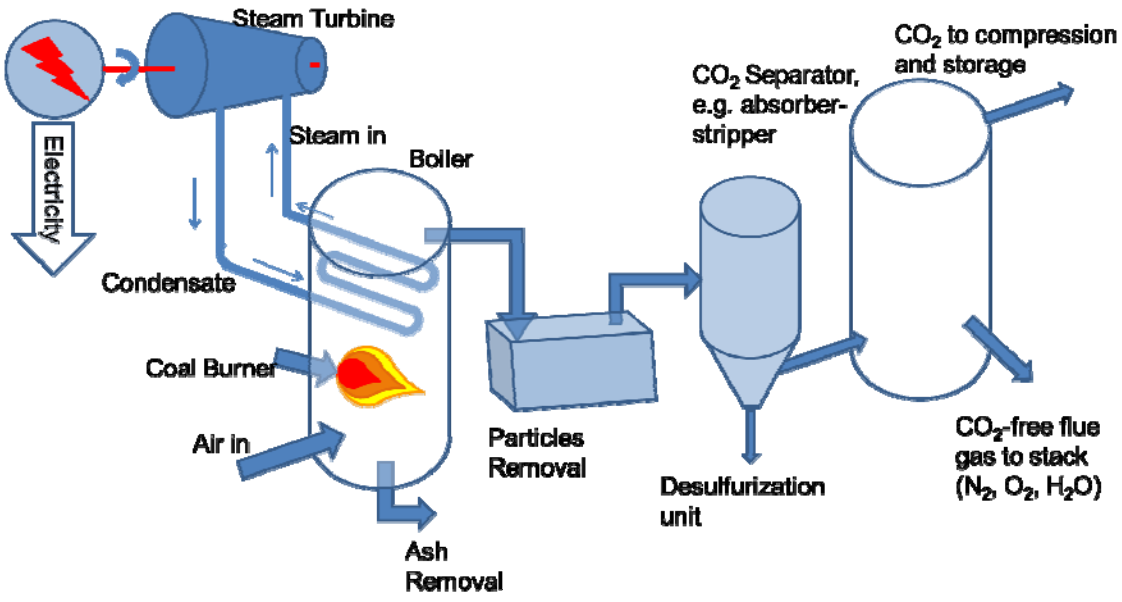

Figure 1.6: Process schematic of a PC power plant with post-combustion capture. The capture method is not mentioned here but may be one of many separation techniques such as solid adsorbents, absorption or membrane separation.

1.3 Post-combustion Capture Methods and the Case for Solid Sorbents

Post-combustion capture allows the flexibility of appending any suitable capture technologies to the power generation process. Absorption, membrane separation and adsorption are the three most likely candidates for carbon capture.

Absorption processes typically employ aqueous solutions of amines such as monoethanolamine (MEA) that bond chemically with acid gases such as CO_2 and can thus be used to remove CO_2 from flue gas. The amines are then stripped of CO_2 in a regenerator and reused, and the concentrated CO_2 can be processed and stored or used. The chief advantage of amine absorption is that it is a widely used process in the chemicals and petroleum industries and can readily be adapted on a large scale to power plant capture. For this reason, they are treated as the "imminent" capture method by researchers and policymakers more interested in other aspects of CCUS such as storage and sequestration. Figure 1.6 shows an amine absorption unit currently operational at the Barry power plant operated by the Alabama Power Company (Southern Company) in Mobile County, Alabama. This unit is capable of capturing CO_2 from a 25MW slipstream from the plant, which is then pumped 15 miles away into a saline formation 3 km underground [23].

Amine absorption has its challenges, the foremost being that it is energetically inefficient. The amine solution contain only 20-25% by weight of amines [24], the rest being water. The water, along with the amines, has to be thermally swung

through the absorption and regeneration cycles and adds greatly to the energy load. Corrosion is another issue that affects all amine absorption processes.

Figure 1.7: Aerial view of the capture unit at Plant Barry operated by Alabama Power Company in Mobile, Alabama. The flue gas intake line on the bottom left supplies a 25 MW slipstream from the power plant to the absorber column in the middle left. (Photo: Southern Company)

Gas separation membranes exploit the differences in the molecular sizes and the adsorption characteristics of CO_2 and nitrogen in polymeric or sometimes, inorganic membranes. They do not require thermal energy to power the separation but flue gas, at nearly atmospheric pressure, has insufficient driving potential to enable economical membrane separation.

Solid sorbents, the third major CO_2 capture technique, overcome many of the problems posed by liquid amine absorption. They may be thought of as immobilized

versions of the amine solutions: CO_2 physically adsorbs onto a stationary solid substrate instead of chemically absorbing into the amine solution. A solid adsorbent does not require an aqueous medium, which reduces thermal energy costs and eliminates corrosion. Traditionally, solid sorbents are packed into sorption beds a few meters long and operated in a pressure swing cycle. This is not a suitable approach for flue gas capture due to the high pressure drops involved and the occurrence of "hot spots". Neither are their dimensions amenable for thermal swing cycles due to the large length scale, which impairs thermal responsiveness. This work focuses on solid sorbents configured into hollow fibers rather than packed beds, which enables them to be used in a Rapid Thermal Swing Adsorption (RTSA) cycle.

1.3.1 Description and Operation of a Hollow Fiber RTSA System

The hollow fiber RTSA concept was envisioned by Lively et al. [25] to combine the benefits of solid sorbents with those of thermal-swing adsorption, which can utilize waste heat to effect the CO_2/N_2 separation. The hollow fiber morphology is useful in shrinking the characteristic length of the system from the order of meters to a few hundred microns, thereby greatly reducing the thermal response times.

A hollow fiber sorbent consists of a CO_2-sorbing material dispersed as suitably-sized particles in a porous polymer matrix arranged in the form of hollow fibers. The polymer matrix serves to enable fiber fabrication and provides mechanical strength as well as flue gas access to the sorbent particles. A key attribute of the polymer matrix is its bi-continuous nature: both the polymer strands and the pores are continuous phases.

The central bore is used as a channel for a heat transfer fluid that helps to accomplish the thermal swing process. A barrier layer is necessary on this channel wall to isolate the heat transfer fluid, namely water and process steam, from the flue gas passing on the outside of the fiber. The three constituent components then are the sorbent material, polymer matrix and the barrier layer, as shown in Figure 1.8.

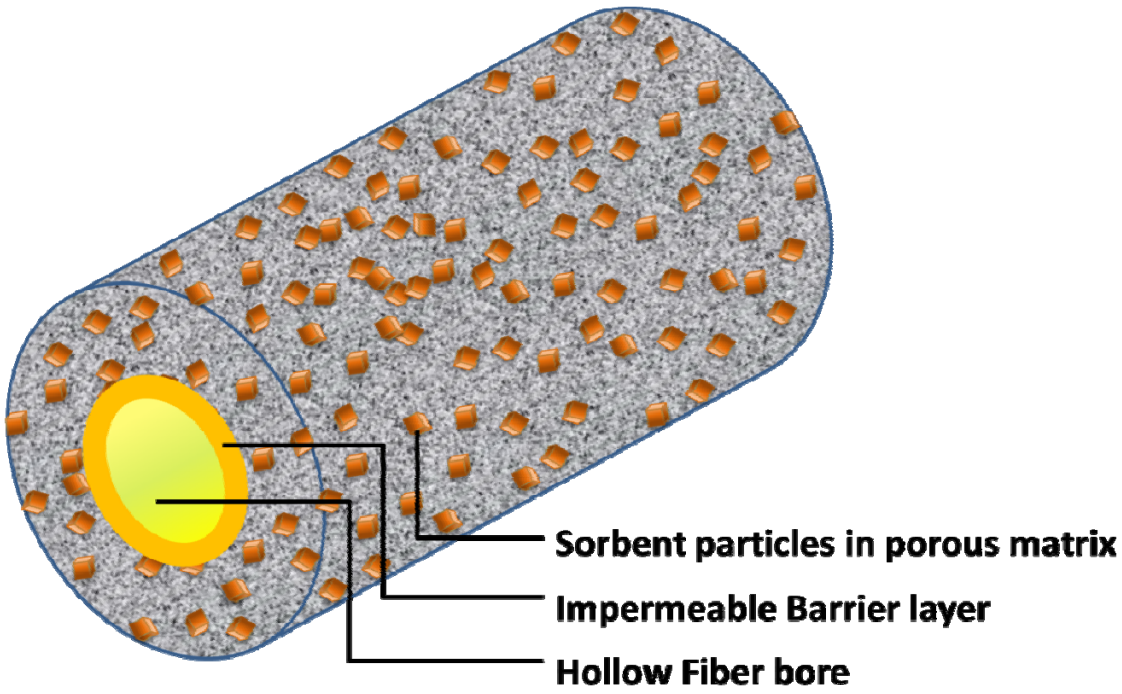

Figure 1.8: Illustration of a fiber sorbent section showing the sorbent particles supported in a porous polymer matrix and the barrier layer isolating the fiber bore (bore side) from the exterior (shell side)

As seen in the figure, a hollow fiber sorbent is essentially a packed sorbent bed where the bed length has been shrunken to the fiber wall thickness, which is less than 0.5 mm thick. This translates to rapid heat transfer aided by heat transfer fluid in the fiber bore. A hollow fiber sorbent may hence be thought of as an *adsorptive heat exchanger*.

The hollow fiber morphology allows the fibers to be mounted lengthwise in a module isolating the fiber bore from the external, or shell side.

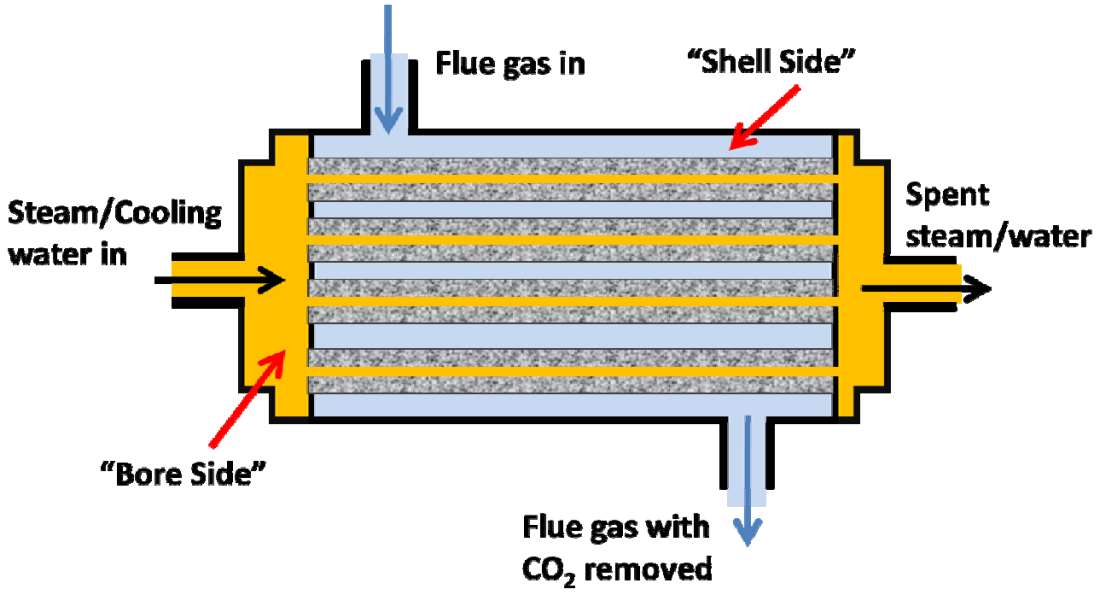

Figure 1.9: Representation of hollow fiber sorbent module during adsorption step showing isolation of the bore side from the shell side

Figure 1.9 shows a typical fiber sorbent setup using the same color scheme as Figure 1.8. It should be noted that both adsorption and subsequent CO_2 desorption occur on the shell side of the system and the bore side only serves to supply and remove heat during desorption and adsorption, respectively.

The arrangement of fibers into an ordered module reduces the flue gas pressure drop while the small fiber diameter increases the sorbent contact area. The operation of the module is very similar to the operation of a packed bed, with an adsorption step for flue gas followed by a desorption step in which the adsorbed CO_2 collects in the shell space and can be removed. The benefit of the lowered pressure drop

manifests as reduced flue gas pumping costs. Optimal operation, with minimal backmixing and high CO_2 capture purity is a *process design* problem requiring innovations such as a nitrogen sweep stage and timing the heat transfer fluid valves. This research instead considers the *materials approach* needed to emplace fiber sorbent components that can successfully capture CO_2 under wet feed conditions under repeated thermal cycling.

1.4 Research Objectives

As discussed in the previous sections, the hollow fiber RTSA system can provide a compact, low-cost carbon capture method with few of the inherent disadvantages of liquid amines and packed beds. Still, for a hollow fiber RTSA system to succeed in an industrial flue gas setting, there are several significant challenges that need to be overcome. PC power plant flue gas contains up to 15% CO_2 by volume, and significant amounts of water vapor and other gases [1]. These factors create complications for certain sorbents and polymers. The adsorbent needs to retain a working CO_2 capacity in the presence of a moisture-laden CO_2 feed. All three components of the fiber sorbents should retain their mechanical integrity on repeated cycling and should be stable at temperatures of 110 °C or higher in the presence of moisture and oxygen. With these challenges in mind, the following objectives have been identified for this research.

1.4.1 To Identify and Validate an Easily Spinnable Polymer with Robust Thermo-Mechanical Properties for the Matrix Phase

The support matrix of the hollow fiber is provided by a glassy polymer. The polymer matrix needs to retain its mechanical integrity and flexibility even at high sorbent loadings and at high temperatures (>100 °C) so that the fibers can be handled and operated without breakage or collapse. In addition, the polymer has to be formed into an open, porous matrix that allows easy access of the flue gas to the supported sorbents. To this end, a suitable glassy polymer has to be identified and a procedure developed to fashion it into an open-porous fiber matrix.

1.4.2 To Incorporate New Sorbent Materials with Good Working Capacity for CO_2

The CO_2 adsorbent is arguably the most important component of the hollow fiber system. Many requirements of the system, such as high capacity for CO_2, low regeneration energy, and reasonable temperature swing are direct attributes of the sorbent material. Hence, a thermally stable sorbent with a preferential adsorption of CO_2 over water and a low heat of sorption needs to be identified and tested. In addition, this sorbent has to be successfully incorporated into the fiber sorbent so that its CO_2 sorption capacity can be fully exploited in fiber form.

1.4.3 To Develop a Technique for the Easy Application of a Barrier Layer to the Fiber Sorbent

Finally, there is a need for a low-permeance barrier on the internal surface of the fiber sorbent to allow for a heat transfer medium (water or steam) to flow through the fiber bore. Since a necessary attribute of the hollow fiber is porosity, it will not be able to contain the heat transfer fluid in the bore without a barrier layer deposited on the inner surface. Lack of a barrier layer will cause steam loss and may clog the sorbent particles, rendering them inactive. To prevent this, a barrier layer that is easy to deposit and that retains its impermeability on repeated thermal cycling in wet environments is desired. An additional consideration is that the barrier should seal off the fiber face so that there is no “lumen-layer bypass” as illustrated in Figure 1.10.

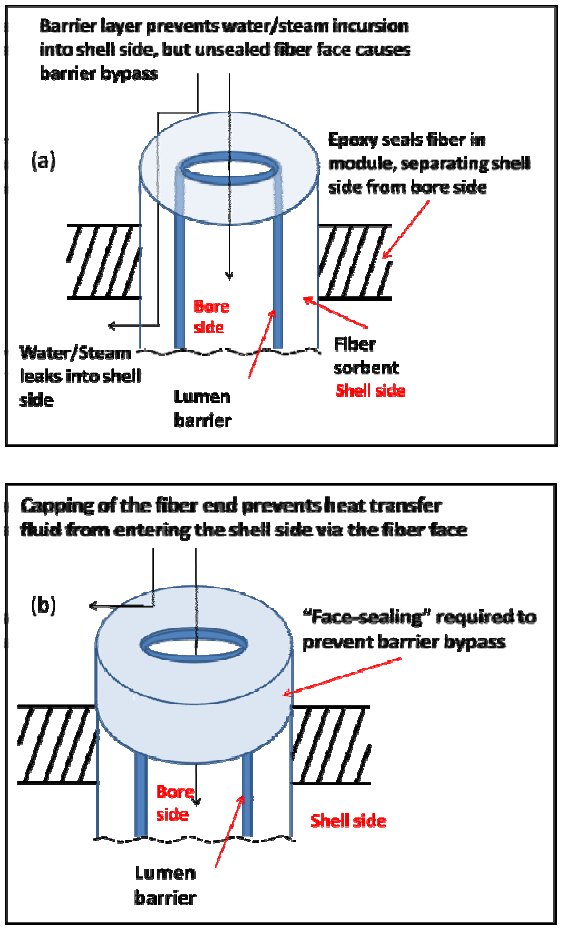

Figure 1.10: (a) Even with a barrier layer, fiber sorbents are prone to steam/water leakage into shell side through the gap between the epoxy potting and the barrier layer. (b) The fiber ends have to be capped with an impermeable material to prevent this bypass and completely isolate the shell side from the bore side.

1.5 Dissertation Organization

Chapter 1 of the thesis has set forth the motivation for PC carbon capture and introduction to and rationale for hollow fiber RTSA.

Chapter 2 covers the background material associated with hollow fiber spinning, transport and adsorption in porous mixed-matrix materials, barrier layer deposition and transport in dense films.

Chapter 3 summarizes the materials used in the course of this research and includes a description of the experimental methods used to synthesize and characterize the fiber sorbents.

Chapters 4-6 describe the selection and demonstration of materials for each component of the hollow fiber sorbent, building off proof-of-concept materials described in previous research [19]. *Chapter 4*, which covers the first research objective, describes the selection of a new matrix polymer and the process and spin conditions required to produce fiber sorbents with the desired porous structure.

In *Chapter 5*, different sorbents are explored for hollow fiber use and are evaluated for integration into the spinning process, availability in hollow fiber form and retention of capacity in wet feeds.

Chapter 6 describes the two different paths to establish a hollow fiber barrier layer and assesses suitable materials for each method.

Chapter 7 reviews the results of this research and identifies future areas of work to improve the hollow fiber RTSA platform.

1.6 References

1. Amann, J.-M.G. and C. Bouallou, *CO_2 capture from power stations running with natural gas (NGCC) and pulverized coal (PC): Assessment of a new chemical solvent based on aqueous solutions of N-methyldiethanolamine + triethylene tetramine.* Energy Procedia, 2009. **1**(1): p. 909-916.

2. Kiehl, J. and K.E. Trenberth, *Earth's annual global mean energy budget.* Bulletin of the American Meteorological Society, 1997. **78**(2): p. 197-208.

3. Boucher, O., G. Myhre, and A. Myhre, *Direct human influence of irrigation on atmospheric water vapour and climate.* Climate Dynamics, 2004. **22**(6): p. 597-603.

4. Forster, P., V. Ramaswamy, P. Artaxo, T. Berntsen, R. Betts, D.W. Fahey, J. Haywood, J. Lean, D.C. Lowe, G. Myhre, J. Nganga, R. Prinn, G. Raga, M. Schulz and R. Van Dorland, *Changes in Atmospheric Constituents and in Radiative Forcing*, in *Climate Change 2007: The Physical Science Basis. Contribution of Working Group I to the Fourth Assessment Report of the Intergovernmental Panel on Climate Change*, S. Solomon, D. Qin, M. Manning, Z. Chen, M. Marquis, K.B. Averyt, M.Tignor and H.L. Miller Editor 2007, Cambridge University Press: Cambridge, United Kingdom and New York, NY, USA. p. 137-141.

5. Le Treut, H., R. Somerville, U. Cubasch, Y. Ding, C. Mauritzen, A. Mokssit, T. Peterson and M. Prather, *Historical Overview of Climate Change*, in *Climate Change 2007: The Physical Science Basis. Contribution of Working Group I to the Fourth Assessment Report of the Intergovernmental Panel on Climate Change [Solomon, S., D. Qin, M. Manning, Z. Chen, M. Marquis, K.B. Averyt, M. Tignor and H.L. Miller (eds.)]*2007, Cambridge University Press: Cambridge, United Kingdom and New York, NY, USA. p. 101.

6. Hegerl, G.C., F. W. Zwiers, P. Braconnot, N.P. Gillett, Y. Luo, J.A. Marengo Orsini, N. Nicholls, J.E. Penner and P.A. Stott, *Understanding and Attributing Climate Change*, in *Climate Change 2007: The Physical Science Basis. Contribution of Working Group I to the Fourth Assessment Report of the Intergovernmental Panel on Climate Change [Solomon, S., D. Qin, M. Manning, Z. Chen, M. Marquis, K.B. Averyt, M. Tignor and H.L. Miller (eds.)*2007, Cambridge University Press: Cambridge, United Kingdom and New York, NY, USA. p. 727-732.

7. Meehl, G.A., et al., *Global climate projections.* Climate change, 2007: p. 747-845.

8. Chandler Jr, A.D., *Anthracite coal and the beginnings of the industrial revolution in the United States.* The Business History Review, 1972: p. 141-181.

9. U.S. Energy Information Administration, *International Energy Outlook 2011*, 2011.

10. Schmalensee, R., T.M. Stoker, and R.A. Judson, *World carbon dioxide emissions: 1950-2050.* Review of Economics and Statistics, 1998. **80**(1): p. 15-27.

11. Nardinelli, C., *Industrial Revolution and Standard of Living.* David R. Henderson, editor, 1993.

12. Ashton, T.S., *The industrial revolution 1760-1830.* OUP Catalogue, 2011.

13. U.S Energy Information Administration, *State Energy Data System (SEDS): 1960-2010*, 2012.

14. U.S. Environmental Protection Agency, *Draft Inventory of U.S. Greenhouse Gas Emissions and Sinks: 1990-2011*, 2013. p. 3-5.

15. Kiehl, J.T., *Geoengineering climate Change: Treating the symptom over the cause?* Climatic Change, 2006. **77**(3): p. 227-228.

16. Pacala, S. and R. Socolow, *Stabilization wedges: Solving the climate problem for the next 50 years with current technologies.* Science, 2004. **305**(5686): p. 968-972.

17. Gough, C., *State of the Art in Carbon Dioxide Capture and Storage in the UK: an experts' review.* International Journal of Greenhouse Gas Control, 2008. **2**(1): p. 155-168.

18. International Energy Agency, *Power Generation from Coal: Measuring and Reporting Efficiency Performance and CO_2 Emissions*, 2008.

19. Lively, R.P., *Hollow fiber sorbents for post-combustion CO_2 capture, PhD Dissertation*, 2011, Georgia Institute of Technology.

20. House, K.Z., et al., *The energy penalty of post-combustion CO_2 capture & storage and its implications for retrofitting the US installed base.* Energy & Environmental Science, 2009. **2**(2): p. 193-205.

21. Singh, D., et al., *Techno-economic study of CO_2 capture from an existing coal-fired power plant: MEA scrubbing vs. O_2/CO_2 recycle combustion.* Energy Conversion and Management, 2003. **44**(19): p. 3073-3091.

22. Herzog, H., *An introduction to CO_2 separation and capture technologies.* Energy Laboratory Working Paper, 1999.

23. Esposito, R., et al., *Integrating carbon capture with transportation and storage.* Energy Procedia, 2011. **4**: p. 5512-5519.

24. Kohl, A.L. and R.B. Nielsen, *Gas purification* 1997: Gulf Professional Publishing.

25. Lively, R.P., et al., *Hollow fiber adsorbents for CO_2 removal from flue gas.* Industrial & Engineering Chemistry Research, 2009. **48**(15): p. 7314-7324.

CHAPTER 2

BACKGROUND AND THEORY

This chapter covers the theoretical concepts necessary to describe sorption and transport in hollow fiber membranes and the principles behind hollow fiber and barrier layer fabrication. Transport in hollow fibers occurs through the porous polymer matrix, the sorbent supported within and through the bulk of the polymer, with different processes governing transport in each phase. In addition, barrier layers fabricated from polymeric materials behave much like low-permeability polymeric membranes.

2.1 Concept of a Hollow Fiber Sorbent

As explained in section 1.3.1, hollow fiber sorbents are comparable to highly miniaturized sorbent beds with up to 75% by weight of sorbent. The key dimension, the bed length, is reduced from a few meters to a few hundred microns, which enables quick thermal responses in a setup otherwise more suited to pressure swing adsorption. The central channel, or lumen, enables the provision of a heat transfer fluid to thermally swing the fiber in a much more efficient way than a heating coil would operate in a packed bed. Thermal cycling is preferred over pressure swing due to the availability of waste heat elsewhere in the plant. As a result, although the fiber sorbents are still randomly packed at the micrometer scale, the fiber/lumen/module system is more ordered and this ordering increases thermal efficiency and reduces response times [1].

Fiber sorbents are fabricated in a manner similar to mixed-matrix membranes via the dry-jet wet quench process [2, 3], wherein a polymer is precipitated from solution due to the action of a non-solvent. The sorbent particles, dispersed in the polymer solution, are trapped in the precipitated polymer lattice, ideally in a *sieve-in-a-cage* type structure. Figure 2.1 illustrates the open nature of such an interface, where the sorbent is fixed to the polymer matrix, but nevertheless provided access to the environment around the porous fiber. In other words, for the fiber sorbent to be successful, both the polymer network and the pore spaces should be continuous and the sorbent should not be occluded by the polymer network.

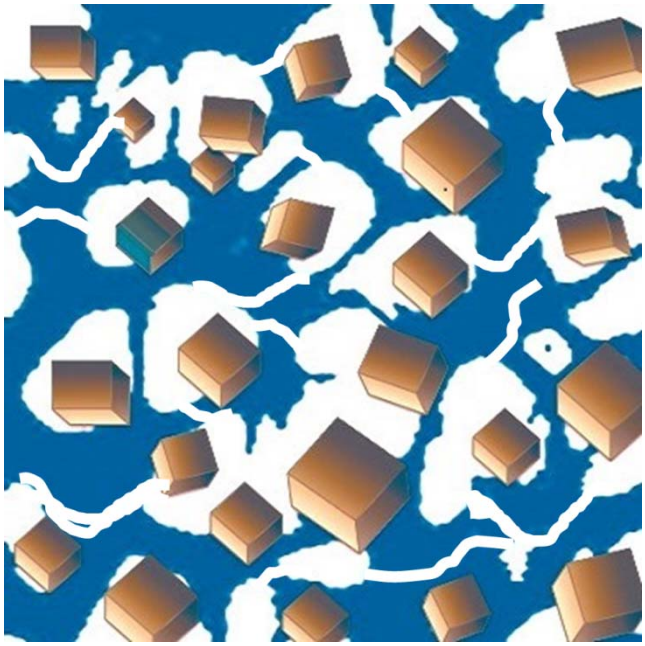

Figure 2.1: Schematic of an idealized "sieve-in-a-cage" pore structure where adsorbent particles are exposed to the ambient gas while supported in the polymer matrix. Both the polymer network (in blue) and the pore spaces (in white) are continuous phases.

2.2 Gas Transport in Hollow Fiber Sorbents

Sorption and gas transport are the two key phenomena governing hollow fiber performance. The sorbent crystals are selected to preferentially adsorb CO_2 over the other components of flue gas but equally importantly, the flue gas components have to diffuse to the sorbent particles, and later, the desorbing CO_2 has to diffuse out of the fiber. Diffusion into and out of the fibers occurs at different regions as shown in Figure 2.2.

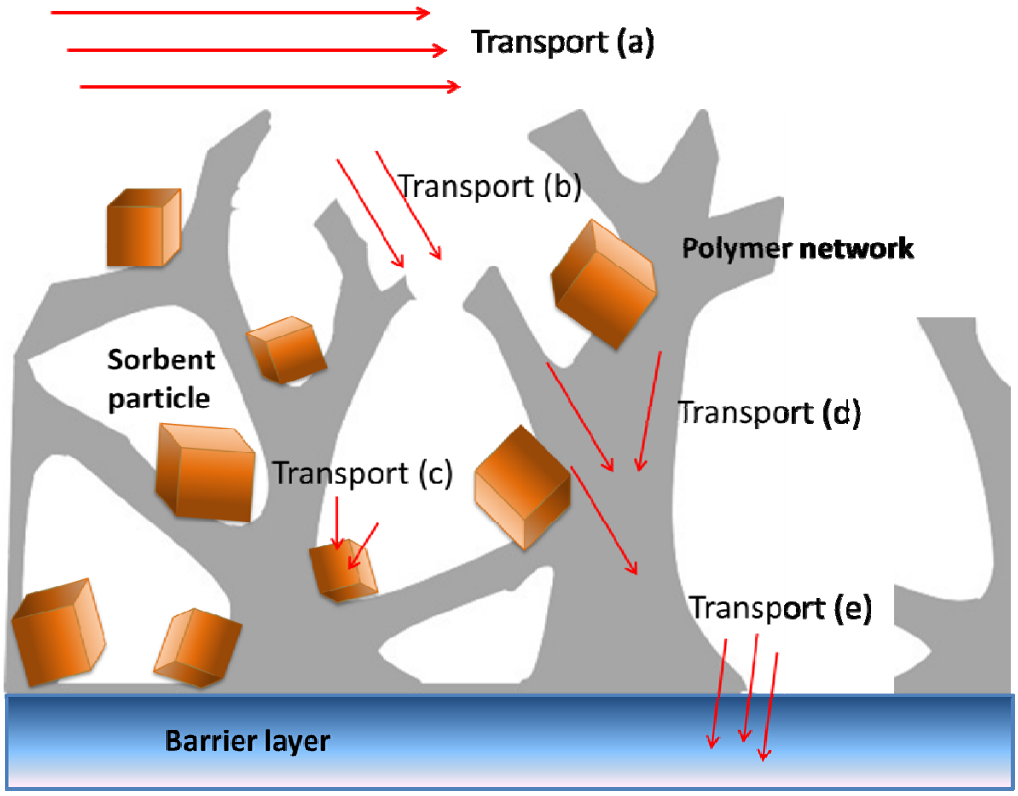

Figure 2.2: Longitudinal section of hollow fiber showing different gas transport regimes: (a) pressure-driven flow of flue gas over fiber surface, (b) diffusion of gas into and out of fiber pore structure, (c) diffusion of gas into and out of sorbent particles, (d) transport of gas molecules through the polymer chains, and (e) very limited transport into and out of the barrier layer isolating the fiber bore.

2.2.1 Gas Transport to the Fiber Surface

During the adsorption step of the thermal cycle, flue gas flows through the module and over the fibers, driven by a slight pressure gradient that may be enhanced by blowers. The flue gas in the fiber module may be considered perfectly mixed, but depending on the geometry of the modules, fiber arrangement and gas velocity, a viscous boundary layer may develop in places along the fiber length. The turbulent flow region, being perfectly mixed, has no diffusion limitations but the viscous sublayer has a velocity gradient and subsequently a concentration gradient across which CO_2 has to diffuse to reach the surface of the fiber. The viscous sublayer can be minimized by changing the fiber arrangement (e.g. cross-flow) or the flue gas velocity.

2.2.2 Diffusion into the Fiber Pore Structure

Within the fiber, there is no pressure gradient to drive convective gas flow, but diffusion occurs due to the thermal energy of the individual molecules and by their interaction with each other and with the pore walls. The continuous pore network within the fibers can be approximated as a series of interconnecting cylindrical channels. Within the network, each gas component diffuses along its gradient and this is responsible for CO_2 reaching the sorbent surface and later, the desorbing CO_2 diffusing into the fiber pores. For simplicity, the gas mixture may be thought of as a CO_2/N_2 binary mixture but this description is applicable to multi-component mixtures as well. The relative dimensions of the pores and the mean free path of the gas molecules determine which of two diffusion phenomena occurs - molecular (bulk) diffusion, or Knudsen diffusion.

2.2.2.1 Molecular or Bulk Diffusion

Molecular diffusion occurs when the vast majority of interactions occur between gas molecules, with little interference from the pore walls. This occurs when the mean free path of the gas molecules *(λ)* is much smaller than the pore diameter *(d_p)*, and gas-gas collisions are much more likely than gas-wall collisions. The mean free path is calculated as in Equation 2.1.

$$\lambda = \frac{k_B T}{\sqrt{2}\pi d^2 p_t} \text{ (m)} \qquad (2.1)$$

Here, p_t is the system pressure (Pa), T is absolute temperature (K), d is the gas molecule diameter (m), and k_B is the Boltzmann constant ($J.K^{-1}$). Molecular diffusion predominates if the ratio λ/d_p is greater than 20 [4]. In a 2-component system, the diffusivity is a function of the system temperature and pressure and gas molecule properties. The molecular diffusion coefficient (D_{AB}) (m^2/s) can be estimated using a suitable relation such as the Chapman-Enskog equation shown below [5]:

$$D_{AB} = \frac{1.86\times10^{-3} T^{3/2} \sqrt{\frac{1}{M_A} + \frac{1}{M_B}}}{p_t \sigma_{AB}^2 \Omega_D} \text{ (m^2/s)} \qquad (2.2)$$

where T is the temperature, M_A and M_B are the molecular weights of the gases (g/mol), σ_{AB} is the effective collision diameter (m) and Ω_D is the collision integral.

2.2.2.2 Knudsen Diffusion

In smaller channels, as the pore dimensions become comparable to the mean free path of the gas molecules, molecule-wall interactions influence the diffusion phenomenon. Knudsen diffusion is said to occur when the ratio d_p/λ is less than about 0.2 [4]. The Knudsen diffusion coefficient ($D_{K,A}$) is written as:

$$D_{K,A} = \frac{d}{3}\left(\frac{8g_c RT}{\pi M_A}\right)^{0.5} \text{ (m}^2\text{/s)} \qquad (2.3)$$

Comparing Equations 2.2 and 2.3, it is seen that the bulk diffusion coefficient (D_{AB}) depends on the system pressure and the gas collision diameter, as would be expected for a process based on intermolecular collisions. The Knudsen diffusion coefficient ($D_{K,A}$) on the other hand is pressure independent and instead varies linearly with the average pore diameter d_p.

In addition, the mutual bulk diffusion coefficient D_{AB} is identical for both components A and B whereas $D_{K,A}$ is different for different gas components. Hence bulk diffusion is a non-selective process but Knudsen diffusion introduces a small selectivity wherein lighter molecules have a higher diffusivity than heavier ones. Measuring the relative rates of diffusion of two gases can thus be a way to determine whether bulk or Knudsen diffusion is the dominant process. Knudsen and bulk diffusion occur not only in the fiber pore structure but also in defective barrier layers, where there may be a macroscopic crack or gap in otherwise dense barriers.

2.2.2.3 Pores of Intermediate Size

In practice, it is not possible to produce fibers with pores of uniform size and depending on the system temperature, pressure and gas used; the diffusion regime may either be bulk diffusion or Knudsen diffusion or intermediate. An effective pore diffusion coefficient can be calculated as the sum of the reciprocals of the molecular and Knudsen diffusion coefficients. (Equation 2.4)

$$\frac{1}{D_{pore}} = \frac{1}{D_{AB}} + \frac{1}{D_{K,A}} \qquad (2.4)$$

The units for the diffusion coefficients are cm^2/s or m^2/s. The effective pore diffusion coefficient is calculated by correcting for the fiber porosity (ε) and the tortuosity (τ), which accounts for the longer path length caused by non-linear pore channels.

$$D_{pore,e} = \frac{\varepsilon}{\tau} \cdot D_{pore} \, (m^2/s) \qquad (2.5)$$

2.2.3 Transport in Dense Polymers

As shown in Figure 2.2, there is movement of gas molecules through the "body" or dense part of the polymer network concurrent to the diffusion through the pore spaces. This is a region of the fiber that consists of the homogenous polymer struts defining the pore structure, formed by precipitation of polymer from solution during fiber

spinning. The same diffusion process also occurs in the barrier layer if it is made of polymeric material. It is important to note that Knudsen and bulk diffusion are several orders of magnitude faster than diffusion through the polymer struts [1] and are the predominant mode of gas transport to and from the sorbent particles. Similarly, a good barrier by design impedes gas transport through it. However, understanding gas transport through the barrier is important to evaluate barrier layer performance.

Diffusion in these dense polymers occurs through a process described by *the solution-diffusion model*. Here, gas molecules encountering the polymer surface sorb or dissolve into the polymer bulk, and then randomly move through the interstices of the polymer chains that constitute them, driven by thermally induced perturbations [6, 7]. If there is a pressure or concentration gradient across the width of the dense layer, there is a net directional diffusion. Thus the flux of gas through the polymer has two components: a kinetic component or diffusion, and an equilibrium component or sorption [8]. Permeability of gas *i* through the polymer, (P_i), is defined as the product of these two components [8]:

$$P_i = D_i \cdot S_i \ \textit{(Barrer)} \qquad \textit{(2.6)}$$

where D_i is the diffusion coefficient and S_i is the sorption coefficient. Since the permeability varies for each gas molecule based on the gas-polymer chemistry and the molecular size and geometry, dense polymers show a relative preference or selectivity for transport of some gases over other, which provides the basis for polymeric membrane separations [9]. This preference may be based on the speed of diffusion, which is affected

by the molecules' size and shape; or on the sorption coefficient, which is controlled by the chemical interactions between the gas and polymer. An overall permselectivity (α_{ij}) for component *i* over component *j* is hence defined as:

$$\alpha_{ij} = \frac{P_i}{P_j} \qquad (2.7)$$

In this work, the permselectivity serves as an important tool to gauge the quality of polymeric barrier layers. The closer the selectivity of a barrier layer is to that of a solution-cast polymer film, the fewer defects it has and more likely it is to be a good barrier.

Transport in polymers begins as gas molecules sorb into the dense polymer. Sorption in polymers is affected by whether the polymer is *glassy* or *rubbery*. This is an aspect of the *amorphous* portion of polymers [10]. All polymers are amorphous to some extent rather than completely crystalline, and this amorphous phase could be rubbery, meaning that the polymer chains have undergone confirmation rearrangement to attain equilibrium (no packing defects). On the other hand, polymers could also be glassy, meaning that the polymer chains have not rearranged themselves to their equilibrium positions. The disequilibrium state of glassy polymers is manifested as an increased or *excess free volume*, the fraction of the polymer that is not occupied by the polymer chains themselves. This enables two modes of sorption: a simple dissolution into the equilibrium polymer and a "hole-filling" of gas molecules into the packing defects. The former is described by Henry's law and the latter by Langmuir's model [11]. The concentration of

sorbed gas in the polymer *(C)* (cc STP/g or mol/g) is hence the sum of the Henry's Law *(C_D)* and Langmuir *(C_H)* contributions:

$$C = C_D + C_H \tag{2.8}$$

which are expanded as:

$$C = k_D p + \frac{C_H' bp}{1 + bp} \tag{2.9}$$

Here k_D is the Henry's law constant (g.atm/mol), C_H' is the Langmuir capacity and b is the Langmuir affinity constant [12]. The sorption coefficient S_i (mol/g.atm), which is the ratio of the concentration term C to the pressure p is written with respect to component i as:

$$S_i = k_{D,i} + \frac{C_{H,i}' b_i}{1 + b_i p_i} \tag{2.10}$$

Diffusion of molecules thus sorbed occurs when gas molecules randomly jump from one sorbed state to another. This is aided by the molecular motions of the polymer chains themselves, which open up jump opportunities for the sorbed gas molecules. Unlike sorbents, polymers do not contain permanent molecule-sized channels for gas diffusion. The diffusion coefficient D_i is proportional to the frequency and length of jumps of the gas molecules from one gap to another and is given by :

$$D_i = \frac{1}{6} \cdot f_i \cdot L_i^2 \qquad (2.11)$$

where f_i is the jump frequency (s^{-1}) and L_i is the jump length of the molecule (m).

2.2.4 Gas Flux Measurement in Fiber Sorbents

The diffusion and sorption coefficients are combined to give the gas permeability P_i, described in Equation 2.6. Permeability of gas component *i* is the gas flux (Q_i/A) (cc STP/m^2) normalized by the thickness of the material (l) (m) and the pressure gradient (Δp) (Pa or atm) that drives diffusion [3, 13] as shown in Equation 2.12 below. Here A is the cross sectional area of permeation.

$$P_i = \frac{Q_i \cdot l}{A \cdot \Delta p_i} \qquad (2.12)$$

Permeability is often measured in a unit called Barrer, which is:

$$1\ Barrer = 10^{-10} \cdot \frac{cm^3(STP) \cdot cm}{cm^2 \cdot s \cdot cm\ Hg} \qquad (2.13)$$

Permeability is a useful quantity to compare polymer membranes of known thickness, but is unsuitable if the thickness is uncertain, as in the case of the barrier layer. It is an intrinsic property of the polymeric material and cannot be applied to

the porous fiber sorbent volume. Here the *pressure normalized flux*, or Permeance *(P_i/l)* comes into play. Permeance is measure in Gas Permeation Units (*GPU*s):

$$1\ GPU = 10^{-6} \cdot \frac{cm^3(STP)}{cm^2 \cdot s \cdot cm\ Hg} \qquad (2.14)$$

In this work, permeance is the relevant measure of permeation through the porous polymer network and later, the increase in permeation resistance as the barrier layer is applied on the fiber bore.

2.2.5 Permeation Porosimetry

One way to analyze the pore structure in fiber sorbents is to flow gas through the fiber wall under pressure and measure the flux. It is important to note that this experiment is **only relevant in the absence of the barrier layer**. With the barrier layer present, the barrier and fiber wall resistances are in series and the barrier resistance controls the rate of diffusion through the fiber wall. Diffusion in that case only occurs due to the molecular diffusion process that transports CO_2 to and the crystal surface, which has been described in Section 2.2.2.

The different transport phenomena in porous solids are described by the Dusty Gas Model [14]. Using this model, the flux through the fiber wall can be simplified into only two components: a pressure-driven Poiseuille component that occurs in the larger channels and a Knudsen diffusion component which occurs in the smaller channels

where the pore dimensions approach the mean free path of the gas molecules. Under usual conditions, a hollow fiber RTSA system yields a mean free path of ~103 nm for nitrogen, calculated as described in Section 2.2.2.2. If pore sizes of 100-300 nm are assumed [2], Knudsen diffusion is the relevant diffusion process.

Molecular diffusion is assumed to be irrelevant in this analysis, since under a pressure gradient, bulk flow dominates in channels that are big enough for molecular diffusion. Diffusion processes through the sorbent particles (described in Section 2.2.6) and through the dense polymer are also assumed to be too slow to influence the overall flux.

Permeation porosimetry involves measuring the permeance through the fiber wall at different pressures and plotting the permeance vs. pressure. For porous fiber sorbents, the plot resembles Figure 2.3 below. There is a pressure-dependent component which represents the Poiseuille flow and the y-intercept that represents Knudsen flow. Knudsen diffusivity is pressure-independent as shown in Equation 2.3 and the pressure dependency of the Poiseuille flow allows us to separate the two components.

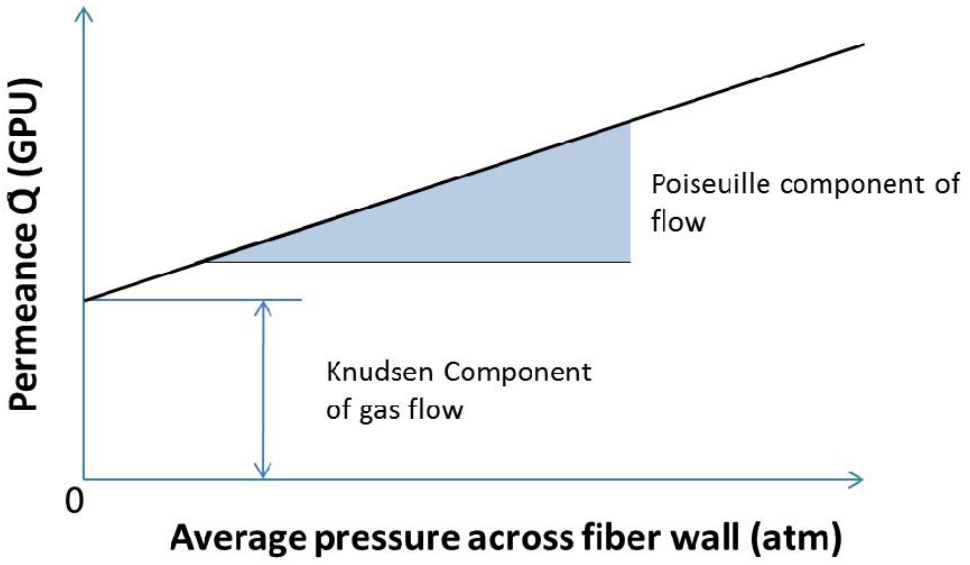

Figure 2.3: Plotting permeance through fiber wall against the average pressure enables calculation of the Knudsen contribution from the y-intercept and the Poiseuille contribution from the slope.

The Knudsen and Poiseuille contributions to this permeance are derived as follows [5, 15]:

$$\dot{Q} = \dot{Q}_{Knudsen} + \dot{Q}_{Poiseuille} \tag{2.15}$$

$$\dot{Q}_{Knudsen} = \frac{2 \cdot \varepsilon \cdot v \cdot r}{3 \cdot R \cdot T \cdot \tau \cdot L_w} \tag{2.16}$$

$$\dot{Q}_{Poiseuille} = \frac{\varepsilon \cdot r_{pore}^2 \cdot p_{avg}}{8 \cdot \mu \cdot R \cdot T \cdot \tau \cdot L_w} \tag{2.17}$$

Here, p_{avg} is the average of feed and permeate pressures (Pa), ε is the fiber porosity (dimensionless), τ is tortuosity (dimensionless), μm is the gas viscosity (Poise), v is the average velocity of the gas (m/s), L_w is the fiber wall thickness (m), T is the temperature (K) and r is the assumed average pore diameter (m).

When $\dot{Q}$ is plotted against p_{avg} as shown in Figure 2.3, the slope *(M)* and intercept *(I)* can be extracted from Equations 2.16 and 2.17:

$$I/M = \frac{16 \cdot v \cdot \mu}{3 \cdot r} \qquad (2.18)$$

The average gas velocity v and the gas viscosity μ may be approximated from the kinetic theory of gases. Then $v = \left(\frac{8 \cdot \mathrm{k}_B \cdot \mathrm{T}}{\rho \cdot \mathrm{M}} \right)^{1/2}$ and $\mu = \left(\frac{0.998 \cdot (\mathrm{M} \cdot \mathrm{k} \cdot \mathrm{T} / \rho)^{1/2}}{\pi \cdot d^2} \right)$.

Here k_B is Boltzmann's constant, M is the molecular weight of the gas, ρ is the gas density, and d is the kinetic diameter of the gas molecule.

$$I/M = \frac{16 \cdot 0.998 \cdot 8^{1/2} \cdot \mathrm{k} \cdot \mathrm{T}}{3 \cdot r \cdot \pi^2 \cdot d^2} \qquad (2.19)$$

This equation shows that the pore radius r can be readily calculated from the ratio I/M at a given temperature. Empirically, Equation 2.19 can be reduced to:

$$d_p = 2 \cdot r = A \cdot T \cdot \left(M/I \right) \qquad (2.20)$$

The coefficient A is an empirical constant that can be estimated for each gas. The above equation can then be used to calculate the average pore diameter in the fiber sorbent.

2.2.6 Transport and Sorption in Microporous Materials

Once the sorbate molecules have traversed the pore network, they reach the surface of the sorbent particles. Sorbents are usually crystalline or amorphous inorganic particles such as zeolites, amine-functionalized amorphous silicas and amorphous carbon. For fiber sorbents, it is advantageous to reduce sorbents to the smallest size that is economically achievable.

The specific surface area available for sorption ($S.A$) (m^2/g) has a hyperbolic relationship with the particle diameter ($d_{particle}$) (m) as shown in Equation 2.6.

$$S.A = \frac{3}{2 \cdot \rho \cdot d_{particle}} \qquad (2.21)$$

However, the energy required to reduce particle sizes by crushing also has an increasing trend as the particle size decreases. Bond proposed a work equation that suggests a non-linear increase in specific energy of comminution as the particle size decreases [16]. Other constraints on particle size reduction include possible difficulty in dispersing sub-micron sized particles, synthesis methods that yield particles of definite size and inability to grind some sorbents without damage. Here, it becomes helpful to

compare the diffusion coefficients of gas in the sorbents with that of the gas in pore network to determine an appropriate particle size. Knudsen diffusion tends to yield diffusion coefficients around 10^{-5} cm^2/s [1] and fiber pores tend to be of the order of tens of microns. Zeolitic sorbents often yield diffusion coefficients $\approx 10^{-5}$ cm^2/s [17]. Even when the diffusion coefficients are 10^{-6} - $10^{-7}cm^2/s$, sorbent particles only need to be less than 1 micron in size to have a comparable diffusion time to the pore spaces surrounding them. As a result, sorbent particles are usually micron-sized, ranging from 1-10 μm. A polydispersity index close to 1 is ideal for dispersion and spinning and yields fibers with higher mechanical strength - i.e., the sorbent particles are completely dispersed and at no point compromise the continuous nature of the polymer phase.

Gas transport in sorbents is heavily dependent on sorption and the thermally facilitated movement of sorbed molecules. An important feature of many adsorbents is their immense internal surface. Commercial adsorbents such as zeolites and amorphous silicas have internal surface areas many orders of magnitude larger than the external surface area, even in powdered form [18, 19]. This surface area occurs in the form of channels and voids approaching molecular dimensions [20, 21] and molecules in these spaces never really leave the force field exerted by the surface. The term surface diffusion describes a process of gas transport along these surfaces. Since this process involves molecules adsorbing on specific sites and hopping from one site to another, surface diffusion is an activated process. The Surface Diffusivity (D_s) (m^2/s) is dependent on the distance between adjacent sorption sites (δ) (m) as follows [22]:

$$D_s = \frac{\delta^2}{4t_j} \tag{2.22}$$

Here t_j is the average time between site jumps (s) and includes the thermal dependence of the diffusivity as:

$$t_j = t_{j0} \cdot \exp\left(\frac{E_a}{RT}\right) \tag{2.23}$$

where E_a is the energy of activation required for the jump (kJ/mol). The term t_{jo} is related to the jump frequency at the thermal diffusion rate.

Equations 2.7 and 2.8 can be combined to provide an expression for temperature dependence of surface diffusivity:

$$D_S = D_{S0} \cdot \exp\left(-\frac{E_S}{RT}\right)(\mathrm{m}^2/\mathrm{s}) \tag{2.24}$$

The pre-exponential term D_{S0} (m^2/s) is the diffusivity when there is no activation barrier, i.e., diffusion at thermal velocity. Surface diffusivity is dependent on the sorbent surface loading, and in the region leading up to monolayer coverage, it increases with increased surface loading [23].

Sorption is often a much more important phenomenon than diffusion when it comes to microporous materials used for CO_2 capture, both from a transport

perspective and as the underlying characteristic of fiber sorbents that allows carbon capture. It is dependent on physical or chemical interactions between the gas molecule and the sorption sites. Zeolite sorption can be explained based on the presence of sorption sites that saturate until complete monolayer coverage is achieved [22, 24]. Zeolites consist of a silica lattice with a definite crystal structure with some sites where the silicon atom has been replaced by an aluminum atom. These tetrahedrally coordinated aluminum atoms require a proton or cation to neutralize its charge and thus form Lewis acid sites which promote strong water adsorption [25].

Zeolites also accommodate physisorption of gas molecules on the pore wall itself [26]. As the aluminum content of the zeolites decreases, the amount of water adsorbed decreases in relation to other sorbed species. Dealuminized and low-aluminum zeolites (SiO_2/Al_2O_3>80) adsorb little water and could be thought of as hydrophobic [27].

The sorption characteristics of zeolites are well described by the Langmuir isotherm, which is an equilibrium equation for the concentration of sorbed molecules (C_i) of species *'i'* at a given system partial pressure (p_i) (Pa or atm) [15]:

$$C_i = \frac{C'_{H,i} b_i p_i}{1 + b_i p_i} \qquad (2.25)$$

Here, $C'_{H,i}$ is the sorbed concentration at complete monolayer coverage (cc STP/g or mol/g), b_i is the pore affinity for the sorbate, and p_i is the sorbate partial pressure [28]. The Langmuir isotherm has a region of approximate linear dependence of

the isotherm on the sorbate partial pressure and flue gas CO_2 sorption often falls in this "Henry's Law regime" of relatively low partial pressure and high temperature [29].

With alternative sorbents, such as amine-functionalized mesoporous silica, chemical interactions between the amines and CO_2 are responsible for adsorption and these are often described in terms of the formation of unstable carbamates and bicarbonates, which is a process aided in the presence of moisture [30]. These chemisorption mechanisms are suggested to be analogous to the reactions of CO_2 in liquid amines, which follow the schematic below [31].

$$2\underbrace{(RNH_2)}_{primary\ amine} + CO_2 \rightleftharpoons \underbrace{RNH \cdot CO_2 \cdot RNH_3^+}_{carbamate}$$

$$\underbrace{RNH_2}_{primary\ amine} + CO_2 + H_2O \rightleftharpoons \underbrace{RNH_3^+ HCO_3^-}_{bicarbonate} \overset{pH}{\rightleftharpoons} RNH_3^+ CO_3^{2-} \qquad (2.26)$$

Amine-functionalized silicas are advantageous in that the number of amine groups, and therefore the CO_2 sorption capacity, are not fixed and may be increased by improving the synthesis procedure. However, since the sorption is predicated on forming chemical bonds between the sorbent and sorbate, the energy required for desorption (the heat of sorption) is much higher for solid amines. The desorption costs for solid amines, as represented by the heat of sorption maybe more than twice that of zeolites and amorphous carbon [32, 33].

2.3 Formation of Hollow Fiber Sorbents

Hollow fiber sorbent fabrication evolved from the dry-jet wet-quench process extensively used to spin hollow fiber membranes for gas separation [34]. Research on zeolite-polymer mixed matrix membranes encountered a defective interface called the "sieve-in-a-cage" morphology [35, 36], where poor adhesion between the inorganic sieve and the polymer caused the sieve to only be supported at certain points on its surface, negatively affecting the separation performance. Hollow fiber sorbents exploit this feature to create a network in which the sorbent particles are loosely held by polymer struts, thereby providing unhindered gas access to the sorbent, as previously illustrated in Figure 2.2.

2.3.1 Modified Dry-jet Wet-quench Spinning for Fiber Sorbents

In the dry-jet wet-quench process to spin polymeric hollow fiber membranes [37], a homogenous polymer solution, or dope, is extruded through a spinneret in a jet into a non-solvent bath, first passing through an air gap. The dope includes a volatile non-solvent that evaporates as the dope passes through the air gap, causing a thin, dense polymer skin to form. This skin eventually forms the separating layer of the hollow fiber membrane. As the polymer jet enters the bath, the non-solvent diffuses into the still-liquid dope beneath the dense skin. The polymer is insoluble in the non-solvent but the non-solvent and the solvent are miscible with each other. When the non-solvent concentration increases above a certain point, the polymer precipitates but retains the cylindrical shape of the dope jet. The solvent-non-solvent phase remains

within this structure, forming polymer-lean nuclei which eventually become the pores of the hollow fiber. The final component of the spinning process is a "neutral" solvent-non-solvent mixture that is extruded within the dope jet, forming a cylindrical cavity within the precipitating polymer: the fiber bore or lumen. The phase diagram illustrating these two phase changes are described in Section 2.3.3.

For spinning hollow fiber sorbents, three major modifications are made to the quench process. First, the sorbent material is thoroughly dispersed in the dope so that the precipitating polymer traps the sorbent particles in its pore network. The sorbents are usually saturated with non-solvent so that they essentially act as "passive fillers" and do not interfere with the precipitation equilibria or kinetics. In essence, the phase diagram is constructed ignoring the sorbent. Secondly, the dense skin formation is dispensed with, since it would hinder gas access to the interior of the fiber. This is accomplished by removing the volatile non-solvent from the dope and by reducing the air gap as much as possible (a small air gap is usually retained to avoid polymer precipitation at the spinneret). The final modification to the spinning process is to add a *pore-former* to the spin dope. The pore-former is an additive that encourages the formation of the pore network as the polymer precipitates, and also suppresses the formation of large macrovoids that could compromise the mechanical strength of the fiber sorbent. This is important to open up the "cage" that comprises the "sieve-in-a-cage" structure and to improve gas access to the sorbent particles.

The experimental setup to spin fiber sorbents is shown in Figure 2.4.

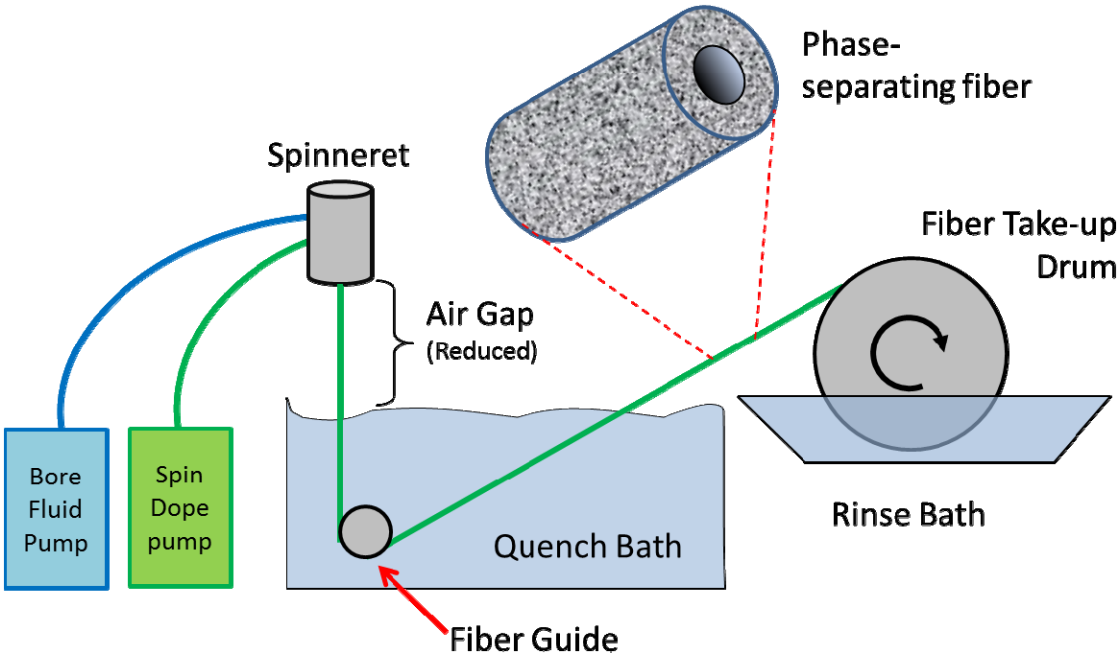

Figure 2.4: Schematic of spinning setup for hollow fiber sorbents. The spin dope and bore fluid are co-extruded through a spinneret into a quench bath where the polymer precipitates into fiber form with the bore fluid forming the fiber lumen. The fiber is taken up on a rotating drum where the phase separation is allowed to continue.

There are a number of parameters that control the dimensions, pore morphology and properties of fibers spun using the dry-wet process. As already described, the dope composition and length of air gap may be modified to control the skin formation. Other parameters include the spinneret design, take up rate and the presence of pore-former in the dope [38].

2.3.2 Fiber Solvent Exchange and fiber drying

Once the fibers are on the take-up drum, they can be cut, and the phase separation is allowed to go to completion in a non-solvent trough. Before the fibers can be dried, they are washed in a series of solvents of decreasing surface tension. If the fiber

is directly taken out of a non-solvent such as water and allowed to dry, the strong capillary forces from the receding water can cause pore collapse, aided by residual solvent in the fiber that may plasticize it [39]. Exchanging the water with a water-miscible organic liquid such as methanol, with a subsequent replacement by a volatile hydrocarbon can allow a gradual decrease in the surface tension and protect the fiber pore structure. The fibers may then be air-dried and vacuum-dried for a more complete removal of adsorbed solvent.

2.3.3 The Ternary Phase Diagram and Dope Preparation

The ternary diagram describes the phase transitions in a 3-component system consisting of polymer, solvent and non-solvent [40]. Figure 2.5 shows a simple ternary diagram showing the single-phase and two-phase regions separated by the *binodal line*. The two transitions discussed in the above section are represented by the yellow arrow (vitrification) and red arrow (phase separation).

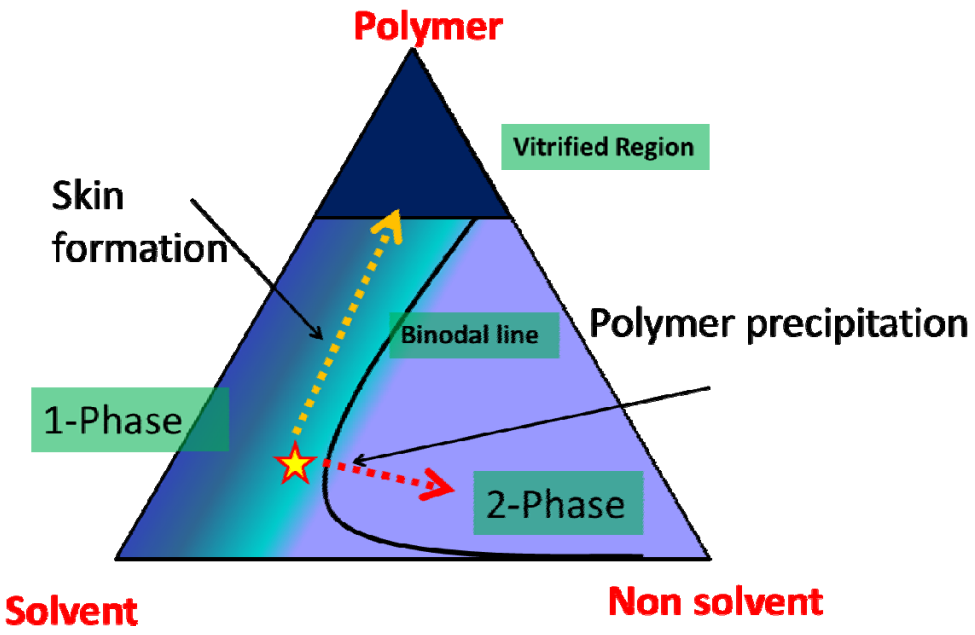

Figure 2.5: Model ternary phase diagram showing the single-phase region marked with a star and transitions into the vitrified region and into the two-phase region. Vitrification occurs as the non-solvent evaporates in the air gap causing the polymer to form a dense, solid skin. As the fiber enters the quench bath, non-solvent diffuses into the dope, causing it to transition across the binodal line and the polymer to precipitate.

For fiber sorbents, the transition marked by the red arrow is the more relevant one. Here, the non-solvent ingress into the dope causes the dope composition to traverse the binodal line. The binodal line separates the one-phase region from the 2-phase region (often passing through a metastable region bound by a spinodal line). As this happens, the system de-mixes into a polymer-rich solid phase and a solvent-non-solvent-rich phase which slowly diffuses out of the fiber as it is wound on the take-up drum.

While deciding on the dope composition, it is important to make the dope close enough to the binodal line that it phase separates while in the quench bath but not

so close that premature polymer precipitation becomes a risk. A convenient practice is to set the non-solvent concentration at 1% below the binodal concentration so that a 1% increase then causes phase separation. The sorbent can be ignored in the phase diagram development if it can be made to act as passive filler.

2.4 Barrier Layer Deposition on Fiber sorbents

There are two ways in which barrier layers may be deposited on fiber sorbents. A barrier material in solution may be **co-extruded** with the fiber sorbent as it is being spun, forming an inner dense layer as the fiber sorbent itself phase-separates. Alternatively, a polymeric barrier may be deposited via **post-treatment** after the fiber has been spun and dried.

2.4.1 Barrier Layer via Co-extrusion

Co-extruded barriers are advantageous in that they can be prepared in-situ and avoid an extra step in the fiber preparation process. However, a face-sealing step is still required to avoid barrier bypass. Additionally, co-extrusion can be a difficult process to optimize and scale up, and a part of the barrier layer is usually porous, adding thermal mass to the fiber without additional sorption capacity. The barrier polymer has to be chosen so that it adheres well to the polymer comprising the fiber sorbent layer.

The spinning process to make co-extruded barriers requires an additional dope pump and the use of a dual-layer spinneret that would enable a barrier dope to be extruded concentrically with the bore fluid and sorbent dope.

To make a barrier using this method, it is not enough to just select a suitable polymer solution. A co-extruded barrier can only be formed as a dense glassy layer on the inner fiber wall. In essence, a dense skin has to be laid on the inside of the fiber, rather than on the outside, as would be done in the case of membrane production. To do this, the bore fluid cannot remain neutral to phase separation in the fiber. Instead, it has to be modified to encourage "internal vitrification" of the polymer. In a membrane spin, the air around the dope jet acts as an extractive medium, removing the solvent and non-solvent via evaporation, thereby causing vitrification of the skin. An attempt was made to spin Torlon® fibers with nitrogen as the bore fluid to encourage internal skin formation via evaporation into the bore. This process can be mimicked by adding a liquid polymer in the bore fluid that would remove the solvent and non-solvent from the dope and cause vitrification on the internal fiber wall. Poly(propylene glycol), or PPG has been proven to be such a polymer in prior research [41] producing "micropillows" with dense skins .

Using such an extractive medium in the bore fluid enables internal skin formation. Simultaneously, phase separation and pore formation occur from the outer surface and propagate inwards as the fiber passes through the quench bath. The process is halted at the internal vitrified layer, where the solvent and non-solvent have been leached

out already. Figure 2.6 illustrates the diffusion processes causing internal vitrification and pore formation in the quench bath.

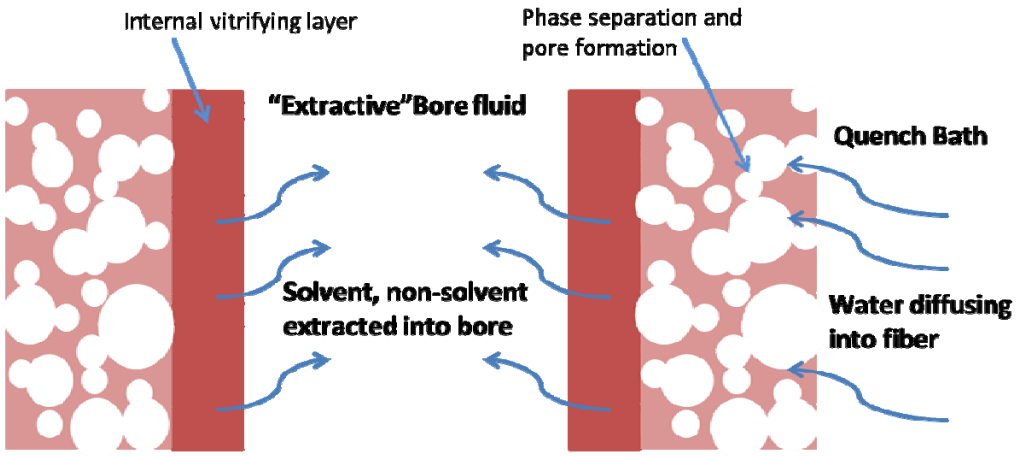

Figure 2.6: Longitudinal cross-section of fiber sorbent co-extruded with an internal dense barrier. The central bore fluid extracts the liquid components from the dope even as phase separation sets in from the quench bath. The resultant porous fiber thus has an internal dense layer that acts as a barrier to mass transfer.

Once the fibers are spooled on the take-up drum, the bore fluid is allowed to diffuse out of the fiber along with the rest of the products of phase separation. The phase separation and solvent exchange processes may have to be modified to account for the dense internal layer retarding the leaching occurring during these processes.

2.4.2 Barrier Layer via Post-treatment

Co-extrusion eliminates a processing step in creating hollow fibers with barriers but significant spinning skill is required to achieve defect-free co-extruded barriers. Post-treatment is the term used to describe any procedure to form an internal barrier layer after the fiber sorbent has been spun, solvent-exchanged and dried.

Typically, a polymer-containing solution or emulsion is flowed through[42] the fiber bore, after which the bore is cleared and remaining film of liquid is allowed to dry, leaving behind a dense barrier layer.

Post-treatment permits any suitable barrier to be cast after the fibers have been potted in the RTSA module. This allows flexibility in choosing the barrier material since there is no need for the barrier polymer to be miscible with the support polymer. Instead, adherence is achieved as the barrier-forming fluid partially penetrates the porous fiber matrix and forms an interlocking barrier-fiber interface. An additional advantage is that the barrier deposition step seals the fiber end faces, avoiding lumen layer bypass. Co-extruded barriers require an additional face-sealing step, somewhat negating their advantage as a single step process. An added advantage is that post-treatment allows deposition of more than one barrier layer, and a series of different steps may be used to improve barrier performance.

Post-treatment processes to deposit polymeric barriers may be split into solution-based processes and emulsion-, or suspension-based processes. The first involves coating the lumen wall of potted fibers with the barrier polymer in solution and allowing the solution to evaporate, leaving a vitrified barrier. Alternatively, sub-micron particles of polymer may be suspended in an aqueous medium and deposited on the lumen wall, followed by drying and agglomeration to form the barrier.

2.4.2.1 Post-Treatment via Emulsion Casting

Emulsion casting using Neoprene® and polyvinylidene dichloride (PVDC) latex has been proven to be an effective way to deposit an internal barrier on the lumen [43]. Emulsions of rubbery polymers are flowed into the potted fiber module; after the bore is cleared out, the polymer particles or micelles remaining on the wall fuse together as they dry, forming a cohesive layer [42]. This is a straightforward step for rubbery polymers where polymer chains interdiffuse easily. Polymers with high glass transition temperatures or semicrystalline natures such as PTFE cannot be readily cast in this manner even if they are excellent barriers and are available in emulsion form. The polymer particles have to be heated above the crystalline melting point [44] in order to sinter into a cohesive layer and if laid too thickly, form "mudcrack" defects [45] that cannot be sealed by sintering.

An important advantage of emulsion post-treatment is that emulsions typically have much lower viscosity than polymer solutions of similar mass loading [46]. Lowered viscosity hugely reduces the chances of fiber blockage during post-treatment. This offers a significant advantage when it comes to multi-fiber coating and in establishing the repeatability and scale-up feasibility of post-treatment as a barrier establishment.

2.4.2.2 Post-Treatment via Solution Casting

Solution casting involves casting followed by evaporation of a polymer solution on the lumen wall. This process is very similar to emulsion casting and conceptually simpler in that the barrier layer is formed via simple solvent evaporation. Whereas the dispersion casting method is limited in its choice of rubbery polymers, solution casting may use any suitable barrier polymer. However, it is essential that the polymer be easily soluble in a solvent that does not also dissolve or swell the polymer constituting the pore network, as this would cause collapse of the entire fiber.

The barrier polymer is required to have low gas permeance and the supporting polymer is required to have good thermal and mechanical properties. In laboratory experience, the pursuit of these goals results in both polymers being soluble in only a few, similar aprotic solvents [47]. Hence the choice of solvent often limits the polymer combinations available to be solution-cast as a barrier. In addition, the post-treatment solutions are orders of magnitude more viscous than emulsions or suspensions. Higher viscosities result in greater pressure drops during post-treatment and make the fibers more susceptible to failure or blockage. These issues underline the need to select a post-treatment solution that minimizes fiber blockage while resulting in a durable lumen layer.

2.5 Summary

In a hollow fiber RTSA system, cost efficiency ultimately relies on three phenomena. The first is the unhindered passage of the sorbing gas component to the sorbent and subsequently back out of it. Different types of diffusion processes come into play to order to effect this. Secondly, the sorbent material in the fiber has to preferentially adsorb CO_2 but at low heats of sorption to reduce the material costs and energy consumption, respectively. The final requirement is an effective barrier between the fiber lumen and the gas interacting with the sorbent layer. These phenomena are controlled by the selection of materials for each fiber component and their methods of fabrication.

Sections 2.1-2.2 of this chapter lay out the microscopic processes underlying the operation of an efficient hollow fiber sorbent and the features of the fiber that control them. The theory behind experiments to quantify them is also discussed. Sections 2.3-2.4 describe the fabrication processes necessary to install the three components of a fiber sorbent (as defined in Section 1.3.1) in order to optimize those fiber characteristics discussed in the previous sections.

2.6 References

1. Lively, R.P., *Hollow fiber sorbents for post-combustion CO_2 capture, PhD Dissertation*, 2011, Georgia Institute of Technology.

2. Bhandari, D.A., *Hollow fiber sorbents for the desulfurization of pipeline natural gas, PhD Dissertation*, 2010, Georgia Institute of Technology.

3. Husain, S., *Mixed matrix dual layer hollow fiber membranes for natural gas separation, PhD Dissertation*, 2006, Georgia Institute of Technology.

4. Treybal, R.E., *Mass-transfer operations*. Vol. 3. 1980: McGraw-Hill New York.

5. McCabe, W.L., J.C. Smith, and P. Harriott, *Unit operations of chemical engineering*. Vol. 5. 1956: McGraw-Hill New York.

6. Mulder, M., *Basic Principles of Membrane Technology Second Edition*1996: Kluwer Academic Pub.

7. Yampolskii, Y., *Polymeric Gas Separation Membranes.* Macromolecules, 2012. **45**(8): p. 3298-3311.

8. Koros, W., et al., *Polymeric gas separation membranes.* Paul, DR, Yampolskii, YP, Eds, 1994.

9. Baker, R., *Membrane Technology and Applications,* 2004: Wiley.

10. Rosen, S.L. and C.S. Brazel, *Fundamental Principles of Polymeric Materials,* 2012: Wiley.

11. Michaels, A.S., W.R. Vieth, and J.A. Barrie, *Diffusion of gases in polyethylene terephthalate.* Journal of Applied Physics, 1963. **34**(1): p. 13-20.

12. Ghosal, K. and B.D. Freeman, *Gas separation using polymer membranes: an overview.* Polymers for Advanced Technologies, 1994. **5**(11): p. 673-697.

13. Kosuri, M.R., *Polymeric membranes for super critical carbon dioxide (scCO$_2$) separations.* 2009.

14. Mason, E.A. and A. Malinauskas, *Gas transport in porous media: the dusty-gas model*. Vol. 17. 1983: Elsevier Amsterdam.

15. Burggraaf, A.J. and L. Cot, *Fundamentals of inorganic membrane science and technology*. Vol. 4. 1996: Elsevier Science.

16. Bond, F.C., *The third theory of comminution.* Trans. AIME, 1952. **193**(2): p. 484-494.

17. Ahn, H., et al., *Diffusion mechanism of carbon dioxide in zeolite 4A and CaX pellets.* Adsorption, 2004. **10**(2): p. 111-128.

18. Lowell, S., et al., *Characterization of porous solids and powders: surface area, pore size and density*. Vol. 16. 2006: Springer.

19. Denoyel, R., et al., *Assessment of the surface area and microporosity of activated charcoals from immersion calorimetry and nitrogen adsorption data.* Langmuir, 1993. **9**(2): p. 515-518.

20. Singh, D., et al., *Techno-economic study of CO_2 capture from an existing coal-fired power plant: MEA scrubbing vs. O_2/CO_2 recycle combustion.* Energy Conversion and Management, 2003. **44**(19): p. 3073-3091.

21. Sing, K.S., *The use of physisorption for the characterization of microporous carbons.* Carbon, 1989. **27**(1): p. 5-11.

22. Do Duong, D., *Adsorption Analysis: Equilibria and Kinetics*1998: Imperial College Press.

23. Carman, P. and F. Raal, *Diffusion and flow of gases and vapours through micropores. III. Surface diffusion coefficients and activation energies.* Proceedings of the Royal Society of London. Series A. Mathematical and Physical Sciences, 1951. **209**(1096): p. 38-58.

24. Burggraaf, A.J., *Single gas permeation of thin zeolite (MFI) membranes: theory and analysis of experimental observations.* Journal of Membrane Science, 1999. **155**(1): p. 45-65.

25. Benesi, H., *Relationship between catalytic activity and nature of acidity of the crystalline zeolites, mordenite and Y faujasite.* Journal of Catalysis, 1967. **8**(4): p. 368-374.

26. Wirawan, S.K. and D. Creaser, *CO_2 adsorption on silicalite-1 and cation exchanged ZSM-5 zeolites using a step change response method.* Microporous and mesoporous materials, 2006. **91**(1): p. 196-205.

27. Chen, N., *Hydrophobic properties of zeolites.* The Journal of Physical Chemistry, 1976. **80**(1): p. 60-64.

28. Ruthven, D.M., S. Farooq, and K.S. Knaebel, *Pressure swing adsorption*1994: VCH Publishers.

29. Ridha, F.N. and P.A. Webley, *Anomalous Henry's law behavior of nitrogen and carbon dioxide adsorption on alkali-exchanged chabazite zeolites.* Separation and Purification Technology, 2009. **67**(3): p. 336-343.

30. Lu, C., et al., *Comparative study of CO_2 capture by carbon nanotubes, activated carbons, and zeolites.* Energy & Fuels, 2008. **22**(5): p. 3050-3056.

31. Serna-Guerrero, R., E. Da'na, and A. Sayari, *New insights into the interactions of CO_2 with amine-functionalized silica.* Industrial & Engineering Chemistry Research, 2008. **47**(23): p. 9406-9412.

32. Wei, J., et al., *Adsorption of carbon dioxide on organically functionalized SBA-16.* Microporous and Mesoporous Materials, 2008. **116**(1): p. 394-399.

33. Choi, S., J.H. Drese, and C.W. Jones, *Adsorbent materials for carbon dioxide capture from large anthropogenic point sources.* ChemSusChem, 2009. **2**(9): p. 796-854.

34. Lively, R.P., et al., *Hollow fiber adsorbents for CO_2 removal from flue gas.* Industrial & Engineering Chemistry Research, 2009. **48**(15): p. 7314-7324.

35. Hillock, A.M., S.J. Miller, and W.J. Koros, *Crosslinked mixed matrix membranes for the purification of natural gas: effects of sieve surface modification.* Journal of membrane science, 2008. **314**(1): p. 193-199.

36. Mahajan, R., et al., *Challenges in forming successful mixed matrix membranes with rigid polymeric materials.* Journal of Applied Polymer Science, 2002. **86**(4): p. 881-890.

37. Loeb, S. and S. Sourirajan, *Sea water demineralization by means of an osmotic membrane*1962: ACS Publications.

38. McKelvey, S.A., D.T. Clausi, and W.J. Koros, *A guide to establishing hollow fiber macroscopic properties for membrane applications.* Journal of membrane science, 1997. **124**(2): p. 223-232.

39. Park, H., et al. *Effect of solvent exchange on the morphology of asymmetric membranes*. in *ACS Symposium Series*. 2000. ACS Publications.

40. Van de Witte, P., et al., *Phase separation processes in polymer solutions in relation to membrane formation.* Journal of membrane science, 1996. **117**(1): p. 1-31.

41. Shan Wickramanayake, W., et al., *Fabrication of hollow, spherical polymeric "micropillows" using a dual layer spinneret.* Journal of Applied Polymer Science, 2011. **121**(5): p. 2835-2842.

42. Lively, R.P., et al., *Formation of defect-free latex films on porous fiber supports.* ACS applied materials & interfaces, 2011. **3**(9): p. 3568-3582.

43. Li, F.S., et al., *Aminosilane-Functionalized Hollow Fiber Sorbents for Post-Combustion CO_2 Capture.* Industrial & Engineering Chemistry Research, 2013.

44. Trimble, D.C., *Method of molding teflon*, 1966, US Patent 3235636, filed Aug 27, 1963, and issued Feb 15, 1966.

45. Lontz, J.F. and W.B. Happoldt, *Teflon Tetrafluoroethylene Resin Dispersion: A New Aqueous Colloidal Dispersion of Polytetrafluoroethylene.* Industrial & Engineering Chemistry, 1952. **44**(8): p. 1800-1805.

46. Srinivasan, C., et al., *Non-Aqueous Suspensions of Antibodies are Much Less Viscous Than Equally Concentrated Aqueous Solutions.* Pharmaceutical Research, 2013. **30**(7): p. 1749-1757.

47. Sumitomo, H. and K. Hashimoto, *Polyamides as barrier materials*, in *Polymer Membranes*, M. Gordon, Editor 1985, Springer Berlin Heidelberg. p. 63-91.

CHAPTER 3

MATERIALS AND EXPERIMENTAL METHODS

A hollow fiber sorbent comprises three functional parts: the sorbent, support matrix and the lumen barrier. Material selection for each component is critical to the performance of the system. This chapter describes the selection process as well as the procedures for performance characterization and supporting experiments.

3.1 Materials

The materials described below were chosen to fit various performance needs for hollow fiber RTSA to be a viable carbon capture technology. While the materials described in the following sub-sections were identified to meet such needs, it is desirable for them to also be commercially available in bulk for economical large-scale production of hollow fiber sorbents.

3.1.1 Polymers for the Fiber Matrix

Torlon®, a polyamide-imide, was chosen as the matrix polymer based on its superior mechanical and spinning properties. It is a widely available engineering polymer with a high reported glass transition temperature of 275 °C and good resistance to creep [1]. Both of these properties are essential for a polymer to withstand repeated thermal cycling and pulsed flow of gas and liquid which occur during RTSA operation.

Specifically, Torlon® 4000T-HV supplied by Solvay Specialty Polymers (Alpharetta, GA) was used owing to its higher molecular weight and good spinnability in a sorbent-filled dope. Torlon® is a random co-polymer made from monomers trimellitic anhydride chloride (TMAC), *m*-phenylenediamine (*m*-PDA) and 4,4′-oxydianiline (ODA) [2] with the following structure.

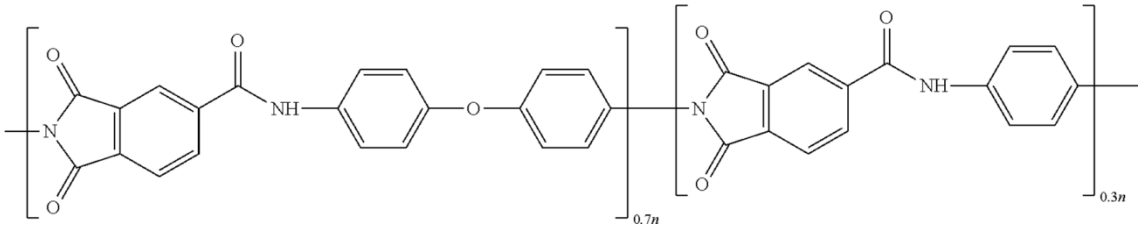

Figure 3.1: Repeating unit of Torlon® showing amide and imide linkages

In addition to Torlon®, a pore-forming polymer was used while making the spin dope. The pore-former is a solvent- and non-solvent-soluble polymer that enhances nucleation in the phase-separating fiber and suppresses macrovoid formation, thereby enhancing fiber morphology in more than one way [3, 4]. As the fiber completes phase separation, the soluble pore-former leaches out into the non-solvent (water) bath, leaving an open-porous fiber behind.

Polyvinylpyrrolidone (PVP) (Mw ~55,000, Sigma Aldrich) was used as the pore-former. It is a benign, water-soluble polymer that has been shown to enhance fiber porosity and improve transport rates [5]. PVP molecular structure is shown in the following figure.

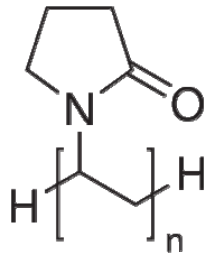

Figure 3.2: PVP molecular structure.

Prior to dope formulation, both PVP and Torlon® were dried overnight under vacuum at 110 °C to remove sorbed moisture.

3.1.2 Sorbent Materials:

Initially, fiber sorbents were spun using Zeolite 13X (powder, ~ 2 μm avg. part. sizes, Sigma-Aldrich) as the sorbent. Dry 13X has an excellent CO_2 capacity; however it completely loses this in the presence of moisture [6]. In any case, 13X was used throughout this project as a stand-in for more expensive or hard-to-obtain sorbents. The spinning techniques were optimized using a Torlon®/13X-based dope and eventually modified for other sorbents, thereby reducing the chance that they would be wasted. This practice was supported by eventual spinning experience where it was realized that sorbents of the same class (zeolites, silicas etc.) could be substituted for each other with few complications arising during spinning.

Another sorbent attribute that was not initially considered, but grew to be important as the project progressed, was its availability in batches >100 g. There exist a wide range of possible solid sorbents for CO_2 capture [7], but some of these are still only

easily synthesized at batch sizes of a few grams at a time. This work focuses on spinning fiber sorbents at the lab scale, which typically requires a minimum of 50 g of sorbent to achieve fibers with 75% sorbent loading by weight. Sorbent synthesis was not considered to be within the scope of the project, and therefore sorbents selected were either available commercially or could be synthesized in larger batches.

The other zeolite framework type considered for this research is the MFI type material ZSM-5. ZSM-5 is a low-alumina zeolite [8] that can be synthesized at a wide range of SiO_2/Al_2O_3 ratios. In particular, it can be synthesized in a pure-silica form called Silicalite-1 that has been proven to yield CO_2 sorption capacity even in wet feeds [9, 10]. This form can be readily synthesized in the lab [11] but requires an aluminum-free precursor and hence is comparatively expensive; nevertheless, MFI zeolites with very high SiO_2/Al_2O_3 ratios are readily available commercially. Our samples were sourced from ExxonMobil and were characterized via SEM imaging and sorption experiments.

ZSM-5 has the crystal structure shown in Figure 3.3 with a 3-dimensional channel network consisting of straight channels along the [010] axis and a sinusoidal channel along a perpendicular [100] axis [12]. The combination of these channels allows gas transport in 3 directions with the [100] channel being smaller at $5.1\text{Å} \times 5.5\text{Å}$ [13]. Hence, CO_2 and N_2, both smaller than the channel dimensions [14] can diffuse readily through the sorbent particles.

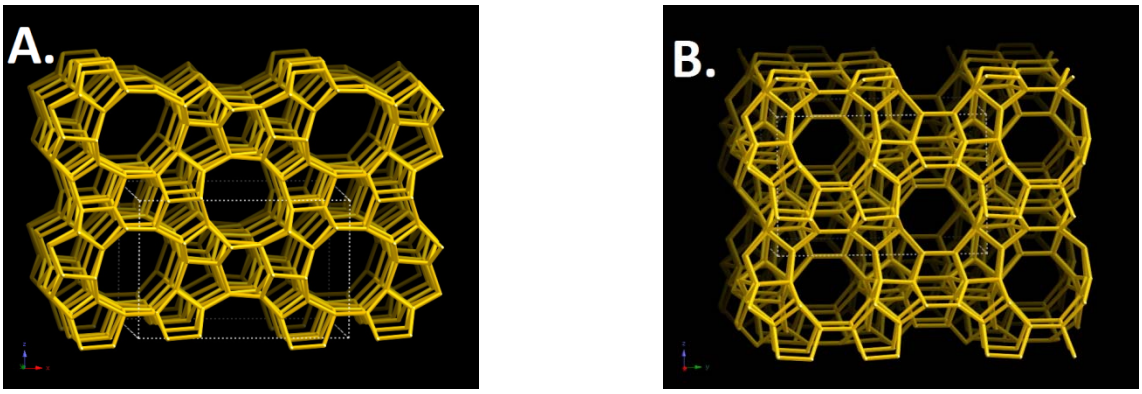

Figure 3.3: MFI framework showing A. the straight channels along [010] and B. the sinusoidal channels viewed along [100]. The two intersecting channels formed by 10-atom rings allow gas transport in 3 dimensions [13].

3.1.3 Barrier Polymers

A number of barrier candidates were tested in this research with varying degrees of success. These include polymer suspensions and neat polymers that could be solution-cast. Polyacrylonitrile (PAN) was one polymer used, owing to its good barrier properties and its solubility in solvents that do not dissolve Torlon®; thereby enabling barrier formation through post-spin solution casting.

PAN is a highly ordered quasi-crystalline polymer that is extensively used for carbon fiber manufacture [15, 16]. It has good film-forming properties and a passable T_g of 95 °C [15]. Though often synthesized as a co-polymer, the main monomer is acrylonitrile, and the homopolymer form is commercially available. An advantage of using PAN is that it undergoes a process called *stabilization* on heating, which can help fortify the cast barrier. On heating between 125°C and 230°C, it forms an insoluble,

infusible cross-lined “ladder” polymer [17, 18] which enhances barrier cohesiveness and introduces the possibility of multiple-layer barrier casting .

The molecular structure of PAN and the stabilization process are illustrated below.

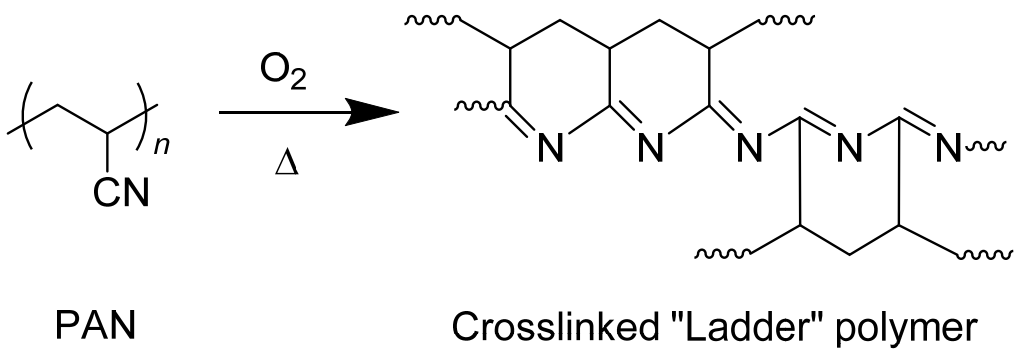

Figure 3.2: Stabilization reaction of PAN in the presence of oxygen at temperatures between 125°C and 230°C, showing one of several possible crosslink mechanisms. The reaction insolubilizes and colorizes the PAN.

Different commercial polymer suspensions were also used to form lumen layers, with varying results. Polytetrafluoroethylene (PTFE) is a good barrier with high melting point (345 °C) and is insoluble in any solvent below this temperature [19]. It can be continuously operated at temperatures up to 290 °C [20]. For barrier formation, it can only be used in the aqueous suspension form (60 wt. % dispersion in H_2O, Sigma-Aldrich).

Similarly, polyolefins such as polyethylene and polypropylene are good hydrophobic barriers but can only be melt-processed due to their non-polar natures. Melt-

casting of barriers is impracticable for hollow fibers because of the high viscosity of polymer melts. However, HDPE-paraffin wax emulsions are commercially available as aqueous suspensions from BYK Additives and Instruments. In this work, a ~30 wt. % HDPE suspension (EMULSION 286, BYK Additives and Instruments) was used as a barrier-forming reagent. Like PVDC and Neoprene®, polyethylene has a very low glass transition temperature (-128.15 °C) [21] which has positive implications for heat sealing of defective barriers.

3.1.4 Solvents

Fiber spinning and barrier layer formation required several solvents and non-solvents. N-methyl-2-pyrrolidone (NMP) (anhydrous, 99.5%, Sigma-Aldrich) was used as the solvent for fiber spinning. Methanol (anhydrous, 99.8%, Sigma-Aldrich) and hexane (anhydrous, 95%, Sigma-Aldrich) were used for solvent exchanging the spun fibers. Tetrahydrofuran (THF) (anhydrous, 99.9%, Sigma-Aldrich) was used in some experiments to encourage Torlon® skin formation. Ethylene carbonate (EC) (98%, Aldrich) and propylene carbonate (PC) (anhydrous, 99.7%, Sigma-Aldrich) were used as solvents for PAN. In addition, Poly(ethylene glycol) (PEG) (average M_n 400, Aldrich) and Poly(propylene glycol) (average M_n ~725, Aldrich) were used as bore fluid additives for co-extrusion of barrier layer with the fiber.

3.1.5 Gases

Oxygen (O_2), nitrogen (N_2), carbon dioxide (CO_2) and Helium (He) gas were used to measure fiber sorbent permeance. In addition, nitrogen was also used to dry post-treated fiber sorbents. Gas mixtures (10 mol% CO_2/ 90 mole% N_2, 10 mol% CO_2/ 10 mol% He/ 90 mole% N_2) were used for thermogravimetric analysis and mass spectrometry. All the gases were obtained from Air Gas.

3.2 Hollow Fiber Preparation

3.2.1 Construction of ternary phase diagram via Cloud Point Technique

The ternary phase diagram serves as a useful reference document that allows methodical alteration of the dope composition for a given polymer/solvent/non-solvent mixture to achieve optimal fiber properties. Whenever a new ternary system is encountered, the ideal spin dope composition needs to be determined. Without the ternary diagram, selecting the best-performing dope composition would be through trial-and-error: a material- and resource-intensive procedure.

As explained in Section 2.3.3, the dope composition is made to be close to the binodal, and the ternary phase diagram indicates the position of the two-phase point at different polymer compositions. Usually, only a portion of the binodal curve has to be made, comprising polymer concentrations those are of interest for fiber spinning or film casting. The viscosity of the polymer solution is an important factor in defining this

region of interest [22]. Fiber sorbent dopes usually contain less than 30% by weight of polymer in the "neat dope", which further decreases on addition of the sorbent. Similarly, the non-solvent concentration has a limited region of interest, namely, the narrow zone in which the dope transitions from a single phase to two discrete phases. The following illustration shows the sub-section of the ternary phase diagram that is of interest for fiber spinning.

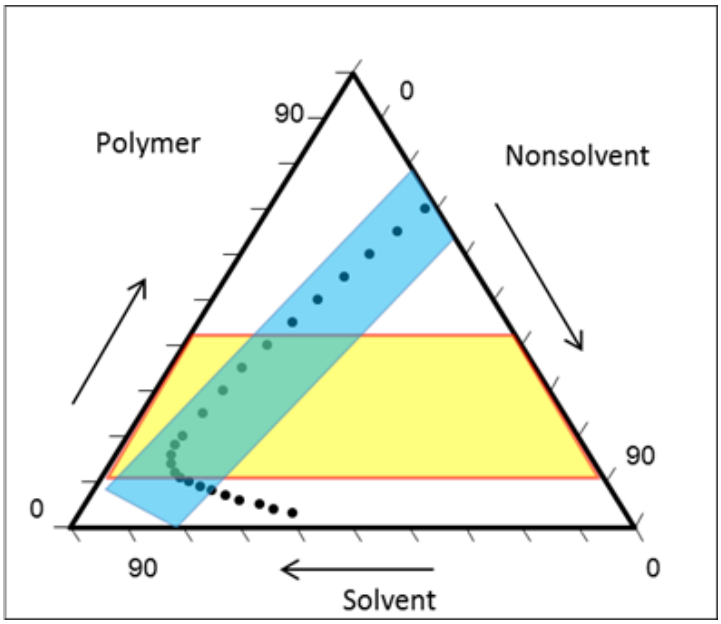

Figure 3.3: Model ternary phase diagram showing the region of interest for fiber sorbent dope formulation. The yellow region represents the polymer concentrations that yield dopes of acceptable viscosity. The blue region represents the area in which the non-solvent concentration becomes important, i.e. causes phase separation. Therefore, the region where the yellow and blue patches overlap is the portion of the phase diagram that is actually constructed. The three axes are parallel to the grid marks shown outside the diagram with the arrows pointing in the ascending direction of each axis.

The cloud point technique is used to construct the binodal curve shown in the figure above. This method involves mixing sample dopes, usually less than 10 g, and noting whether the completely dispersed mixture is a single-phase solution, a two-phase

mixture with clearly undissolved polymer, or a translucent “cloudy” mixture indicating the threshold of phase separation. It is important to keep the samples tightly closed and to ensure that they are thoroughly mixed. The temperature is noted as well, since the binodal curve is extremely temperature-sensitive.

One way to obtain cloud points at different polymer concentrations is to prepare a polymer solution within the desired polymer concentration range and add incremental amounts of non-solvent, followed by thorough mixing. This is continued till the point where the polymer does not dissolve, which is determined to be the “cloud point” [3]. The experiment is repeated for different polymer concentrations. This can be a laborious process because adding small amounts of non-solvent always causes local polymer precipitation even when the overall composition occurs in the single-phase region. Re-dissolution of the precipitated polymer can be time-consuming for small samples, since small sample jars restrict dope movement and dissolution.

In this work, a number of samples of varying polymer and non-solvent concentrations are prepared and allowed to mix completely on a rolling mixer. The mixed samples are then visually examined to determine at what non-solvent concentration phase separation sets in for each polymer concentration. This is a superior method since the one-phase and two-phase samples can be compared side-by-side to accurately define the phase-separation point. It is also less time-consuming since the polymer and non-solvent concentration increments are initially chosen to be very large, resulting in fewer samples. Once the rough position of the binodal is determined, the increments are made smaller in

that region till finally, the binodal line is determined at polymer and non-solvent increments smaller than 1 wt. %.

While the binodal can be constructed ignoring the sorbent, which is later added in as passive filler, it does have to include the pore-former which strongly affects the position of the binodal curve. Considering the pore-former as a fourth component requires a 3-dimensional ternary diagram. This may be circumvented by setting a fixed polymer to pore-former ratio and considering them a single component. In this work, a 4:1 ratio of polymer to pore-former was set and found to yield acceptable pore structure.

3.2.2 Sorbent Dope Preparation

Once the binodal has been constructed, it can be used to determine a suitable dope composition sans the sorbent. The sorbent content is then calculated based on the desired sorbent loading in the spun and dried fibers. In this work, the fibers were targeted to contain 75% by weight of sorbent when dry. To achieve this level, the spin dope composition needed to contain roughly 3 times as much sorbent as Torlon®. The remaining components; NMP (solvent), water (non-solvent) and PVP (pore-former) are then adjusted to remain in proportion to the Torlon®. As an example, if the ideal composition via the ternary diagram were determined to be 16% Torlon®/ 4% PVP/ 72% NMP/ 8% water, the spin dope would contain 10.8% Torlon®/ 2.7% PVP/ 48.6% NMP/ 5.4% water/ 32.4% sorbent.

In this research, sorbent dopes are made in sizes 100 g - 500 g. Dope sizes are determined based on the amount of sorbent available, number of fibers required to be produced and whether the spin is "unproven" or "established". "Unproven" spin dopes are usually made in larger quantity because of the expected dope wastage during spin parameter optimization.

Pure polymer dopes for membrane spinning can be mixed in sealed jars on a heated roller within days to weeks, but sorbent dopes require the sorbent to be dispersed finely and cannot be mixed on a roller. A special procedure involving a *prime dope* and *dispersion solution* has been developed to prepare sorbent dopes [10].

A week before the dope preparation, the dried sorbent is placed in a moisture saturation chamber with some water to saturate the pores and turn the sorbent into passive filler. Concurrently, the Torlon® and PVP are dried overnight under vacuum at 110 °C. Once the polymers are dried and cooled to room temperature, 20% by wt. of the total required Torlon®, PVP, NMP and water are mixed in a suitably sized jar with a PTFE-lined lid and placed on a heated roller till the polymer dissolves to form the *prime dope*. This is usually achieved in a few days. Since there is wastage while transferring the solution to the final dope jar, more prime dope is prepared than will eventually be used.

Once the prime dope is ready for use, the remaining solvent and non-solvent (80% by weight of the total NMP and water and all of the required sorbent) are placed in a different glass jar (usually 1 liter capacity) to prepare the *dispersion solution*. The sorbent from the moisture saturation chamber is added in. The dispersion solution

requires completely suspending sorbent particles in the above-mentioned NMP-water mixture. This is achieved via sonication, wherein a sonication horn (Model: 20A1000 ULTRA 1000 AUTO-TRAC, manufactured by Dukane, St. Charles, IL) is immersed in the sorbent/NMP/water mixture and operated for three 1-minute cycles with 30-second gaps between cycles. This allows for complete dispersion of the sorbent, but the sorbent will settle if allowed to stand. Quickly, the prime dope (containing 20% of the total Torlon®, PVP, NMP and water) is weighed into the dispersion solution and sonicated for two more cycles. The sonicated mixture is now both well-dispersed and resistant to gravity settling.

The remaining Torlon® and PVP (80% of the total required) are then added to the sonicated mixture and set on a hot plate maintained at 60 °C. It is stirred by means of an anchor impeller (Model 409 Heavy Duty Mixer, Troemner) at high shear rates (100-200 rpm depending on dope viscosity) till the polymer dissolves completely. This may take 4 hours or longer. Evaporation during this time is minimized by closing the jar with a lid provided with a hole for the impeller to pass through.

3.2.3 Preparation of other dopes and polymer solutions

Pure polymer solutions for co-extruding lumen barriers and for fiber post-treatment are prepared in a straightforward way by mixing the requisite components in a glass jar, sealing it with a PTFE-lined lid and rolling the jar on a heated roller till the polymer dissolves and a transparent solution is obtained. The sorbent dope as prepared in the Section 3.2.2 may also be left overnight on the roller to remove air bubbles

(degassing) introduced during high-shear mixing. Further degassing is achieved by loading the dopes into the pumps and leaving them standing overnight.

3.2.4 Fiber Spinning and Solvent Exchange:

The spin dope thus prepared is loaded into a previously cleaned 1 liter syringe pump (Teledyne ISCO, Lincoln, NE). Another pump is filled with the bore fluid and the outlets are connected to the corresponding spinneret fittings. The fibers are spun and solvent-exchanged as described in Section 2.3. For dual-layer fiber spins, the barrier dope has to be added concentrically to the sorbent dope on its inner surface. In this case, spinnerets with three channels are used. The innermost channel is called the bore needle where the bore fluid is pumped. The channel surrounding the bore needle is called the core dope channel and the outermost channel is the sheath dope channel. The core needle maybe recessed in order to off-set “die swell” [23], an expansion of the extruded dope jet as it exits the core channel.

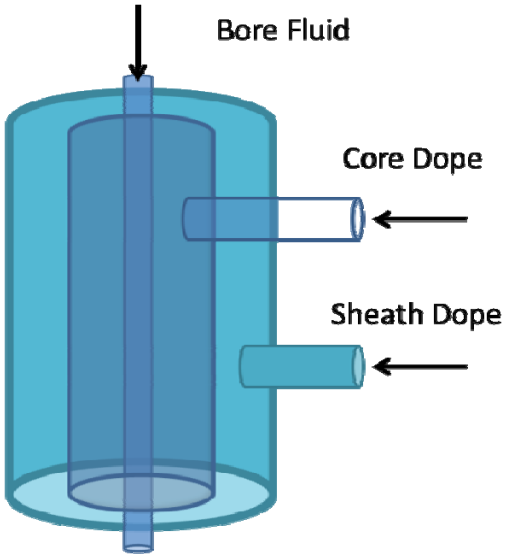

Figure 3.4: Schematic of a dual-layer spinneret showing bore fluid, core and sheath dope channels. The core and sheath dopes enter the spinneret laterally but are extruded concentric to the bore fluid.

Once the fibers are spun, they are allowed to phase-separate on the take-up drum for 15-30 minutes, after which they are cut and transferred to a trough of water for 3 days, with the water being changed each day. Following this, they are transferred to a 1-liter measuring jar and the jar is filled with methanol, and the methanol is replaced every 20 minutes. After an hour (3 methanol batches), the procedure is repeated with hexane (1 hour, 3 batches of hexane). The fibers are taken out, air-dried and then dried overnight in a vacuum oven at 110 °C. They can now be used for testing and module construction.

3.2.5 Syringe Extrusion of Solid Fibers:

When investigating a new dope composition or sorbent material, it is not always prudent or feasible to prepare a spin dope and attempt a full-scale hollow fiber spin. Instead, small dopes (≈ 10 g) may be prepared and extruded through a plastic syringe (Becton, Dickinson and Company, NJ) into a 1L beaker filled with de-ionized (DI) water at the planned quench bath temperature. The mock spin thus performed helps to confirm dope spinnability and produces solid fibers whose sorption characteristics may be measured via TGA or packed bed sorption. Additionally, they can be analyzed via SEM to study if a satisfactory pore structure has been achieved. The absence of a bore limits the use of syringe-extruded fibers but they provide a quick way of identifying and remedying problems that may arise during a large-scale spin, saving material and effort.

Syringe extrusion produces fibers with much larger diameters (> 1.5 mm) than spun fibers but this can be corrected by applying force intermittently on the syringe. This causes a pulsed flow of the dope, where a drop of the dope leaves the syringe drawing out a long “tail” of reduced diameter. This section of the extruded fiber typically has more dimensions better resembling hollow fibers. For purposes of extrusion, solid fibers are considered analogous to hollow fibers with walls half as thick as the diameter as solid fibers. Once sufficient fiber has been extruded, the phase separation and solvent exchange are performed the same way as for hollow fibers.

3.3 Barrier Layer Formation via Post-treatment

Before characterization or post-treatment, the solvent-exchanged and dried fibers are potted in brass or SS modules that yield a shell-and-tube configuration [24]. This establishes a bore side and a shell side wherein fluids can then be pumped through the bore and allowed to diffuse to the shell side for fiber permeability characterization. Alternatively, liquids for post-treatment can be flowed through the fiber bore; the bore is swept clean and then dried in order to establish an internal barrier.

3.3.1 Fiber Post-treatment Process:

The post-treatment process to establish an internal barrier on fiber modules involves the fiber modules connected vertically to the downstream port of a 3-way valve supported on a metal frame. One of the upstream ports is connected to the discharge line of an ISCO pump, and the other to a nitrogen cylinder set at a low pressure, usually, 5-15 psig. The module is made without compression fittings and is attached to the 3-way valve via Ultra-Torr fittings from Swagelok (Solon, OH) which can withstand repeated disconnects [25].

Post-treatment experiments require slight modifications depending on the type of solution or suspension used. The method to coat the fiber lumen with PVDC has been previously described [26] . When ethylene carbonate (EC) is used as solvent, the entire feed system including the pump barrel, pump discharge line, 3-way valve and fiber

module are wrapped in heating tape and maintained at 50 °C since EC freezes at 37 °C. The setup below in Figure 3.5 is for PAN-EC solution casting.

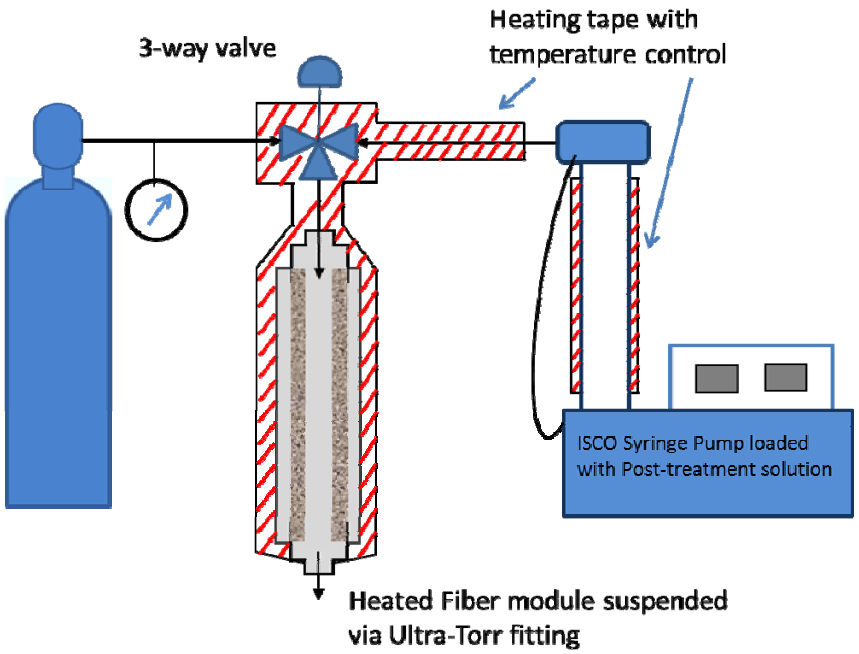

Figure 3.5: Experimental setup for PAN-EC solution-cast lumen barrier. The fiber module is suspended from a 3-way valve and heated PAN-EC solution is flowed through the fiber bore, following which nitrogen gas is used to clear the bore and then dry the PAN film left behind on the lumen wall.

The post-treatment solution, typically 5-12 wt. % PAN in EC, is loaded into the warmed pump barrel. The solution flow path from the pump to the module is kept at 50 °C and the solution is run through the module at 30 ml/hr.

While the PAN solution is being pumped through the modules, a sudden increase in the pump pressure may occur, which indicates fiber blockage. This can sometimes be resolved by stopping the pump and waiting for blockage to clear itself. If this does not occur, the 3-way valve may be switched to nitrogen flow, and the pressure is

slowly increased till the blockage is cleared. Fibers in this work were found to withstand up to 180 psig pressure under such conditions before failure occurred. Fiber blockages were typically due to particulates in the PAN solution obtained commercially or due to residue in the improperly cleaned syringe pump. Once these sources were identified, instances of blockage were reduced dramatically.

If there are no blocks, the PAN is pumped through the fiber till it appears at the downstream end of the module. After this point, the flow is continued for 1 minute, at the end of which the pump is stopped, and the valve is switched to nitrogen. The nitrogen flow is typically started off at 20 psig at the cylinder. It is important to maintain a low nitrogen pressure because at high pressures, the nitrogen diffuses sideways into the fiber wall instead of pushing out the PAN solution through the bore, thereby causing a perforated barrier layer to be formed. To further avoid this, the shell side fittings are kept capped to restrict the gas and solution flow to the bore side. As the nitrogen displaces the PAN solution in the fiber bore, the solution will flow out till the nitrogen starts bubbling out of the downstream end of the module. The cylinder pressure is maintained at 20 psig for 5 more minutes and then lowered to 5 psig to conserve nitrogen and to increase the rate of EC evaporation by increasing the temperature of the drying lumen layer. Meanwhile the heating tape around the module is heated up to 85 °C, at which point a temperature overshoot is usually observed. Once the temperature has stabilized, it is set to 125 °C for 6 hours (or overnight for convenience) to allow complete evaporation of the EC. Since EC has a very high boiling point (260 °C), constant nitrogen flow is maintained to reduce EC partial pressure around the drying film. Since the post-treatment process can yield non-uniform coating along the fiber length and at each face of the fiber,

the module is then turned over and post-treated from the other side to yield a uniform barrier. The dried modules are cooled and are ready for further heat-treatment to induce PAN ladder formation, but usually a permeance measurement experiment is done at this stage.

3.3.2 Film Casting with PAN:

The PAN solution was also cast into films to measure PAN permeance, study film integrity and to observe PAN crosslinking. To cast the film, about 5 g of the PAN-EC solution was poured onto a level glass plate that had been pre-heated to 60 °C. It is important to keep the PAN-EC solution above the EC freezing point of 37 °C throughout the casting process. Once the solution has been poured onto the plate, the film is cast by moving a doctor knife over the solution, spreading it to uniform thickness. The film, along with the glass plate is heated to 60°C in air for 6 hours and dried overnight in a vacuum oven at 100 °C to completely remove the solvent.

3.3.3 PAN Crosslinking:

As mentioned earlier, PAN crosslinking has been reported to occur between 125 °C and 250 °C. Colorization and insolubilization have been observed on heating PAN at 180 °C for 3 hours in air. In this work, the deposited PAN barrier was stabilized by heating the fiber module for 1 hour wrapped in heating tape at 190 °C as an approximation of these conditions.

3.4 Fiber Testing Methods:

3.4.1 Permeance Measurement:

Pure gas permeance is used as a measure of the transport properties of the fiber pore structure, and also the efficacy of the barrier layer, once formed. Gas is flowed from the bore side to the shell side at a constant pressure and the gas flux is measured to study the fiber wall resistance. The shell and bore sides are physically isolated by potting the fibers in a brass or SS module as previously described in Section 3.3. The module, placed in a constant-temperature box is connected to different gases in turn. This is done by connecting one bore-side end of the module to the gas supply, capping the other end, and connecting one shell-side fitting to a bubble flow meter. For each gas, the upstream (bore side) pressure is set and allowed to equilibrate. During this time, the gas being fed on the bore side will establish a steady pressure differential across the fiber wall (more universally, this may be described as a *differential in thermodynamic activity*). A good test for completion of this process is to watch for increasing or decreasing trends in the gas flux across the fiber wall. For fiber sorbents, this takes less than 5 minutes due to the open nature of the fiber pore structure, but once the barrier has been cast, the equilibration process may take more than 30 minutes. The pressure equilibration process is illustrated in Figure 3.6.

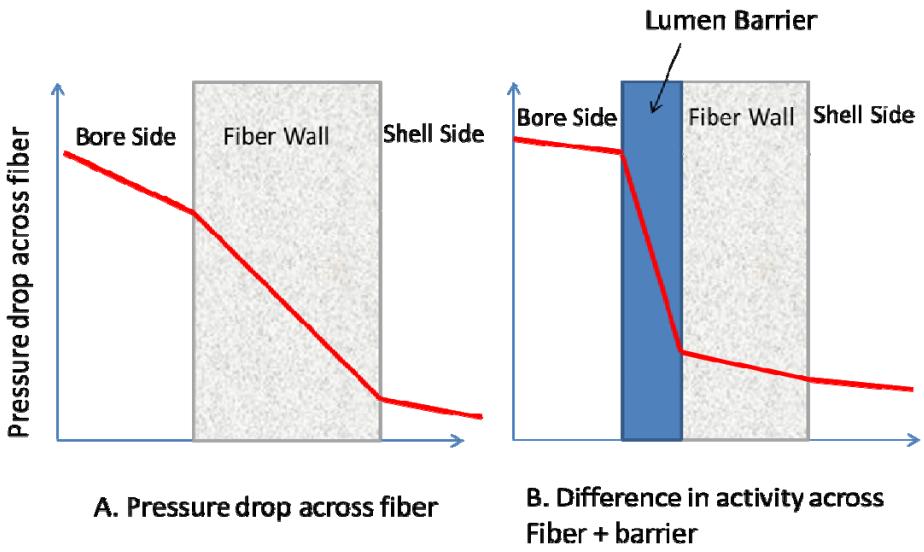

Figure 3.6: Established thermodynamic activity profiles during permeation across bare fiber sorbent wall (A.) and with lumen barrier (B.). The pressure equilibrates quickly for bare fiber since it has a low resistance to flow as shown by the very similar profiles for fiber and empty space (bore and shell side). On casting an internal barrier, a steep activity gradient is set up across the barrier, which takes longer to reach equilibrium and controls the flow across the fiber wall.

Once equilibrated, the flow across the fiber wall is measured using the bubble flow meter. Three readings are taken at each pressure, observing for upward or downward drifts which may indicate incomplete equilibration. The flux is measured at 3-5 bore side pressure values, typically between 5 to 100 psig for each gas. The downstream (shell side) is assumed to be at atmospheric pressure. In this work, the bare fiber sorbents were usually tested from 5-30 psig owing to their high permeance, and the fibers with barriers were tested up to 100 psig in order to get a measurable gas flow. There was at least some degree of overlap in upstream pressure between the two experiments so that the reduction of permeance at a given pressure on casting the internal barrier could be directly observed.

3.4.2 Dense Film Permeation:

Gas flux through dense films is best measured by arranging the film in a permeation cell in a "constant volume and variable pressure" setup. The film is mounted or "masked" between two halves of the cell so that it presents a well-defined area for permeation. The entire system is evacuated before a known amount of gas is introduced upstream of the film. The gas flux is then inferred from the pressure rise in the downstream chamber. This is a widely used method to measure diffusion coefficients in a dense film [27]. As the gas is introduced in the upstream region, there is an initial unsteady state where the introduced gas dissolves into the evacuated polymer. This is observed as a lag phase, where the downstream pressure does not increase and then increases non-linearly. As the polymer saturates, there is a linear pressure increase, from which the gas flux, and hence the permeability are calculated. The permeability for gas A, P_A is measured in Barrers as:

$$P_A = \frac{Q_A \bullet l}{\Delta p \bullet A_s}$$
$$Q_A = \frac{V_R}{R \bullet T} \bullet \left(\frac{dp}{dt} \right) \qquad (3.1)$$

Here, Q_A is the gas flow rate calculated from the downstream pressure rise $\left(\frac{dp}{dt} \right)$ (torr/s), downstream volume V_R (cc), gas constant R (J/mol.K) and temperature T (K). l is the film thickness (micron), Δp is the pressure differential across the film (Pa or psi) and A_s is the permeation area (cm^2).

3.4.3 Pressure Decay Sorption:

The equilibrium CO_2 sorption capacity for the sorbent and fiber can be measured via pressure decay sorption, previously described for polymers [28]. Here, the sorbent sample is carefully weighed and placed in a stainless steel sample cell. Powder samples are enclosed in a porous SS filter and capped with aluminum foil, both of which are carefully weighed, but fiber samples may just be packed into the sample call. The cell is connected in series to a stainless steel reservoir and then to a manifold that provides a vacuum connection, supply of sorbate gas and access to the atmosphere via a vent. The sample cell and reservoir can be isolated via needle valves and are provided with pressure transducers (Honeywell Sensing & Control, Morristown, NJ). The experimental setup, shown below, is immersed in a constant temperature oil bath provided with a circulating heater.

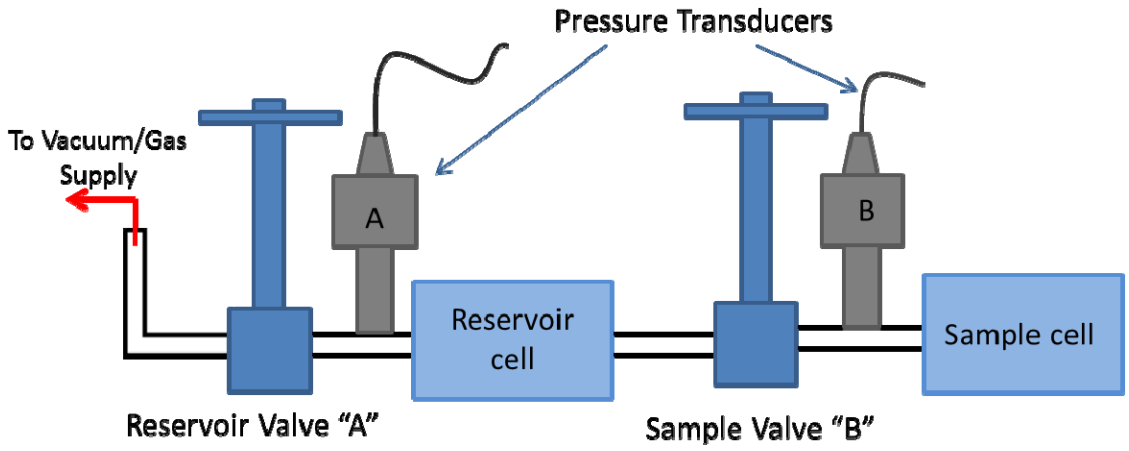

Figure 3.7: Sample and reservoir cell arrangement for pressure decay sorption. The reservoir and sample cells are isolated by needle valves A and B, and the whole arrangement is immersed in an oil bath to obtain sorption coefficients at different pressures.

Both valves A and B are opened; the system is heated to 110 °C and left under vacuum overnight to dry the sample. Once the bath has been cooled down to the temperature of interest (45 °C), both needle valves are closed, and the manifold is pressurized with the gas of interest. Valve A is opened to introduce some gas into the reservoir where it is allowed to reach thermal equilibrium for 30 minutes. Now, the sample cell valve B is opened for 1 sec and then closed tightly. This introduces a small amount of gas from the reservoir to the sample cell. This process may be automated by providing an additional pneumatic valve to the sample cell that is triggered by the computer interface that the pressure transducers input to. This would enable quick gas injection to the sample. The transducers A and B are connected to a computer interface that records the pressures before and after the opening of the sample valves. The sample adsorbs the introduced gas, which is observed as decay in the sample cell pressure. The pressures are recorded till the sample has attained equilibrium with the introduced gas. For fiber sorbents, this is usually achieved within 3 hours.

Sorption isotherms are obtained by repeating the above experiment for different pressures in the region of interest. The sorption capacity at each pressure (S) (mol/g) is obtained from a simple mole balance:

$$S = \frac{(V_1 - V_P) \bullet (p_{2,i} \times Z(p_{2,i}) - p_{2,f} \times Z(p_{2,f}))}{R \bullet T \bullet (V_P \times \rho_P)} \qquad (3.2)$$

Here V_1 and V_P are the volumes of the sample cell (cc) and the sample, $p_{2,i}$ and $p_{2,f}$ are the initial and final sample cell pressures (psi), Z is the compressibility factor at each pressure and ρ_P is the sample density (g/cc). Once the capacity is obtained at each pressure, the isotherm is obtained by plotting the cumulative capacity against the fugacity. The relevant isotherm model may be fitted on to the data using non-linear regression analysis [29, 30].

3.4.4 Kinetic Sorption:

Pressure decay sorption is useful to study equilibrium sorption capacity, but cannot effectively capture the kinetics of sorption. The setup described in the previous section can obtain pressure measurements at 0.5 second intervals, which is nevertheless too slow to measure zeolite sorption rates, especially with heat effects that occur in the closed cell.

Kinetic sorption describes an experiment where sorbents, either as fibers in a module or sorbent in a packed bed are fed a gas stream containing the sorbate gas which is sorbed preferentially and delayed as it passes through the bed. Nitrogen gas is supplied to purge the system and 10% CO_2/10% He/80% N_2 gas is used as the probe gas. Here, He acts as the inert tracer whereas CO_2 is the sorbate. Both the gas streams are metered to the system via mass flow controllers. The gases are routed to the sorbent bed or fiber module either directly or through a bubbler filled with DI water. The bubbler saturates the gas feed with moisture to simulate a wet feed. The effluent from the bed is

sent to an OmniStar GSD30x mass spectrometer (Pfeiffer Vacuum, Asslar, Germany). Additional connections allow for bed and mass spec. evacuation via a vacuum pump and a module bypass. The experimental setup is shown in the below schematic. The sorbent bed and the mass spectrometer feed line can be heated independently of the other components.

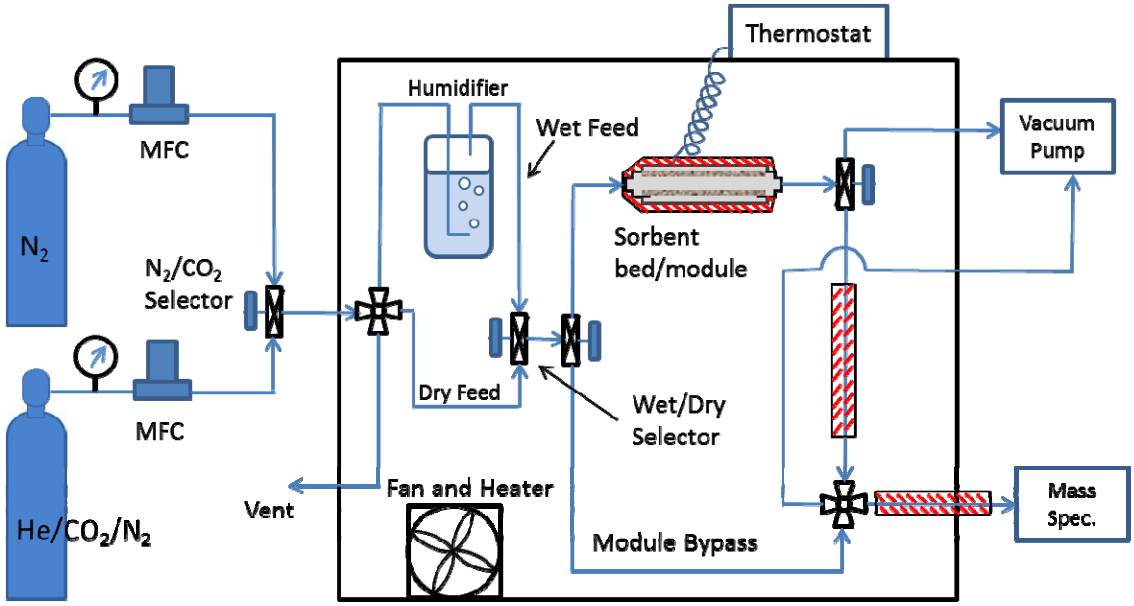

Figure 3.8: Packed bed sorption system to study CO_2 breakthrough curves in wet and dry feed. N_2 or CO_2/He/N_2 mixture is supplied to the packed bed system via mass flow controllers (MFCs). The gases may be saturated with moisture by passing through humidifier. The effluent is analyzed in a mass spectrometer. The bed is re-activated by heating while connected to vacuum. Pure N_2 is then flowed through the bed and the effluent is again analyzed to verify removal of the sorbed gases.

The sorbent bed or module is first connected to the vacuum pump and dried overnight at 125 °C. It is then switched to 20 sccm of flowing N_2 and the vacuum/mass spec. selector is set to "mass spec." N_2 is flowed till the bed effluent shows

no trace of desorbing gases or moisture. The humidifier and bed/bypass lines were housed in a temperature-controlled box set at 35 °C but the line downstream to the bed was kept heated at 150 °C to prevent moisture condensation. Once the bed is dry, it is allowed to cool under flowing N_2. Subsequent bed activation was simply done under N_2 at 110 °C.

For dry sorption experiments, the two wet/dry selector valves are switched to bypass the humidifier. They should already be in this position during the drying step. With N_2 flowing through the bed, the $He/CO_2/N_2$ mixture is set to flow at 50 sccm. The flow through the bed is switched to the gas mixture using the N_2/CO_2 selector. The nitrogen flow is stopped at the flow meter, and the 4-way valve feeding the bed is set to "vent", and the N_2/CO_2 selector is switched back to N_2 to depressurize that line. The selector is switched back to CO_2 and the 4-way valve is switched back to feed the bed. This is a minor disruption in the bed feed gas and does not register in the mass spec. reading. The breakthrough curve is soon observed in the mass spectrometer and flow is continued till the CO_2 and He reading roughly overlap. At this point, a desorption experiment may be performed by switching the feed flow back to N_2. The CO_2 line is vented as described previously. In both sorption and desorption experiments, the CO_2 sorption capacity is measured as the area between the CO_2 and He curves. This is because the system has a certain amount of axial dispersion or backmixing, which is captured by the He signal. Figure 3.9 illustrates this method of analysis. Desorption is continued till the mass spectrometer registers only nitrogen.

For wet sorption experiments, the feed gas is routed through the humidifier via the 2 dry/wet selector valves. Pure water sorption may be studied by saturating N_2 gas by passing it through the humidifier while bypassing the (dried) sorbent bed. Once the water signal has stabilized, the N_2 is routed through the bed and the water breakthrough is recorded. Similarly, CO_2/water competitive sorption can be studied by saturating the He/CO_2/N_2 mixture with moisture (verified via the mass spectrometer) and then passing the saturated feed through the sorption bed.

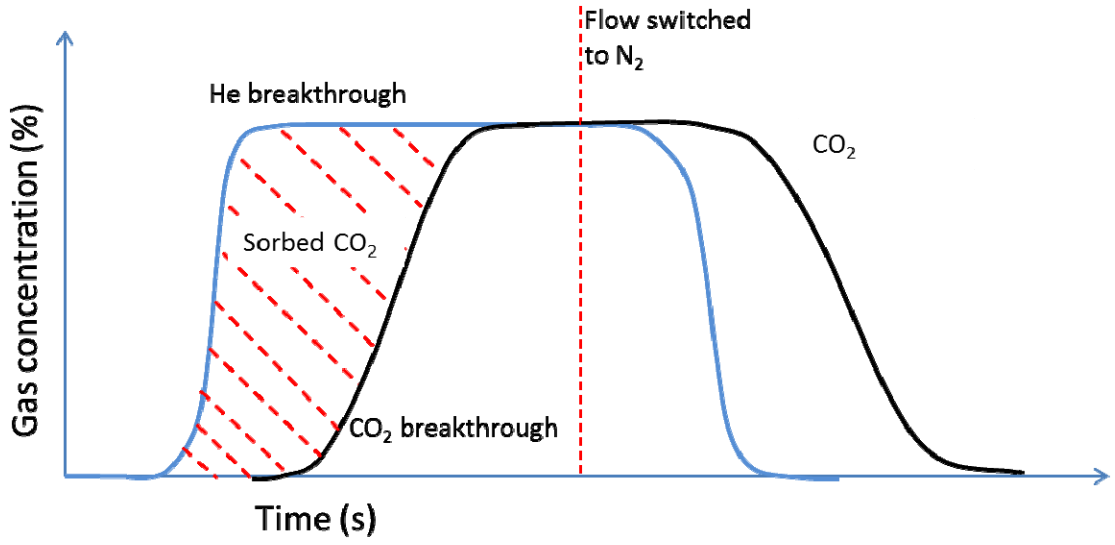

Figure 3.9: Chromatographic sorption experiment uses CO_2 as the sorbate and He as the inert tracer. The helium signal captures the degree of backmix in the system. CO_2 sorption capacity is obtained as the area bound between the He and CO_2 curves. On switching back from the gas feed to N_2, desorption begins more quickly than breakthrough and the CO_2 signal has a long "tail".

The amount of CO_2 sorbed (mole) is readily obtained as the product of the area of the curve (units in %-sec) multiplied by the feed gas flow rate (sccm). The sorption capacity is obtained as the ratio of the amount of CO_2 sorbed to the dry weight of sorbent in the bed.

3.4.5 Thermo Gravimetric Analysis (TGA):

TGA proved to be valuable in analyzing polymer decomposition, water and solvent sorption in spun fibers, and more importantly, to study sorption under repeated thermal cycles. The TGA model was Netzsch STA 409 which allows automation of the temperature protocol described below.

For studying CO_2 sorption under thermal cycling, He gas and 10% CO_2/90% He were used. Optionally, a bubbling apparatus could be connected to the He or He-CO_2 lines and filled with water. Gas passing through de-ionized water in the bubbler could thus be saturated with moisture to enable TGA sorption measurements in wet gas feeds. It is important to note that the water in the bubbler gets saturated with CO_2 and it is advisable to replace it before each experiment. The sample was loaded into the TGA and dried under 30 ml/min He at 115 °C for 36 hours. At the end of this drying step, the sample was cooled to 100 °C, and the gas flow was manually switched to 30 ml/min of 10% CO_2/90% He via a 3-way valve. The sample was cycled between 100 °C and 45 °C at 4 K/min heating/cooling rate with a 30 minute soak at each temperature. The difference in sample mass between 45 °C and 100 °C is taken as the "working capacity" of the sorbent in an RTSA scenario. After 5 cycles, the temperature is increased to 115 °C and then cooled in 15 °C increments to 40 °C with a 30 minute soak at each temperature. This stepped cooling provides the sorption capacity at each temperature, which can be used to calculate the heat of sorption via the van't Hoff's equation [31]:

$$\frac{d \ln K}{dT} = \frac{\Delta H_S}{RT^2} \qquad (3.3)$$

Here, K is the equilibrium sorption constant (dimensionless), R the gas constant (J/mol.K), T the absolute temperature (K) and ΔH_S is the heat of sorption (J/mol). K can be obtained as the sorption capacity at each temperature T. The equation can be integrated to obtain ΔH_S from a plot of $\ln K$ vs. $1/T$:

$$\ln\left(\frac{K_1}{K_2}\right) = \frac{\Delta H_S}{R}\left(1/T_1 - 1/T_2\right) \qquad (3.4)$$

3.4.6 Scanning Electron Microscopy (SEM):

SEM analysis was extensively used to measure the fiber dimensions as well as to study the pore structure and the barrier layer. Hitachi S-800 (FEG) and LEO 1530 (TFE) (Zeiss) microscopes were used for this purpose. Fiber samples were soaked in hexane and immersed in liquid nitrogen. They were sheared under liquid nitrogen using a pair of fine point tweezers to obtain a level viewing surface. For calculating fiber dimensions, 6-10 fiber samples were obtained from each batch of fiber to be measured. The samples were chosen from different fiber pieces and the diameters were measured at 45° intervals so that each sample had 4 measurements. The collected measurements were averaged to obtain the mean fiber dimensions.

3.5 References

1. Solvay Specialty Polymers. 2013 [cited 2013 Sep 16]; Available from: http://www.solvayplastics.com/sites/solvayplastics/EN/specialty_polymers/Spire_Ultra_Polymers/Pages/Torlon.aspx.

2. Robertson, G.P., et al., *Structural determination of Torlon< sup>®</sup> 4000T polyamide–imide by NMR spectroscopy.* Polymer, 2004. **45**(4): p. 1111-1117.

3. Kosuri, M.R., *Polymeric membranes for super critical carbon dioxide ($scCO_2$) separations.* 2009.

4. Qin, J.-J., et al., *Cellulose acetate hollow fiber ultrafiltration membranes made from CA/PVP 360 K/NMP/water.* Journal of membrane science, 2003. **218**(1): p. 173-183.

5. Amirilargani, M., et al., *Effects of coagulation bath temperature and polyvinylpyrrolidone content on flat sheet asymmetric polyethersulfone membranes.* Polymer Engineering & Science, 2010. **50**(5): p. 885-893.

6. Rege, S.U. and R.T. Yang, *A novel FTIR method for studying mixed gas adsorption at low concentrations: H_2O and CO_2 on NaX zeolite and γ-alumina.* Chemical engineering science, 2001. **56**(12): p. 3781-3796.

7. Choi, S., J.H. Drese, and C.W. Jones, *Adsorbent materials for carbon dioxide capture from large anthropogenic point sources.* ChemSusChem, 2009. **2**(9): p. 796-854.

8. Olson, D., W. Haag, and R. Lago, *Chemical and physical properties of the ZSM-5 substitutional series.* Journal of Catalysis, 1980. **61**(2): p. 390-396.

9. Duval, J.-M., et al., *Adsorbent filled membranes for gas separation. Part 1. Improvement of the gas separation properties of polymeric membranes by incorporation of microporous adsorbents.* Journal of membrane science, 1993. **80**(1): p. 189-198.

10. Lively, R.P., *Hollow fiber sorbents for post-combustion CO_2 capture, PhD Dissertation*, 2011, Georgia Institute of Technology.

11. Wirawan, S.K. and D. Creaser, *CO_2 adsorption on silicalite-1 and cation exchanged ZSM-5 zeolites using a step change response method.* Microporous and Mesoporous Materials, 2006. **91**(1): p. 196-205.

12. Olson, D., et al., *Crystal structure and structure-related properties of ZSM-5.* The Journal of Physical Chemistry, 1981. **85**(15): p. 2238-2243.

13. Baerlocher, C. and L. McCusker, *Database of zeolite structures.* http://www.iza-structure.org/databases, 2012.

14. Scholes, C.A., S.E. Kentish, and G.W. Stevens, *Carbon dioxide separation through polymeric membrane systems for flue gas applications.* Recent Patents on Chemical Engineering, 2008. **1**(1): p. 52-66.

15. Allen, S., et al., *The barrier properties of polyacrylonitrile.* Journal of membrane science, 1977. **2**: p. 153-163.

16. Prescott, R., *Pocess for the Manufacture of Continuous High Modulus Carbon Yarns and Monofilaments*, US Patent 3533743 A, filed May 28, 1968, and issued Oct 13, 1970.

17. Beevers, R., *The physical properties of polyacrylonitrile and its copolymers.* Journal of Polymer Science: Macromolecular Reviews, 1968. **3**(1): p. 113-254.

18. Dalton, S., F. Heatley, and P.M. Budd, *Thermal stabilization of polyacrylonitrile fibres.* Polymer, 1999. **40**(20): p. 5531-5543.

19. Tuminello, W.H. and G.T. Dee, *Thermodynamics of poly (tetrafluoroethylene) solubility.* Macromolecules, 1994. **27**(3): p. 669-676.

20. Drobny, J.G., *Technology of fluoropolymers,* 2008: CRC Press.

21. Gaur, U. and B. Wunderlich, *The glass transition temperature of polyethylene.* Macromolecules, 1980. **13**(2): p. 445-446.

22. Peng, N., T.-S. Chung, and J.-Y. Lai, *The rheology of Torlon® solutions and its role in the formation of ultra-thin defect-free Torlon® hollow fiber membranes for gas separation.* Journal of membrane science, 2009. **326**(2): p. 608-617.

23. Han, C.D. and L. Segal, *A study of fiber extrusion in wet spinning. II. Effects of spinning conditions on fiber formation.* Journal of Applied Polymer Science, 1970. **14**(12): p. 2999-3019.

24. Djoekita, G., D.Q. Vu, and W.J. Koros, *Pervaporative introduction of organic vapors into high-pressure gas feeds.* Journal of Applied Polymer Science, 2001. **80**(2): p. 311-315.

25. Swagelok Company. *Ultra-Torr Vacuum Fittings*. 2007 [cited 2013 September 3]; Available from: http://www.swagelok.com/downloads/webcatalogs/EN/ms-01-32.pdf.

26. Lively, R.P., et al., *Hollow fiber adsorbents for CO_2 removal from flue gas.* Industrial & Engineering Chemistry Research, 2009. **48**(15): p. 7314-7324.

27. O'Brien, K., et al., *A new technique for the measurement of multicomponent gas transport through polymeric films.* Journal of membrane science, 1986. **29**(3): p. 229-238.

28. Koros, W.J. and D. Paul, *Design considerations for measurement of gas sorption in polymers by pressure decay.* Journal of Polymer Science: Polymer Physics Edition, 1976. **14**(10): p. 1903-1907.

29. Wong, Y., et al., *Adsorption of acid dyes on chitosan—equilibrium isotherm analyses.* Process Biochemistry, 2004. **39**(6): p. 695-704.

30. Foo, K. and B. Hameed, *Insights into the modeling of adsorption isotherm systems.* Chemical Engineering Journal, 2010. **156**(1): p. 2-10.

31. Do Duong, D., *Adsorption Analysis: Equilibria and Kinetics*1998: Imperial College Press.

CHAPTER 4

FORMATION OF SINGLE-LAYER TORLON® FIBER SORBENTS

4.1 Overview of Fiber Sorbent Spinning with Torlon®

This chapter discusses the challenges involved in forming durable, heat-resistant fiber matrices that retain their mechanical integrity on repeated thermal cycling along with easy transport in and out of the sorbent particles. It provides the rationale for the selection of Torlon® for the RTSA platform and its application to the spin dope development process. The later part of the chapter details the optimization of the spinning process and the challenges encountered therein. Fiber characterization via helium porosimetry, TGA sorption and SEM analysis are also reported.

4.2 Selecting a Matrix Polymer for High-Temperature Application

The matrix polymer provides the structural framework and mechanical strength to the hollow fiber. The hollow fiber RTSA project originally tested polysulfone and PEBAX® as possible matrix polymers, but Cellulose Acetate (CA) was found to be a better candidate as it is both inexpensive and easily spinnable [1]. Cellulose acetate is widely used for industrial membranes and hence is readily adapted to the RTSA platform. The molecular structure is provided in Figure 4.1.

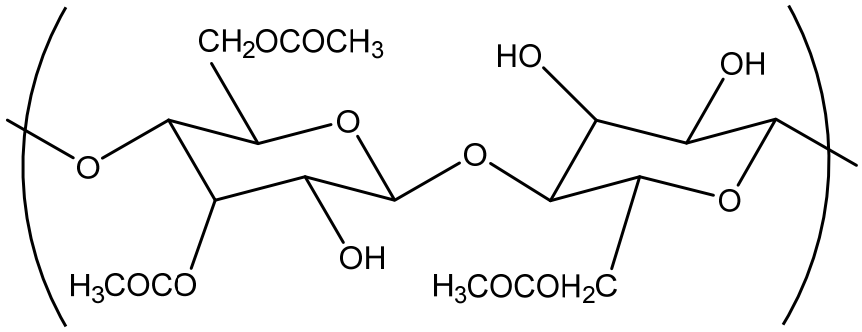

Figure 4.1: Molecular structure of cellulose acetate showing partial random acetylation of the -OH groups.

Despite its positive traits, cellulose acetate degrades at higher temperatures in the presence of oxygen or UV radiation [2, 3]. Its glass transition temperature (185-210 °C) is depressed in the presence of humidity [4], which impacts barrier layer formation and post-treatment. This is compounded by the fact that it is soluble in a number of solvents with low dielectric constants (relative permittivity), such as acetone, that makes it impossible to solvent-cast barrier materials that only dissolve in solvents with higher dielectric constants. Hence there appears the need to substitute cellulose acetate with a more durable, less soluble polymer.

4.2.1 Hollow Fibers from Torlon®

Since the matrix polymer performs a structural, rather than a separation function, it is better chosen from a class of polymers called *engineering plastics*. These typically have better mechanical properties and solvent resistance, especially at elevated temperatures [5]. Examples include polyethylene terephthalate (PET), polycarbonates, poly(tetrafluoroethylene) (PTFE) and polyamides such as Nylon 6,6 and Kevlar®.

Polyamides in particular are known for their superior mechanical strength and chemical resistance arising from hydrogen bonding between the amide groups that occur in their backbones [6].

Many engineering polymers are not commonly spun into hollow fiber membranes owing to their low permeability or processibility (e.g. PTFE); however, they are promising candidates for the RTSA platform if they can be processed via the dry-jet wet-quench method. Polyamide-imides, manufactured by Solvay Plastics under the trademark Torlon®, are among those that are soluble in a common industrial solvent (NMP) but are resistant to attack by less polar solvents. In addition, they combine the strengths of polyamides and polyimides to the extent that they are considered among the best-performing engineering polymers on par with polymer composites. Torlon® grades have a reported ultimate tensile strength up to 22,000 psi [7], more than three times that of cellulose acetate [8, 9]. For this work, the grade chosen was Torlon® 4000T HV, the high-viscosity, additive-free granular form supplied by Solvay Polymers. 'HV' indicates that the polymer has higher molecular weight than other grades. Lower viscosity grades were found to be difficult to extrude at high shear rates since sorbent dopes contain up to 35% by weight of sorbent.

Prior research in the Koros group has established Torlon® as a viable candidate for producing plasticization-resistant membranes for high pressure CO_2 separations [10]. This chapter discusses the production of open-porous fibers from Torlon® that retain their structural integrity and flexibility during thermal cycling and the high-pressure conditions that occur during fiber post-treatment. Torlon® membranes are

spun from dopes containing up to 34% Torlon® by weight along with a volatile solvent. Sorbent dopes use a much lower Torlon® content to accommodate the sorbent itself and also discourage skin formation.

4.3 Sorbent Dope Development

The process as laid out in Section 2.3.1 sets forth the dope development philosophy for fiber sorbents. The volatile component of the dope is dispensed with, but the solvent (NMP) and non-solvent (water) are retained from research on membrane spinning. Torlon® is soluble in a number of polar aprotic solvents including NMP, DMF and DMSO but NMP is less volatile (b.p. 202 °C) and relatively safer and environmentally benign [11]. Similarly, water is the obvious non-solvent of choice over organic liquids such as methanol. PVP was retained in the dope not only for its pore-forming ability [12] but also since it provides a means of increasing dope viscosity without increasing the polymer content of the spun fibers.

4.3.1 Torlon®/NMP/Water Ternary Phase Diagram

Sections 2.3.3 and 3.2.1 detail the process of developing the ternary phase diagram via the cloud point technique. The Torlon®-NMP-water ternary diagram was constructed at 50 °C since this was the planned quench bath temperature. The temperature is important for spin dopes since they are designed to be very close to the phase separation line. It is quite possible for the binodal line to move past the dope composition on cooling. In this work, it was observed that spin dopes would often get

cloudy when cooled to room temperature. This may be exacerbated by the evaporation of solvent and non-solvent from the dope and so the dope was kept covered. The ternary diagram is shown in Figure 4. 2.

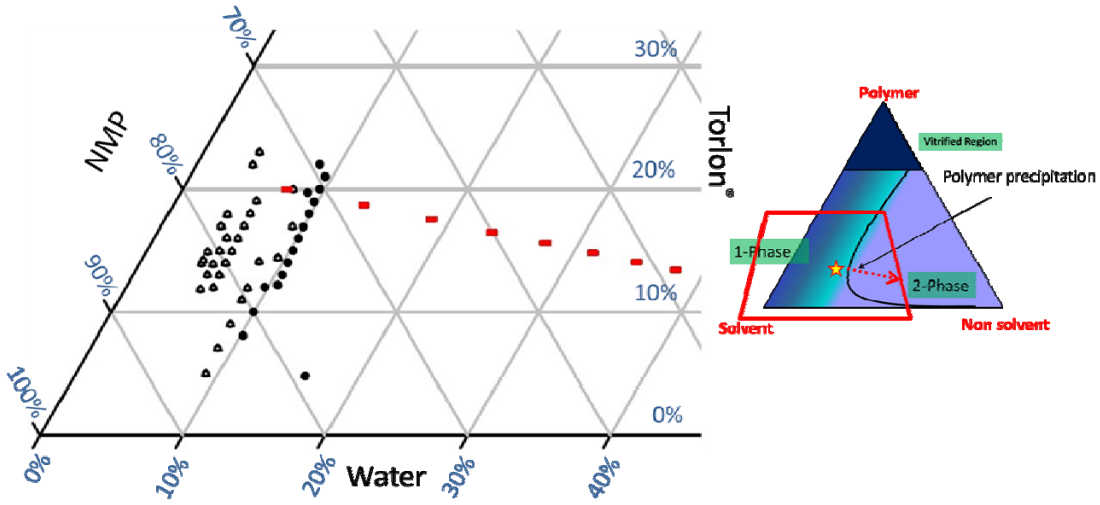

Figure 4.2: Torlon®/ NMP/ Water ternary phase diagram at 50 °C with single-phase (○) and 2-phase (●) regions. The dashed red line represents the effect of adding water to a dope that initially contains 20% Torlon®/7% water/73% NMP. The smaller inset represents the ternary phase diagram as a whole, with the relevant area outlined in red.

The open symbols (○) represent the single phase region and the solid circles represent the 2-phase area. A smaller schematic of the ternary phase diagram is provided to show the region where the cloud point experiment was actually performed.

It is observed that the phase separation curve lies close and parallel to the 10% water line for the range of Torlon® concentration studied. Typically, phase separation occurred at 9-9.5 wt. % water in the dope. Incorporation of PVP into the process is described in the Section 4.5.

4.3.1.1 Preliminary Dope Development

The first variable probed while developing a dope was the dope viscosity. At lower polymer concentrations, the dope viscosity was too low to allow extrusion at high extrusion rates, whereas dope mixing became difficult at high polymer content. More dilute dopes also have the advantage of larger dope volume, which reduced sorbent and polymer wastage during trial spins. The rough starting point for dope development was the cellulose acetate/13X composition previously used for RTSA sorbents [13]. This composition contained 10 wt. % of cellulose acetate and 30 wt. % of saturated zeolite. In the absence of zeolite, the cellulose acetate constituted 14.3% by weight of the solution, as indicated in Table 4.1.

Table 4.1: Dope composition for CA/13X sorbent dopes with and without the 13X content.

Dope Component	Concentration in Spin Dope (%)	Concentration ignoring zeolite content (%)
Cellulose acetate	10	14.3
PVP	4	5.7
NMP	49.3	70.4
Water	6.7	9.6
13X	30	--

Hence Torlon® dopes were also studied primarily between 10-22 wt. % polymer concentration (ignoring the zeolite content). It was found that Torlon® solutions were less viscous than those of cellulose acetate and also accommodated less water. The initial trial polymer solution contained 16 wt. % Torlon® and 8.3 wt. % water.

4.4 Trial Spin at 75% Zeolite Targeted Loading:

Having decided on a 16% Torlon® polymer solution as the base for a spin dope, a trial spin was attempted to produce fiber sorbents with 75% by weight of zeolite loading. Zeolite 13X was used as the stand-in sorbent for the trial spin. It was saturated for a week as described in Section 3.2.2.

4.4.1 Spin Dope Compositions and Spinning Parameters

Unlike fiber membranes, fiber sorbents benefit from thin walls or high draw rates. One of the goals of sorbent spinning is to maximize sorbent loading per length of fiber, i.e. the fiber volume per volume of bed. This is best achieved by increasing fiber wall thickness and diameter as long as diffusional constraints do not set in. Membranes on the other hand require increased surface area per volume of bed, and benefit from small, thin-walled fibers. With this in mind, the dope and bore fluid flow rates were set very high and the core-to-bore flow ratio was set at 1:3. The air gap between the spinneret and the needle was decreased to 4 cm to discourage any skin formation. The temperature of the dope pump, spinneret and quench bath were all set to 50 °C. Elevated quench temperature improves the fiber structure by improving the fiber

porosity and discouraging skin formation within the bath [14]. Since the phase diagram had been made at 50 °C as well, this was the overall operating temperature for the spin. Skin formation on the internal wall was avoided by choosing a solvent-rich bore fluid. 80:20 NMP/water was retained as a practicable bore fluid based on prior cellulose acetate spinning experience.

The trial dope composition after including the zeolite content is given below along with the spin conditions for one spin state (state 2).

Table 4.2: Dope composition and spinning condition for initial Torlon®/13X trial spin.

Dope Component	Concentration in Spin Dope (%)
Torlon®	10.8
NMP	51.2
Water	5.6
13X	32.4

Spin Parameters	
Core Flow Rate	600 ml/hr
Bore Flow Rate	200 ml/hr
Bore Composition	20:80 Water:NMP
Operating Temperature	50 °C
Take-up Rate m/min	16 m/min
Air Gap	4 cm

4.4.2 Results of Trial Spin

The spin was successful in producing hollow fiber sorbents although the dope was less viscous than a comparable cellulose acetate dope. Fiber breaks did occur but did not prevent the successful collection of fibers. The fibers obtained were allowed

to phase-separate, then solvent-exchanged and dried as for a standard membrane fiber, and analyzed via SEM, TGA and constant-pressure permeation.

4.4.2.1 SEM Analysis of Fibers

Sample SEM micrographs of the fibers are provided below in Figure 4.3 and 4.4. The average I.D. and O.D were 563 μm and 1125 μm respectively. The most prominent features observed were the eccentricity of the fiber bore with respect to the outer wall and the presence of large radial macrovoids. The bore eccentricity was later found to be an artifact of the misaligned spinneret, and was eliminated in subsequent spins as shown shortly. In spite of the non-centered bore and macrovoids, the dried fiber sorbents had good mechanical strength and could be handled and potted easily.

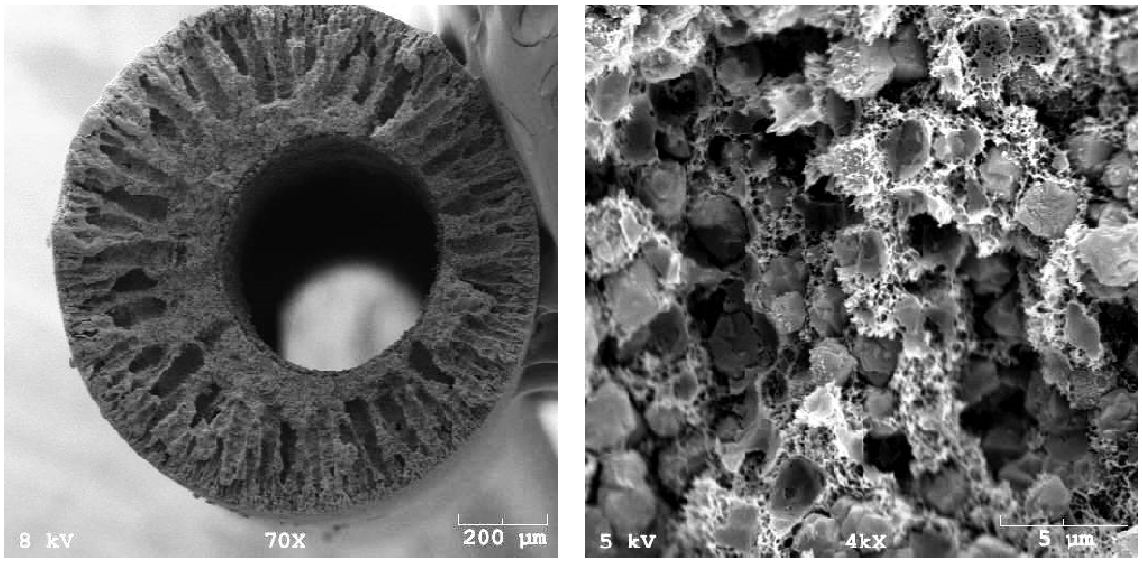

Figure 4.3: Cross-section of fiber sorbents showing (A.) macrovoids and bore eccentricity, and (B.) Pore structure with zeolite crystals well-dispersed in an open polymer matrix. The empty sockets represent areas where the sorbent crystals are seated in the network.

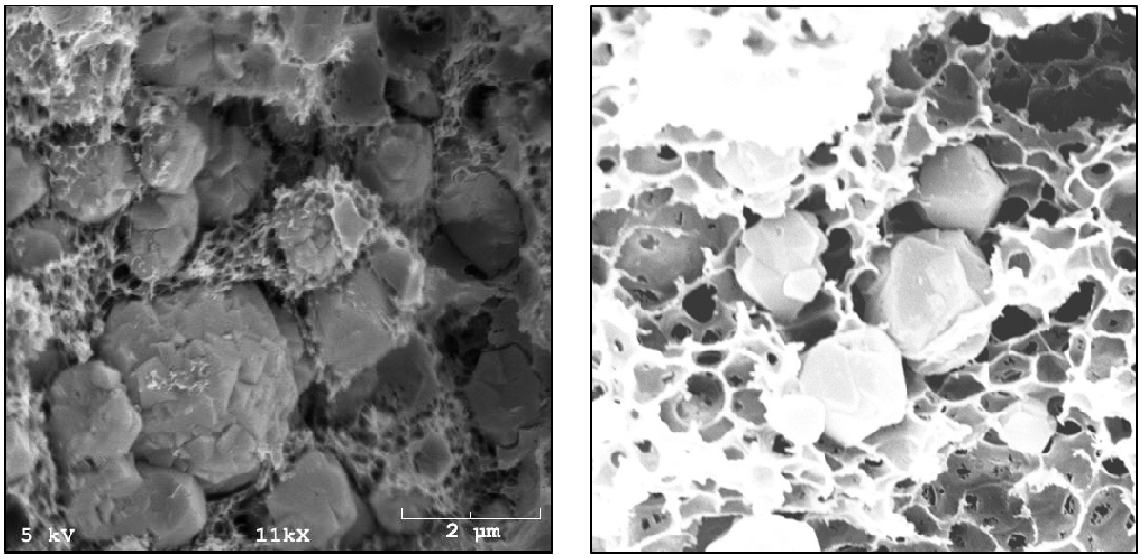

Figure 4.4: Closer view of (A.) Torlon® pore structure showing the "sieve-in-a-cage" interface between 13X and polymer, and (B.) CA/13X spun under similar conditions. The CA fibers showed a more closed-cell configuration that was reflected in permeance measurements.

The other feature observed were macrovoids extending inward from the outer wall, and to a lesser extent, from the inner wall. Macrovoids weaken the fiber and reduce the linear sorbent loading. They are formed due to differential stresses in polymer-lean solvent/coagulant nuclei near the fiber walls where phase separation starts [15]. The counter-diffusion of solvent and coagulant into the nucleus and the resultant volumetric increase causes it to grow in a tear-drop shape towards the fiber bore. It has been proposed that increasing the bath temperature could discourage macrovoid growth by delaying phase separation till greater coagulant diffusion has occurred and by increasing the elasticity of the precipitating polymer [14]. In any case, the macrovoids were not serious mechanical limitations to the use of the fibers. Another way of suppressing macrovoids is to use a complexing agent such as lithium nitrate or an additive such as PVP [16]. This was the approach pursued in subsequent spins to reduce the size of

macrovoids and improve the pore structure. In these fibers, the fiber pore structure itself had an open, "sieve-in-a-cage" structure in the region between macrovoids. As desired, both the inner and outer walls lacked a dense skin. The sorbent crystals were held loosely but securely in a socket formed from the precipitated polymer. Overall, the desired pore structure was achieved apart from the occurrence of macrovoids.

4.4.2.2 Permeance Measurement

Fibers were potted in modules as described in Section 3.3 and connected to the permeation system to measure nitrogen permeance at constant pressure. Owing to the eccentricity of the bore, the fiber diameter could not be said to be representative. Still, assuming an O.D of 1125 μm yielded an average nitrogen permeance of 31,583 GPUs at 1.2 psi Δp. For comparison, cellulose acetate fibers spun at similar condition (dope composition in Table 4.1.) had permeances an order of magnitude smaller, at 4125 GPUs close to atmospheric pressure. There are two possible explanations for this discrepancy. One reason could be the presence of the large macrovoids in the Torlon® fibers which decrease the effective diffusion length through the fiber wall, causing the fiber to present a lower resistance to gas flow than would be expected from the measured wall thickness. It was observed in the SEM images that the macrovoids at some points stretched from the bore almost to the outer wall of the fiber, an issue exacerbated by the eccentricity of the fiber bore. This would cause gas to short-circuit through the voids rather than diffuse through the fiber wall proper. Additionally, the cellulose acetate fibers used for comparison also exhibited a closed-cell morphology (shown in Figure 4.4.) that could have depressed their permeance. Closed cells occur when nuclei form and grow slowly

during phase separation, as opposed to instantaneous demixing that occurs during spinodal decomposition [17]. However, the permeance measurement was useful in establishing the feasibility of spinning high-permeance, open-porous fibers with Torlon® as the matrix. Subsequent modifications were made to the dope to further improve gas transport, detailed in Section 4.5.

4.4.2.3 Sorbent Loading Calculation via TGA

The spin dope had been prepared so that the dried fibers would contain 75% by wt. of zeolite sorbent. However, the targeted sorbent content does not necessarily match the final zeolite loading. The exact loading may be obtained by simply burning the fiber sorbents in air in the TGA leaving behind only the zeolite.

Fiber samples from solvent exchange were loaded into the TGA and heated at 125 °C for 36 hours under nitrogen sweep at 30 ml/min to remove sorbed moisture. The temperature was then ramped to 200 °C and held there for 2 hours to remove sorbed NMP, followed by a slow ramp (5 K/min) to 700 °C under air flow at 30 ml/min. The temperature was held at 700 °C for 2 hours to complete the fiber burn off.

The results of the burn off experiment are shown in Figure 4.5. The fiber lost about 14% of its mass in water and a further 1.5% in NMP. NMP is known to hydrogen-bond with Torlon® and is difficult to remove [15]; however, it does not impact fiber sorbent separation the way it does for membranes. Eventually only 60% of the original fiber was left at 700 °C. This implies that sorbent loading was 69.7% of the dry

weight of fiber (or 60% of the saturated fiber) against a target of 75%. The reduced loading was attributed to the fact that the zeolite was saturated with moisture prior to being weighed out for spinning. The simplest way to make up for this discrepancy is to simply increase the targeted loading so that the actual loading increases in tandem.

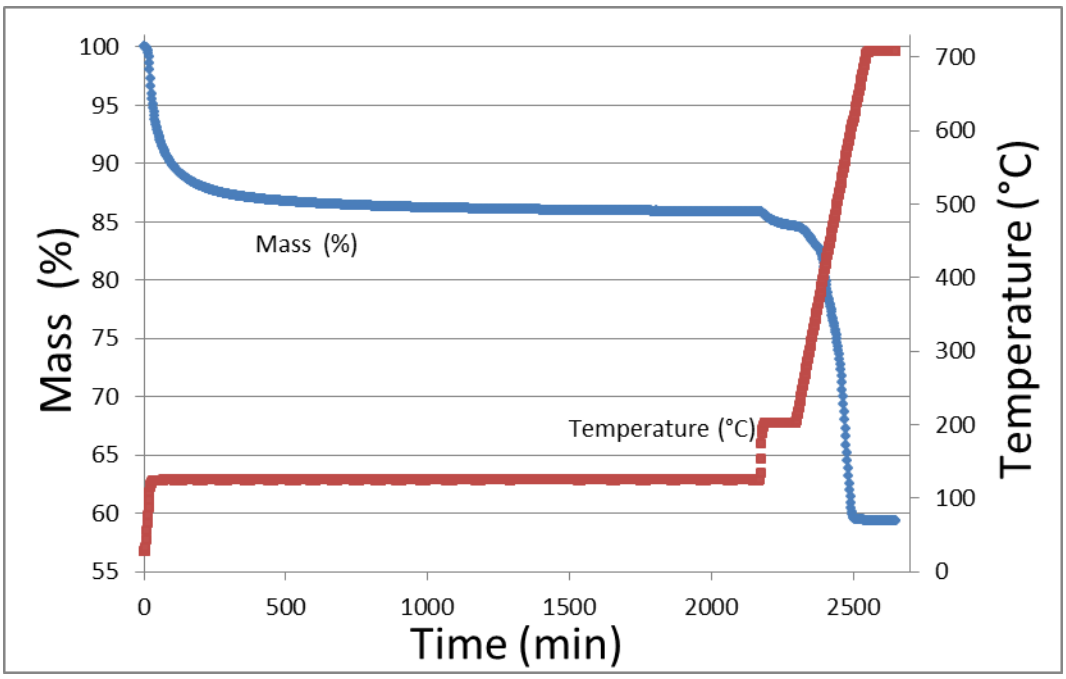

Figure 4.5: Fiber burn off in TGA showing mass loss due to desorption of water at 125 °C and NMP at 205 °C, followed by oxidation leaving behind the siliceous sorbent.

4.4.2.4 TGA Thermal Cycling

Finally, the working capacity of the fibers was estimated by thermally cycling the fibers in the TGA and inferring the capacity at each temperature from the change in mass of the sample. The TGA protocol for this experiment is described in Section 3.4.5. The lengthy drying process allowed the calculation of the dry weight of

fiber, which formed the basis for the capacity calculation. The gas used was 10% CO_2/90% He to allow capacity calculation at partial pressures that occur in the field, i.e. ≈ 0.1 atmospheres.

The figure below shows the temperature program with the corresponding results. The three regions of the thermal profile are the initial drying step at 115 °C (under dry helium), thermal cycling between 45 and 100 °C under 10% CO_2/90% He and a final stepped cooling to estimate the heat of sorption. There were 5 thermal cycles, which were used to calculate the equilibrium capacities at 45 and 100 °C, and the working capacity on swinging the sorbent between these temperatures.

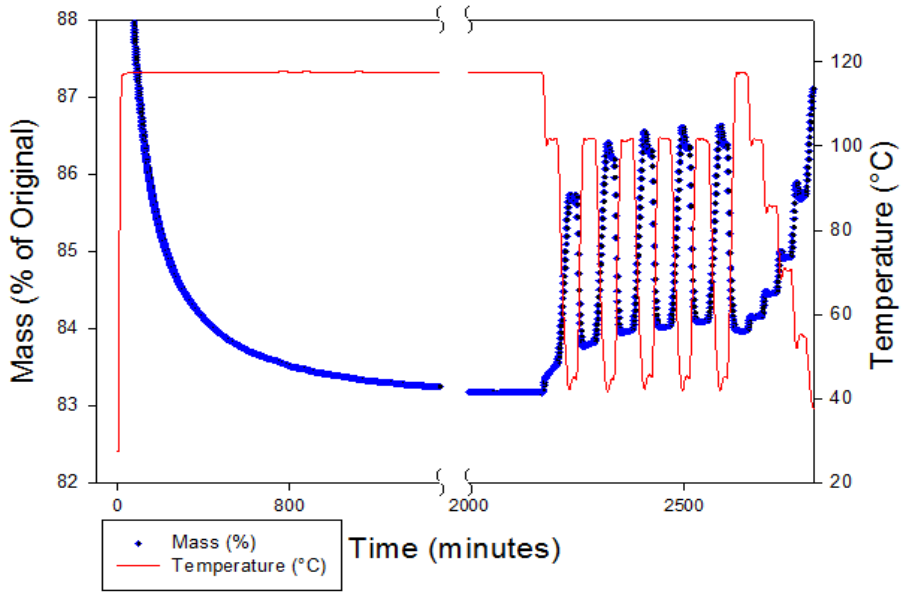

Figure 4.6: Thermal cycling of Torlon®/ 13X fiber in TGA with an initial 36-hour drying step. There was a mass loss of about 17% on drying under helium at 115 °C, and the remaining mass was used as the dry weight of fiber.

The dry weight of fiber was found to be around 83% of the total weight of saturated fiber. The average capacity at 45 °C was 0.83 mmol CO_2/g of dry fiber and at 100 °C was 0.19 mmol/g, yielding an average working capacity of 0.64 mmol/g between these temperatures. This compares favorably with CA/13X fibers with the same loading previously spun, for which the corresponding values were 0.73 mmol/g, 0.13 mmol/g and 0.60 mmol/g respectively.

It is important to note that the capacities listed above were for the fiber and not just the sorbent. They may be understood as the weight-averaged capacity of the polymer and zeolite. The capacities were back-calculated from known capacities for 13X from literature and from Torlon® isotherms (Figure 4.7) separately obtained via pressure decay sorption. The isotherms were fitted to the dual-mode sorption using the Microsoft Excel Solver add-in. Doing so allowed the calculation of the Torlon® CO_2 capacity at 45°C and 100 °C at 0.1 atm partial pressure.

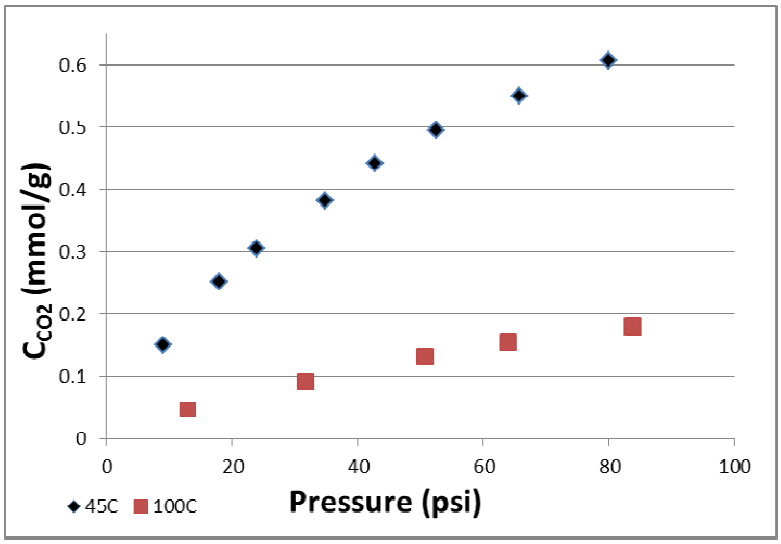

Figure 4.7: CO_2 Sorption isotherm for Torlon® 4000T HV at 45 °C and 100 °C.

The capacities for Torlon® thus calculated, 13X capacity from literature [18, 19], and the expected and measured sorption capacities of the 69.7 wt. % 13X fibers are listed in Table 4.3. The equilibrium and swing capacities for 13X are much higher than those calculated from the fiber. This was attributed to the fact that the fiber sorbents were activated only at 115 °C as high temperature activation is not feasible with spun fibers. As mentioned previously, the capacities match those of 13X/CA fibers and also match swing capacity for 13X crystals determined from chromatography experiments under the same temperature cycling [13], which are a more realistic representation of hollow fiber use in RTSA systems.

Table 4.3: Sorption and working capacities of 13X, Torlon® and fibers containing 69.7 wt. % of sorbent. Absolute capacities are higher for 13X reported here [1] as it had been activated at 400 °C.

Material		Capacity at 45 °C	Capacity at 100 °C	Working Capacity
		Units are in mmol CO_2/g sorbent		
13X		1.8	0.54	1.26
Torlon® 4000T HV		0.15	0.016	0.13
69.7% 13X / 30.3% Torlon®	**Estimated**	1.3	0.38	0.92
	Measured	0.83	0.19	0.64

The heat of sorption for Torlon®/13X and CA/13X fibers were estimated from the stepped cooling at the end of the TGA experiment. The natural log of the sorbed

content was plotted against the inverse of the corresponding temperature, and this was fitted to the linearized Van't Hoff equation. The estimated heat of sorption for Torlon®/13X fibers was 38.8 kJ/mol and for CA/13X it was 39.5 kJ/mol, compared to a literature value of 37.2 kJ/mol for pure 13X [20]. Also evident in Figure 4.6 on Page 110, the mass change curve followed the temperature program very closely. This, coupled with the fact that the swing capacity is similar to what is expected from literature values supports the argument that Torlon® framework provides ready gas access to the sorbent crystals: the primary requirement of the polymer matrix.

4.5 Introduction of PVP and Reduction in Macrovoids

Having observed the benefit of adding PVP to spinning porous cellulose acetate sorbents, it was decided to add PVP to Torlon® dopes as well. The main goals were to improve the pore structure and reduce the occurrence of macrovoids. PVP also provided a useful way to increase dope viscosity without increasing the Torlon® content in the dope, which would have increased the sorbent content correspondingly, potentially causing problems in sorbent dispersion.

4.5.1 Development of Torlon®/PVP/Water/NMP Phase Diagram

Two percent PVP by weight was added to the 17% Torlon® dope and found to be miscible with Torlon®-NMP solutions. The solution was stable on standing and showed no signs of degradation on storage. PVP was expected to significantly affect the phase separation equilibria as well as phase separation during fiber spinning. Based

on this expectation, a new phase diagram was prepared to include PVP with Torlon®. To eliminate one variable, the Torlon®: PVP ratio was arbitrarily set at 4:1. The concentrations of PVP and Torlon® were summed and plotted along the polymer axis. The cloud point determination was performed as described in Section 2.3.3. The relevant section of the new phase diagram is provided below.

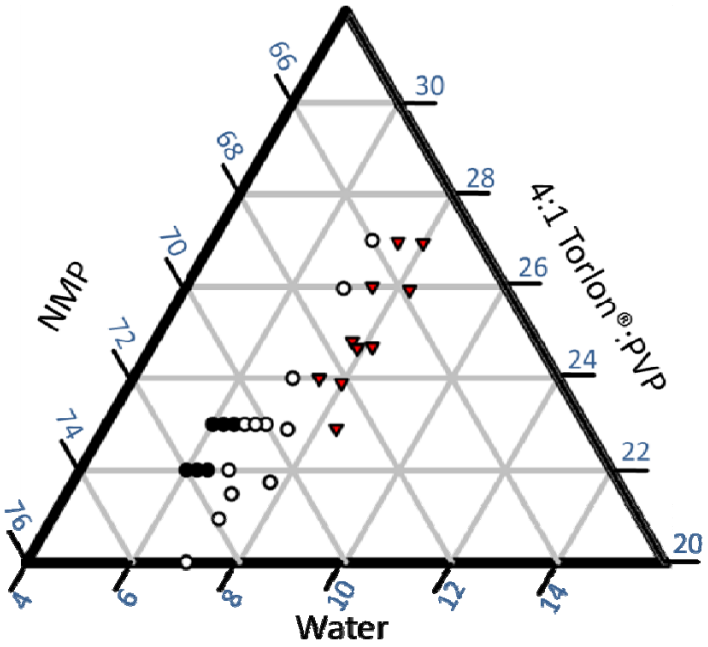

Figure 4.8: Selected section of Torlon®-PVP/ NMP/ Water ternary phase diagram at 50 °C with single-phase (●), cloudy (o) and 2-phase (▼) regions. The units are % of each component by weight. Only the region of interest (20-32% Torlon®/PVP and 4-16% water) is shown in this figure.

It was observed that the new compositions had a significant non-solvent concentration range which produced cloudy solutions, which are represented by open circles (o) above. This cloudiness was not widely observed in Torlon®-only solutions. Since cloudy solutions are prone to phase separation on cooling or due to water absorption during dope preparation, it was decided to set their lower limit as the

acceptable single-phase region. This was observed between 6.5-7% by weight of water for the range of polymer concentrations probed. Overall, phase separation occurred at a lower non-solvent concentration than for polymer solutions lacking PVP. This is attributed to PVP acting as a non-solvent rather than an inert pore former, thereby depressing the amount of water required for phase separation. A polymer solution with 21% by weight of polymer yielded a dope that was deemed most spinnable.

Since the non-solvent concentration was to be set at 1% away from the phase separation line, the dope was designed to contain 5.8% water by weight. Of the 21% polymer content, the Torlon® and PVP were 16.8% and 4.2% by weight each, maintaining the ratio at 4:1 in accordance with the ternary phase diagram. The dope makeup with and without the sorbent were as shown in Table 4.4.

Table 4.4: Revised dope composition with PVP pore former included.

Dope Component	Concentration in Prime Dope (%)	Concentration in Spin Dope (%)
Torlon®	16.8	11.2
PVP	4.2	2.8
NMP	73.2	48.7
Water	5.8	3.8
Sorbent	--	33.5

4.5.2 Spin Results

The revised dope was easily spun into large-dimension fiber sorbents with fewer fiber breaks even at higher spin temperatures (Table 4.5). High-silica ZSM-5 (Si: Al ratio of 40, ≈2μm crystals) was used as the stand-in sorbent. The fibers were solvent-exchanged and dried as before; then the fiber dimensions, capacity and permeance were measured. The fibers were heated in the TGA under air flow to burn off the organic content and were revealed to contain 69.2 % dry sorbent by weight.

Table 4.5: Spin conditions with revised dope composition.

Spin Parameters	
Core Flow Rate	800 ml/hr
Bore Flow Rate	300 ml/hr
Bore Composition	20:80 Water: NMP
Operating Temperature	50 °C
Take-up Rate	25 m/min
Air Gap	4 cm

4.5.2.1 SEM Analysis

SEM imaging showed that the macrovoids had been significantly reduced in size upon addition of PVP and mostly confined to the periphery of the fibers. Also as

expected, the bore eccentricity had been eliminated. The pore structure was examined and the polymer structure supporting the fiber was found to be porous.

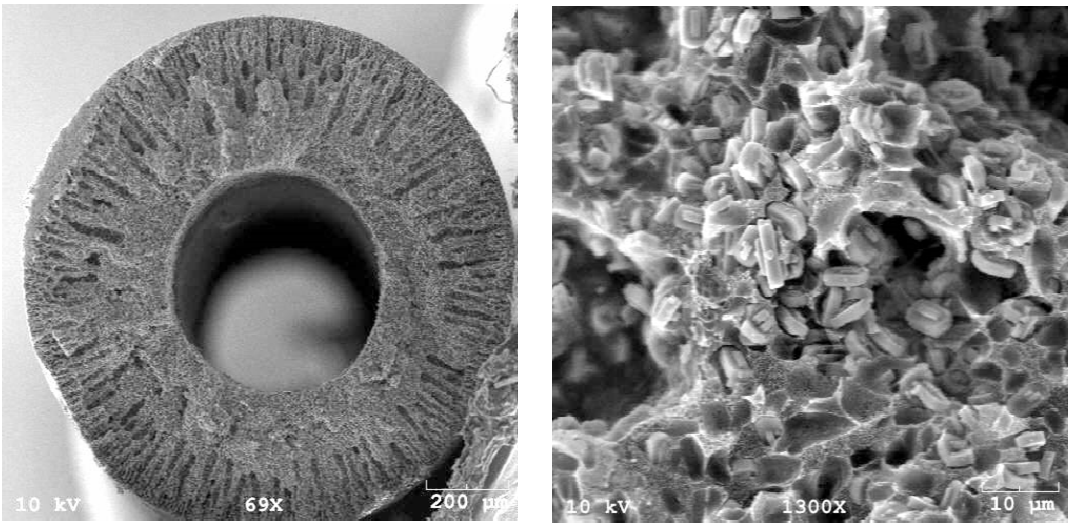

Figure 4.9: Cross-section of fiber sorbents showing (A.) reduced macrovoids on addition of PVP, and (B.) fiber pore structure with zeolite crystals well-dispersed in the open polymer matrix.

4.5.2.2 Permeance Measurement and Porosimetry

Nitrogen permeance measurements were performed on fibers with outer diameters 1208±42 µm and the permeance was plotted against average system pressure to estimate the fiber pore dimensions as set forth in Section 2.2.5. Helium permeance was approximately 2.65 times that of nitrogen implying considerable Knudsen diffusion occurring. The permeance was lower than that of the fibers spun without PVP (Section 4.4.2.2) but this could be attributed to the reduction in macrovoids that would have depressed the effective thickness of the fiber and increase gas flux. Later experiments proved nitrogen permeances greater than 15000 GPUs at < 25 psi pressure drops could be

consistently obtained on other spins based on this dope makeup. The permeance data is shown in the Figure 4.10.

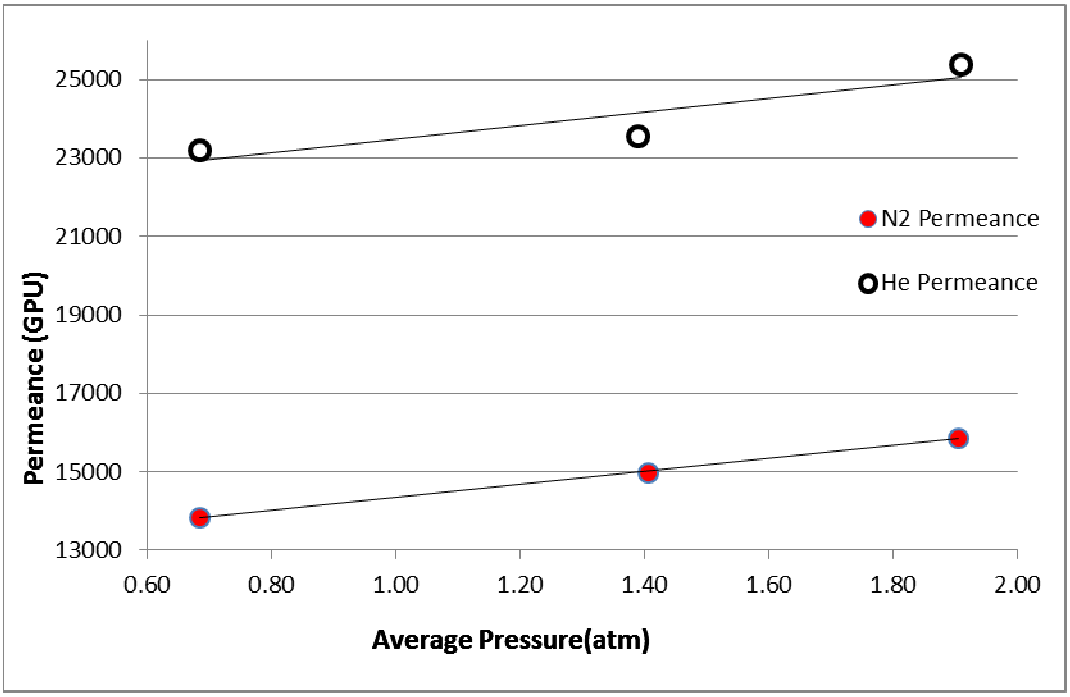

Figure 4.10: Plot of average nitrogen and helium permeance vs. average system pressure for fiber sorbents spun with 3% PVP in the dope.

The ratio of Knudsen to Poiseuille flow contributions to gas flux, measured as (Intercept/ (Slope*average p)) was 9.2, which implies that the Knudsen contribution to flow dominated over Poiseuille contribution at the test pressures. The ratio of slope to the intercept in the permeance vs. pressure curve was used to estimate the average pore diameter based on Knudsen diffusion. For fibers spun as above, the d_{pore} was estimated to be 132 nm based on nitrogen diffusion and 149 nm based on helium diffusion. At 20 psi, the mean free path for nitrogen diffusion is 73 nm, therefore the diffusion primarily occurs in the transition region between Knudsen and molecular diffusion.

4.6 Summary and Conclusions

Torlon® was tested as a matrix polymer and was found to be readily adaptable to the fiber sorbent platform. It produced sorbent dopes that could be easily prepared and readily spun into robust fibers that retained their mechanical strength even at high sorbent loadings. Initially, the Torlon®/NMP/water phase diagram was prepared and used to spin test fiber sorbents that were found to display a desirable pore structure and high permeance. However, this dope was prone to fiber breakage during spinning and produced fibers with a large number of macrovoids. To remedy this, PVP was introduced in the dope as a pore former and macrovoid suppressant. A separate phase diagram was developed to include PVP and a new preferred spin dope composition was identified. Fibers were spun based on this concentration with far fewer breakages during spinning: an important requirement for industrial production. SEM analysis showed that macrovoids had been significantly reduced as well. High wall permeance was retained and the permeance measurement was used to estimate the ratio of Knudsen to Poiseuille contributions to flow. It was found that Knudsen flow was dominant over Poiseuille flow implying small channels. The estimated pore sizes revealed that the diffusion process would lie in the transition region between molecular and Knudsen diffusion. Thus, the final dope composition and spin conditions were used for subsequent spins to produce fibers described in subsequent chapters.

4.7 References

1. Lively, R.P., et al., *Hollow fiber adsorbents for CO_2 removal from flue gas.* Industrial & Engineering Chemistry Research, 2009. **48**(15): p. 7314-7324.

2. Lawton Jr, T. and H. Nason, *Effect of Ultraviolet Light on Cellulose Acetate and Nitrate.* Industrial & Engineering Chemistry, 1944. **36**(12): p. 1128-1130.

3. Lucena, M.d.C.C., et al., *The effect of additives on the thermal degradation of cellulose acetate.* Polymer degradation and stability, 2003. **80**(1): p. 149-155.

4. Shogren, R.L., *Preparation, thermal properties, and extrusion of high-amylose starch acetates.* Carbohydrate polymers, 1996. **29**(1): p. 57-62.

5. Mittal, V., *High performance polymers and engineering plastics*2011: Wiley. com.

6. Page, I., *Polyamides as engineering thermoplastic materials*. Vol. 121. 2000: i, Smithers Rapra Publishing.

7. Solvay Specialty Polymers. 2013 [cited 2013 Sep 16]; Available from: http://www.solvayplastics.com/sites/solvayplastics/EN/specialty_polymers/Spire_Ultra_Polymers/Pages/Torlon.aspx.

8. Brydson, J.A., *Plastics materials*1999: Butterworth-Heinemann.

9. Rao, P.R. and P.V. Diwan, *Permeability studies of cellulose acetate free films for transdermal use: influence of plasticizers.* Pharmaceutica Acta Helvetiae, 1997. **72**(1): p. 47-51.

10. Kosuri, M.R. and W.J. Koros, *Defect-free asymmetric hollow fiber membranes from Torlon®, a polyamide–imide polymer, for high-pressure CO_2 separations.* Journal of membrane science, 2008. **320**(1–2): p. 65-72.

11. Lee, K.P., et al., *Toxicity of N-methyl-2-pyrrolidone (NMP): Teratogenic, subchronic, and two-year inhalation studies.* Fundamental and Applied Toxicology, 1987. **9**(2): p. 222-235.

12. Miyano, T., T. Matsuura, and Sourirajan, *Effect of polyvinylpyrrolidone additive on the pore size and the pore size distribution of polyethersulfone (victrex) membranes.* Chemical Engineering Communications, 1993. **119**(1): p. 23-39.

13. Lively, R.P., *Hollow fiber sorbents for post-combustion CO_2 capture, PhD Dissertation*, 2011, Georgia Institute of Technology.

14. Chung, T.s. and E.R. Kafchinski, *The effects of spinning conditions on asymmetric 6FDA/6FDAM polyimide hollow fibers for air separation.* Journal of Applied Polymer Science, 1997. **65**(8): p. 1555-1569.

15. Kosuri, M.R., *Polymeric membranes for super critical carbon dioxide ($scCO_2$) separations.* 2009.

16. Qin, J.-J., et al., *A high flux ultrafiltration membrane spun from PSU/PVP (K90)/DMF/1, 2-propanediol.* Journal of membrane science, 2003. **211**(1): p. 139-147.

17. Van de Witte, P., et al., *Phase separation processes in polymer solutions in relation to membrane formation.* Journal of membrane science, 1996. **117**(1): p. 1-31.

18. Hyun, S.H. and R.P. Danner, *Equilibrium adsorption of ethane, ethylene, isobutane, carbon dioxide, and their binary mixtures on 13X molecular sieves.* Journal of Chemical and Engineering Data, 1982. **27**(2): p. 196-200.

19. Chue, K., et al., *Comparison of activated carbon and zeolite 13X for CO_2 recovery from flue gas by pressure swing adsorption.* Industrial & Engineering Chemistry Research, 1995. **34**(2): p. 591-598.

20. Cavenati, S., C.A. Grande, and A.E. Rodrigues, *Adsorption equilibrium of methane, carbon dioxide, and nitrogen on zeolite 13X at high pressures.* Journal of Chemical & Engineering Data, 2004. **49**(4): p. 1095-1101.

CHAPTER 5

IDENTIFICATION AND TESTING OF SORBENT MATERIALS

5.1 Introduction

Sorbent particles are the main component of the hollow fiber system, and high capacity for CO_2, low regeneration energy, and reasonable temperature swing magnitude are key attributes required for the sorbent material. Identification of a thermally stable sorbent with a preferential adsorption of CO_2 over water and a low heat of sorption is the focus of this chapter.

As discussed earlier, an additional requirement for this research was the availability of the sorbent in large batches to allow formation of sufficient fiber sorbents. As noted in Chapter 4, the optimal dope composition had 33.5% by weight of sorbent (Table 4.4). Typically at least 150 g of dope is required to produce a sufficient amount of hollow fiber. Therefore at least 50 g of sorbent is required to spin a batch of hollow fibers at high sorbent loading (≈75% by weight). Many novel sorbents are not available in batches this size, which complicates their study in even small scale RTSA systems.

In this study, sorbents were typically tested to assess sorption capacity and kinetic performance of sorbent powders via TGA and packed bed experiments. Morover, incorporation into the fiber spinning process and sorption performance of the resultant fibers was investigated. Since the three fiber components (sorbent, matrix polymer and

lumen barrier) were being optimized simultaneously, it was found convenient to use 13X as the stand-in sorbent in experiments involving barrier formation and dope optimization trials, eventually to be replaced by more suitable sorbents.

5.2 Choice of Sorbents for CO_2 Capture

The first class of sorbents considered for CO_2 capture was zeolites. Zeolite 13X, the most commonly used adsorbent, exhibits a good swing capacity for CO_2. However, it is not practicable in wet feeds, as water competitively adsorbs [1], severely limiting CO_2 sorption capacity. It was hoped that by choosing zeolites with a small number of surface acid sites, (i.e. large Si:Al ratio) this preference for water may be overcome, because it is the presence of these active sites that causes competitive adsorption of water [2]. As an example of this, silicalite-1, the pure silica version of zeolite ZSM-5 (MFI framework), was identified for testing. While silicalite-1 has a lower capacity for CO_2 than 13X [3], it nominally has zero acid sites. Therefore it could potentially retain its CO_2 capacity in a wet feed environment [4].

Siliceous solids can be made better CO_2 adsorbents by making them more basic, thereby increasing the sorption capacity for the acidic CO_2. Zeolites are typically acidic compounds, but their alkali metal salts may be weakly basic; whereas amorphous silicas are usually neutral. Sorbents can be made more basic by one of three ways: amine-functionalization, nitrogen-substitution and cation-exchange [5]. Amine-functionalization is more applicable to amorphous silicas, whereas nitrogen-substitution and cation exchange are more relevant to zeolites.

Cation substitution can increase zeolite alkalinity by replacing less alkaline metal ions with more alkaline ones. Zeolites are Bronsted acids as their crystal structure has aluminum atoms occurring intermittently. Since aluminum is trivalent, it usually occurs with a hydrogen ion that renders the whole structure electrically neutral but acidic.

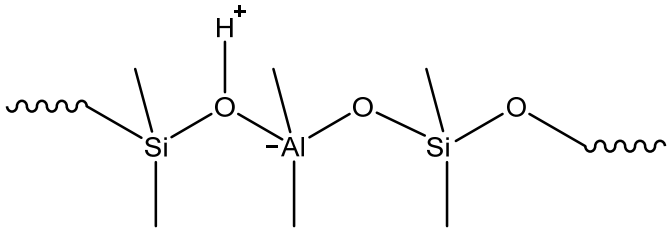

Figure 5.1: Zeolite framework with a Si-O-Al bridging cluster with the associated H+ ion.

The acidic H^+ shown in Figure 5.1 may be replaced with alkaline and alkaline earth metal ions to increase the alkalinity. Intuition suggests that larger, more alkaline atoms such as K, Rb and Cs will make the zeolites more alkaline than smaller ones like Na and therefore make for better CO_2 sorbents. In practice however, the smaller atoms like lithium provide a higher CO_2 capacity per gram of sorbent. This could be explained by the heavy Rb and Cs atoms increasing the zeolite density (lower porosity), in addition to the CO_2 dipole interaction being more pronounced for smaller atoms like lithium [6], leading to increased capacity. Cation substitution was not pursued in this work, especially since the focus was on low-aluminum zeolites like ZSM-5.

Treatment with amino-silanes is also not applicable for zeolites since they cannot penetrate many zeolite channels. However, zeolites can be treated with ammonia

or small alkyl amines to render them more basic. The mechanism of functionalization is also different from that of amine-grafting. Instead of covalently tethering amine groups to the pore surface, nitrogen may be directly incorporated in the silicate structure as well as in the surface silanol groups. At lower temperatures, the surface silanol groups get aminated, with preference for amination of the Si—OH···Al acid sites [7].

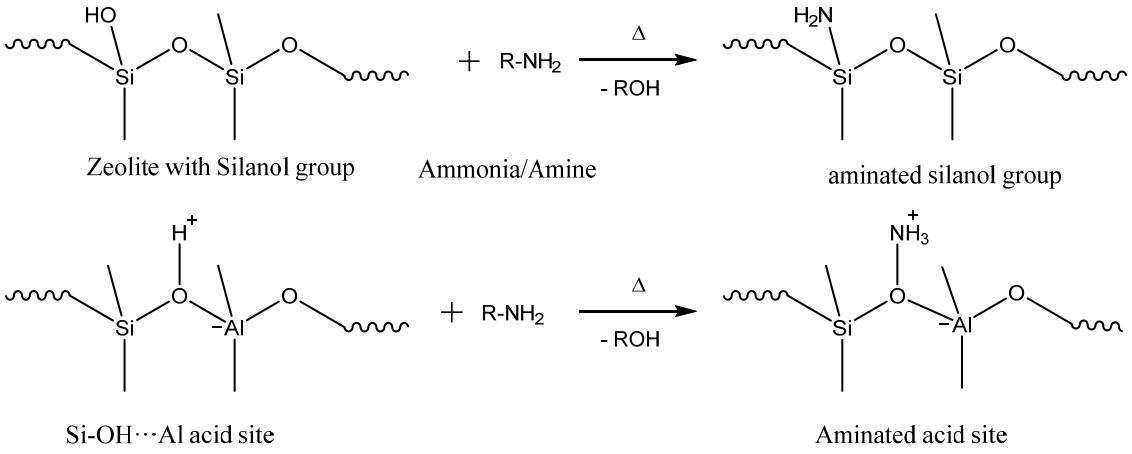

Figure 5.2: Reaction of ammonia with zeolite resulting in amination of acid sites.

At higher temperatures, the ammonia attacks the oxygen atoms in the silicate framework itself. Nitridation, or nitrogen-substitution, describes such a method where the oxygen atoms in the "silyl ether" groups that form the silicate skeleton are replaced by nitrogen atom to form more basic "silyl amine" groups [8]. There is evidence that the nitrogen substitution itself does not affect the zeolite crystal structure since it is a simple exchange of oxygen for nitrogen atoms [9]. The following schematic illustrates the chemistry of nitrogen substitution near silicon and aluminum atoms in the silicate matrix.

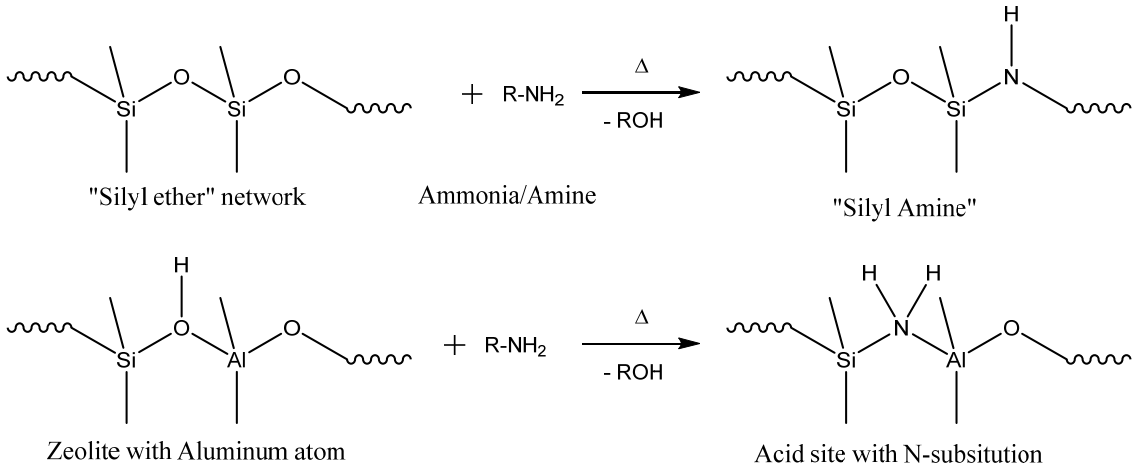

Figure 5.3: Nitrogen substitution of framework oxygen atoms.

The primary requirements for nitridation are high temperature and removal of the water formed when ammonia is used as the nitrogen source. Literature reviews indicate that temperatures higher than 500 °C are required to break the Si-O bond but nitridation may be achieved at 550-850 °C [10] or even lower [11]. At higher temperatures, there may be a loss of zeolite crystallinity, so in this work, ammonia treatment was carried out at 550 °C at low pressure to remove moisture formed.

Amorphous silicas such as MCM-48 are atomically disordered as the name suggests, but are synthesized in such a manner that they have medium-range (≈100 Å) ordering, and at longer scales (1 μm), even exhibit facets [12, 13]. An additional aspect of the medium-range ordering is that the silicas contain large channels in the mesopore size regime [14]. This makes them mesoporous molecular sieves analogous to the microporous zeolites. MCM-48, for example, has ordered 3-dimensional channels in the size range 20-100 Å, as shown in the Figure 5.4.

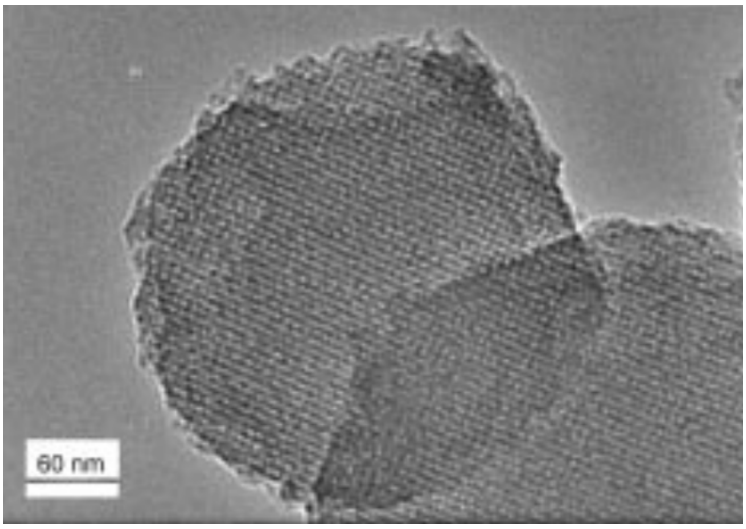

Figure 5.4: TEM image of MCM-48 showing mesopore channels [15].

Apart from improving transport through the solid phase, these channels provide an immense internal surface area that allows functionalization of the silica surface with organic amine compounds [16, 17]. This is a means of increasing the alkalinity of solid sorbents that is not afforded to zeolites, which have sub-nanometer pores. Organic silanes containing amine groups can be tethered to the channel walls, simulating an amine system where the amines are not in solution and the amine recovery process is much less energetically expensive. Such sorbents may be referred to as solid amines. Additionally, amine-CO_2 sorption chemistry makes the presence of moisture favorable to the adsorption of CO_2 by encouraging the formation of bicarbonates and carbonates. This is a huge advantage in the context of flue gas capture, where the feed gas is often moisture-saturated. However, solid amines, which exhibit chemical adsorption, have a higher heat of sorption than zeolitic sorbents, which undergo physisorption (Section 2.2.6).

The rest of this chapter discusses, in series, the attempts to produce and incorporate CO_2 sorbent materials into the hollow fiber setup. The relative performance of different sorbents not just in themselves but their suitability for hollow fibers is studied.

5.3 13X Sorbent in Torlon® Fibers

In this work, moisture-saturated zeolite 13X was used as the stand-in sorbent for many purposes: for example, to test a new matrix polymer (Torlon®), or to produce fibers for developing barrier deposition procedures. It was thought to be prudent to use the readily available 13X for these experiments, then replace it with practicable sorbents like ZSM-5 once the risks of wastage or failure were diminished. For example, 13X was used while optimizing the dope composition for Torlon®-based fiber sorbents; and the characterization of the 13X in those fibers was used to validate the suitability of Torlon® as a matrix polymer. The fibers thus produced have been described in Section 4.4. The 13X retained its swing capacity and kinetics in TGA sorption experiments, validating the ability of Torlon® to form open, porous networks.

Subsequently, 13X was used in experiments to co-extrude an internal barrier layer along with the fiber sorbents, the results of which are discussed in Chapter 6. In addition, 13X was subjected to ammonia treatment to incorporate amine groups in the aluminosilicate framework, potentially improving the CO_2 capacity and overcoming the competitive water sorption.

5.4 Aminated Silicas

Amine-functionalized mesoporous silicas were also targeted for assimilation into the fiber sorbent work. MCM-48 silica with covalently bound amines was obtained from Exxonmobil and its sorption capacities were studied in the TGA.

5.4.1 MCM-48 TGA sorption

The as-received sorbent was found to have a working capacity of 0.43 mmol CO_2/g between 45 °C and 100 °C at 0.1 atm CO_2 partial pressure. TGA thermal cycling was also performed with a wet helium feed and with a simulated wet feed of 7-8% CO_2, 2-3% H_2O and remainder helium. The CO_2 capacity in wet feed was then estimated as the difference between the sorption capacities in He-H_2O and He-H_2O-CO_2 feeds.

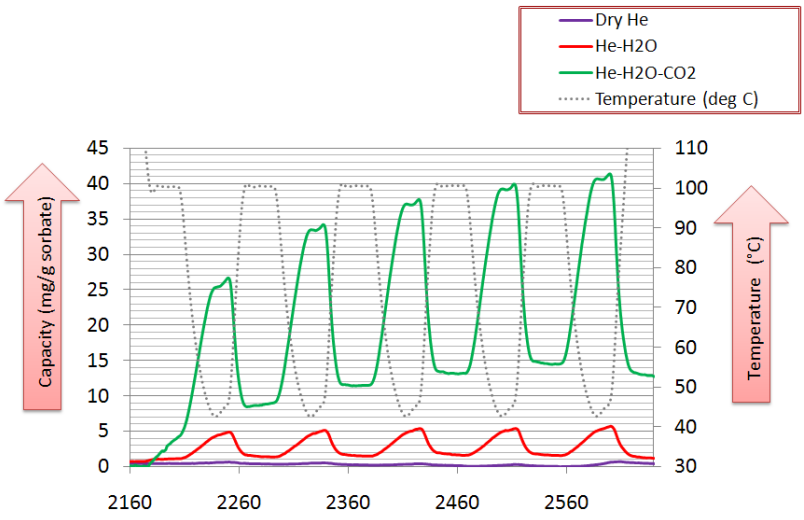

Figure 5.12: Thermal cycling of amine-functionalized MCM-48 in wet CO_2 feeds showing the enhanced sorption of CO_2 in wet feeds. (Horizontal axis is time in seconds)

This calculation returns a conservative value for the sorption capacity for CO_2 because it assumes water in the He-H_2O-CO_2 mixture adsorbs independently, when in fact CO_2 is the favored sorbate and water adsorbs largely in conjunction with CO_2. Still, the experiment provides a useful way to determine if a sorbent is likely to retain any capacity for CO_2 in the presence of moisture, and helps weed out hydrophilic sorbents. The as-received sample of MCM-48 had a slightly enhanced working capacity of 0.46 mmol/g in such an experiment.

5.4.2 Syringe extrusion of CA/MCM-48 fibers

The silica sample was then prepared for incorporation into a cellulose acetate dope. Problems arose while trying to incorporate the MCM-48 into the fiber dope to attempt a "syringe extrusion", a small-scale exploratory fiber extrusion technique. It was difficult to disperse the silica in the dope and its extremely low density made the dope difficult to stir, so the dope had to be diluted prior to mixing. Even after dilution, visual inspection suggested that the sorbent was incompletely dispersed.

In addition, dynamic light scattering (DLS) experiments suggested that the silica particles were prone to form aggregates as large as 20 μm. The sample was subject to size-classification via centrifugation and size-reduction via milling. The first method involved settling a suspension of the sorbent in water for 1 hour and collecting the supernatant suspension which was then centrifuged to recover the sorbent. This method was expected to exclude the heavier agglomerates which would have settled out of the

suspension. The second method involved shaking the sample (without grinding medium) in a ball mill (Spex Sampleprep 8000M shaker mill).

While these methods were effective in obtaining smaller sized silica particles, the sorption capacity was severely affected, as shown in Table 5.2.

Table 5.2: Degradation of CO_2 capacity in processed MCM-48 sample

MCM-48 Sample	Working Capacity (mmol CO_2/g)	Average particle size via DLS (μm)
As-received	0.43	20
Settled in water, centrifuged	0.25	0.73
Ball-milled for 30 min with no grinding medium	0.25	5

Ball milling with ceramic grinding media was found to be especially destructive to the sorbent integrity and was abandoned. More disturbingly, there was significant reduction in the sample capacity even in the relatively benign processing step involving centrifugation and air-drying; hence the sample was not expected to withstand the dope preparation process which involves sonication and stirring under heat.

To investigate this suspicion, the as-received MCM-48 sample was loaded into the cellulose acetate dope (target final loading 42% by weight), and syringe-extruded to produce solid fibers. The dried fibers were subjected to thermal cycling in the TGA

under a dry CO_2 feed, at which point they only yielded a cycle capacity of about 0.13 mmol CO_2/g, as opposed to an expected capacity of 0.19 mmol/g. The reduction in capacity during dope preparation and separation processes such as centrifugation was attributed to the thermal and hydrolytic degradation of the aminated sorbent. This, in addition to the relatively low loading that could be achieved with amine-functionalized silica, led us to focus on sorbents with good mechanical stability that could be loaded more readily into the sorbent dope. It is still possible that with a mono-disperse, more mechanically stable silica base, amine-functionalized sorbents could endure the dope preparation process. High nitrogen-loading of the sorbent, if achieved, could compensate for its low mass loading in the fiber, thereby producing high-capacity fiber sorbents.

5.5 13X Nitridation and Testing

Nitridation, or nitrogen substitution, was attempted on zeolite 13X to increase its basic nature. Nitrogen substitution has been used to improve the catalytic properties of zeolites for certain reactions [8], but it was envisioned that this would also improve its CO_2 capacity.

5.5.1 Nitridation procedure

About 100 g of 13X was placed in a quartz tube provided with a fritted disc halfway down the length of the tube. Argon and ammonia gas connections were provided such that the fritted disc was downstream of the 13X sample. A gas sweep could then be provided over the sample, with the porous fritted disc preventing it from being

blown downstream. The quartz tube was placed in a tube furnace and heated to 550 °C. The schematic of the experimental setup is as follows.

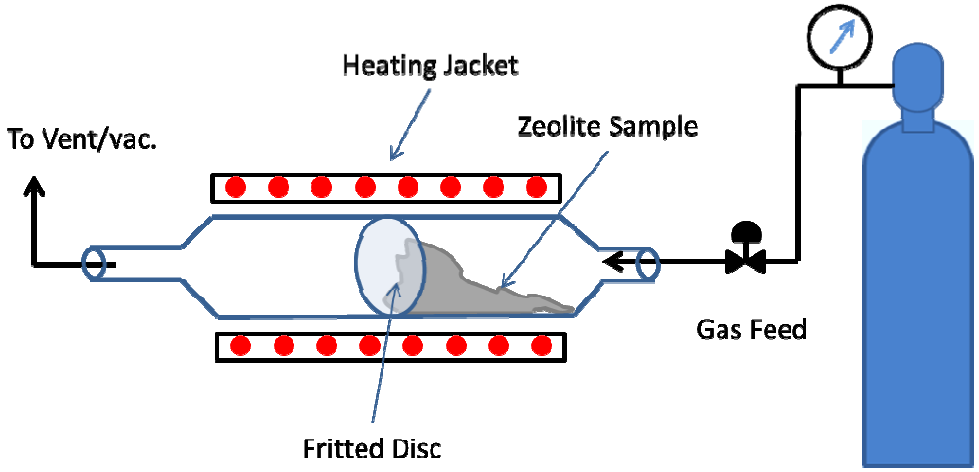

Figure 5.5: Experimental setup for zeolite nitridation under ammonia flow at 100 torr.

The upstream was sealed and the tube was held under vacuum overnight to dehydrate the sample. Nitridation was performed by flowing ammonia gas at 10 torr for 10 hours at 550 °C, following which the sample was cooled to room temperature.

5.5.2 Characterization of Nitrided 13X

The nitrided samples were analyzed under SEM and no change in the crystal size was observed.

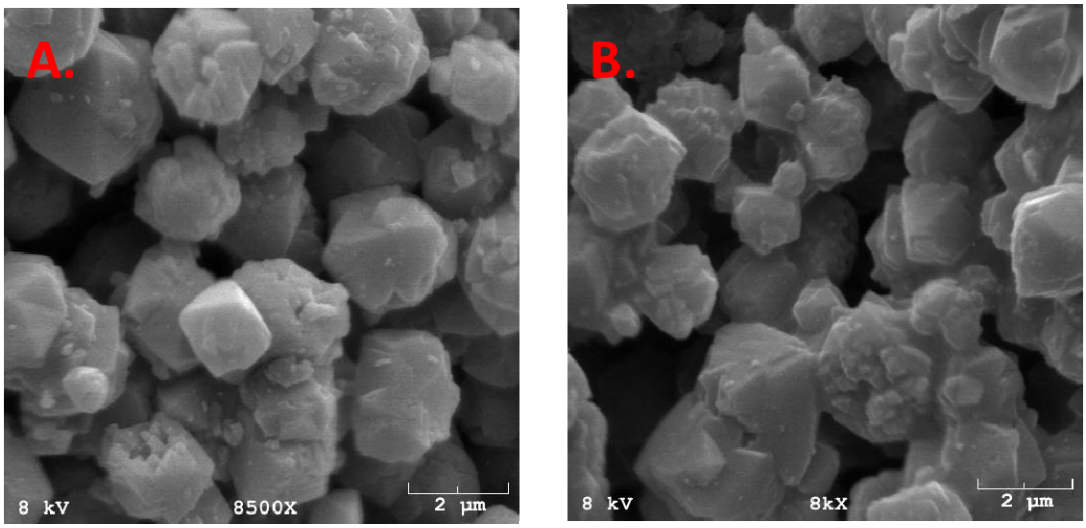

Figure 5.6: SEM images of A. untreated zeolite 13X and B. 13X after nitridation with ammonia at 550 °C.

5.5.3 TGA Analysis of Nitrided 13X

The nitrided 13X was subjected to TGA thermal cycling to measure the CO_2 sorption capacity. The experimental protocol utilized the 36-hour drying procedure followed by cycling between 45 °C and 100 °C that was described in Chapter 3.

5.5.3.1 Thermal cycling under dry CO_2

TGA sorption was performed under dry 10% He/ 90% CO_2 mixture. The drying step showed a smaller decrease in mass than in un-treated zeolite and fiber samples (5% weight loss for nitrided 13X vs. 18% for other samples), but this was to be expected since the nitrided zeolite had not yet adsorbed moisture and CO_2 from the atmosphere. The averaged CO_2 capacities were 1.53±0.16 mmol/g 13X at 45 °C and 0.49±0.16 mmol/g at 100 °C, which yielded a working CO_2 capacity of 1.05 mmol/g

between these temperatures (Figure 5.7). This is not significantly different from the CO_2 capacity of untreated 13X (Section 4.4.2.4), indicating that nitridation had not significantly improved CO_2 affinity.

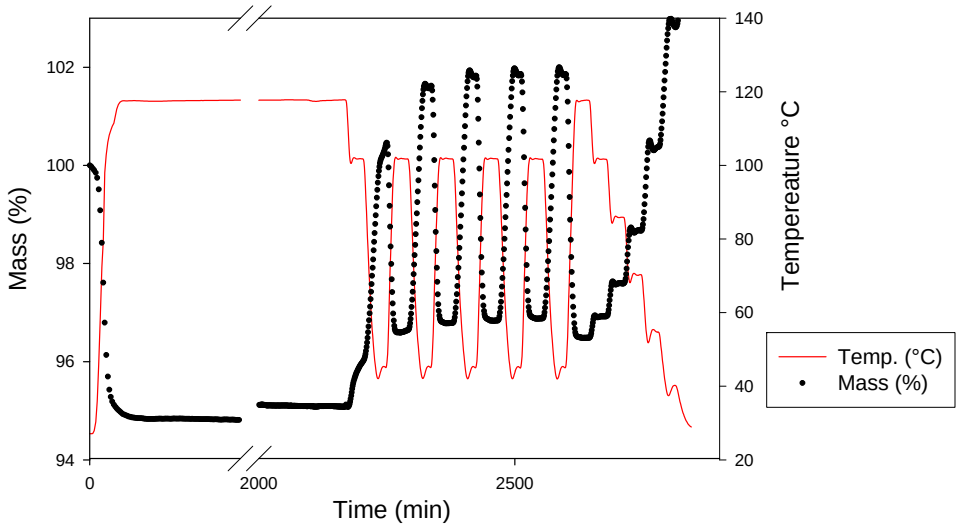

Figure 5.7: Thermal cycling of nitrided 13X in a 10% CO_2 atmosphere at atmospheric pressure. The sample showed rapid response to the thermal signal and the CO_2 capacity showed no significant increase due to post-treatment.

The sample was also cycled repeatedly under a dry 10% CO_2 feed between 145 and 100 °C. In spite of an observed drift in the mass measurement, the 13X was found to retain its capacity over 16 cycles in 24 hours, yielding a swing capacity of 1.06±0.05 mmol/g (Figure 5.8). These experiments showed that, while nitridation experiments did not appear to have increased the CO_2 capacity significantly, the treated solid was still stable and retained its sorption kinetics.

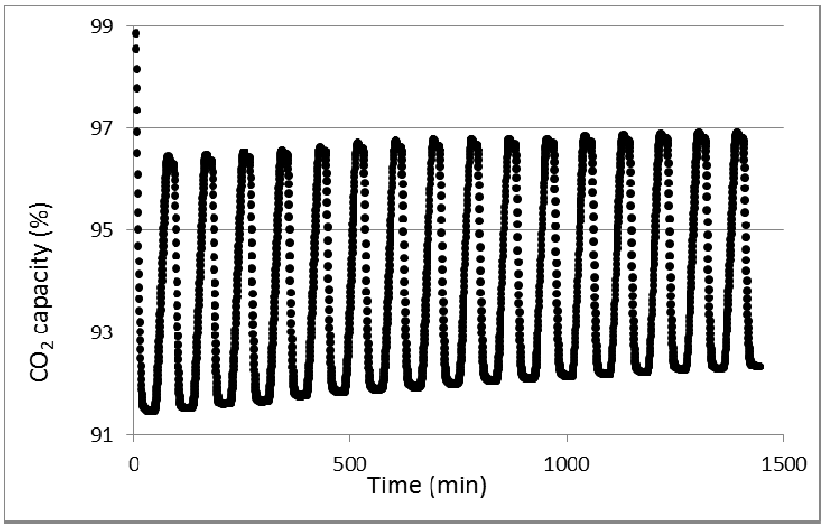

Figure 5.8: Thermal cycling of nitrided 13X between 45 and 100 °C under 10% CO_2 showed that there was no change in the CO_2 capacity on repeated cycling.

5.5.3.2 Thermal cycling under wet feed

The nitrided zeolite was also tested under moisture-saturated He and He-CO_2 gas feeds. The experimental setup for wet TGA sorption measurement was discussed in Section 3.4.5. In each case, the sample was dried under helium flow at 115 °C and then exposed either to helium gas or 10% CO_2/ 90% He mixture that had been saturated with moisture by passing through the water-containing bubbling apparatus.

The TGA results for both experiments showed the zeolite showed an accumulating, irreversible sorption over the course of the experiment that had not been observed in CO_2 sorption. This is characteristic of water adsorption on activated 13X [18], a sign that nitridation had not succeeded in suppressing 13X preference for water.

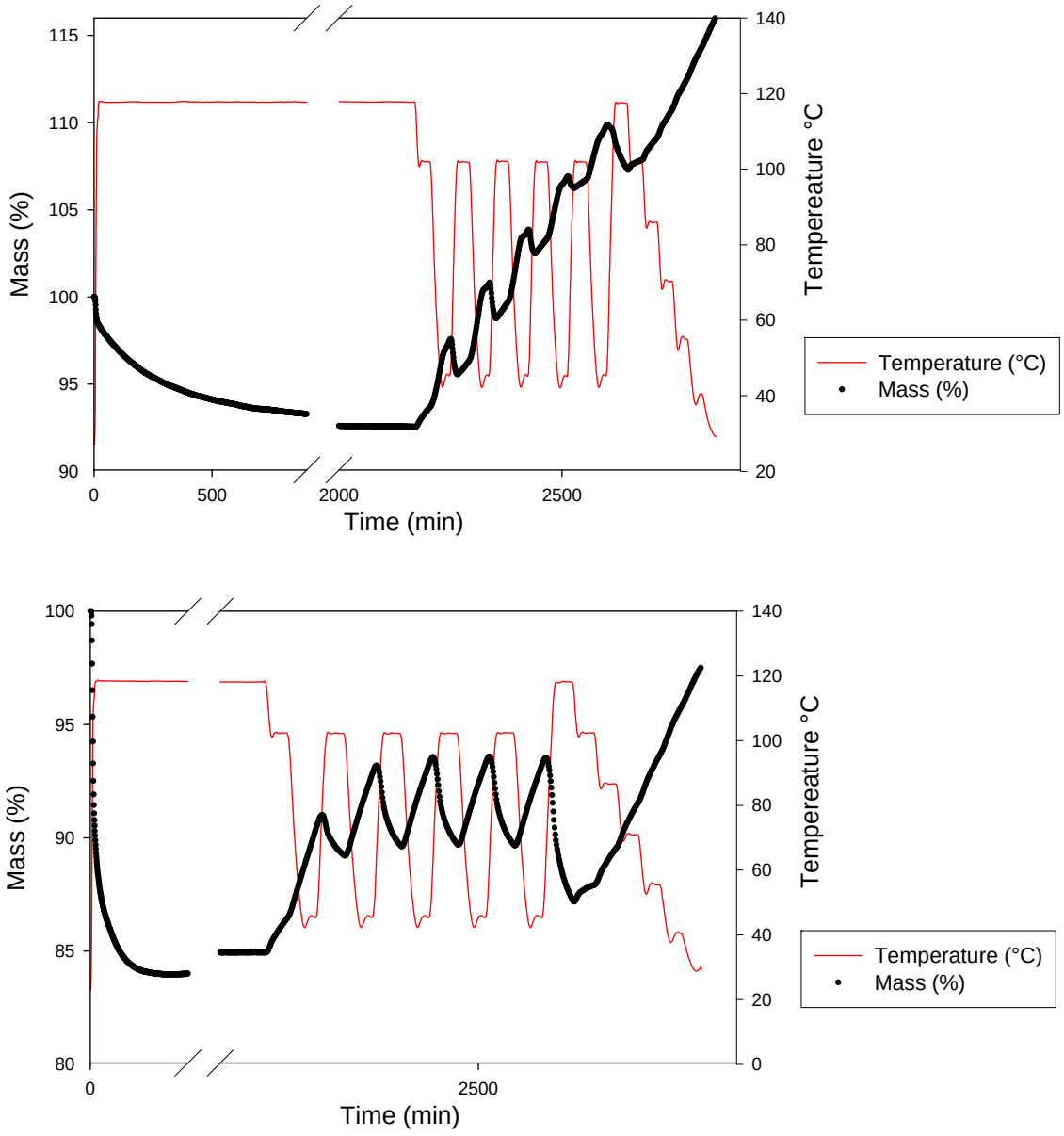

Figure 5.9: TGA sorption of nitrided 13X under (1) wet CO_2-He feed and (2) wet helium feed. An irreversible water uptake is observed when the zeolite is exposed to the wet gas feed.

Despite the above complications, the swing capacity between 45 °C and 100 °C was estimated and expressed as mass of total adsorbate adsorbed rather than in

mmol/g. The results are tabulated below and indicated that the swing capacity of wet CO_2/H_2O feed was about the same as that of just wet helium.

Table 5.1: Working capacity of Nitrided 13X for different gas feeds.

Gas Feed	Working Capacity (g/100 g)	Working Capacity (mmol/ g)
He-H_2O	4.5±0.16	2.49±0.09
He-CO_2	4.6±0.24	1.05±0.05
He-CO_2-H_2O	4.45±0.79	---

These results suggested that nitridation was not helpful in suppressing water adsorption in 13X. This could possibly be because amination, rather than nitridation had occurred. Amination of zeolites is easily reversed via hydrolysis. Stability of nitrided products at high temperatures and in the presence of moisture has been called into question before [19, 20], and my studies support these concerns.

5.5.4 Attempt to incorporate nitrided 13X into spin dope

A trial spin was attempted with the nitrided 13X, with the dope composition discussed previously in Chapter 4 (Table 4.4). Unfortunately, when the nitrided zeolite was added to the dope being prepared, there was significant degassing of the sorbent with vigorous bubbling. Fumes rose from the dope along with a strong smell of ammonia and the dope was stored in the lab hood until the bubbling subsided. The

cooled dope was found to be dark grey in color and was more viscous than usual. Mixing the dope with the anchor impeller did not improve its consistency and eventually it had to be discarded.

The unsuccessful experience with trying to incorporate nitrided 13X in the spinning process suggested that the nitridation was easily reversible and could not endure the dope mixing process. It is likely that amination (Figure 5.2), rather than actual nitridation was the predominant process occurring, since amination is easily reversed by hydrolysis. Furthermore, there was no evidence of enhanced CO_2 adsorption under wet feeds as demonstrated by TGA analysis. At this juncture, it was decided to explore other options for hydrophobic sorbents rather than expend more energy on a modification process that had only been applied to catalysis hitherto.

5.6 Silicalite-1 as a hydrophobic sorbent

Silicalite-1, the pure silica form of ZSM-5 [21] is a hydrophobic zeolite with channels that allow transport in 3 directions (Figure 3.3). The MFI crystal structure is formed during synthesis via a liquid crystal templating mechanism, where a bulky organic molecule such as tetrapropylammonium hydroxide (TPAOH) provides the template for the condensing silicalite structure. This allows the zeolite to be synthesized free of aluminum ions, thus yielding an infinite Si: Al ratio. However, since it could not be sourced commercially like many other zeolites, lab synthesis of silicalite-1 was undertaken to establish that it could be produced in the lab if needed.

5.6.1 Silicalite-1 lab synthesis

Silicalite-1 was synthesized in the lab using a TPAOH-based recipe [22] in a round-bottomed flask with reflux. The target yield was 5 g; however when the sample was dried, ground and calcined, the ultimate yield was only around 2 g. An XRD of the sample revealed that it closely resembled that in literature [22].

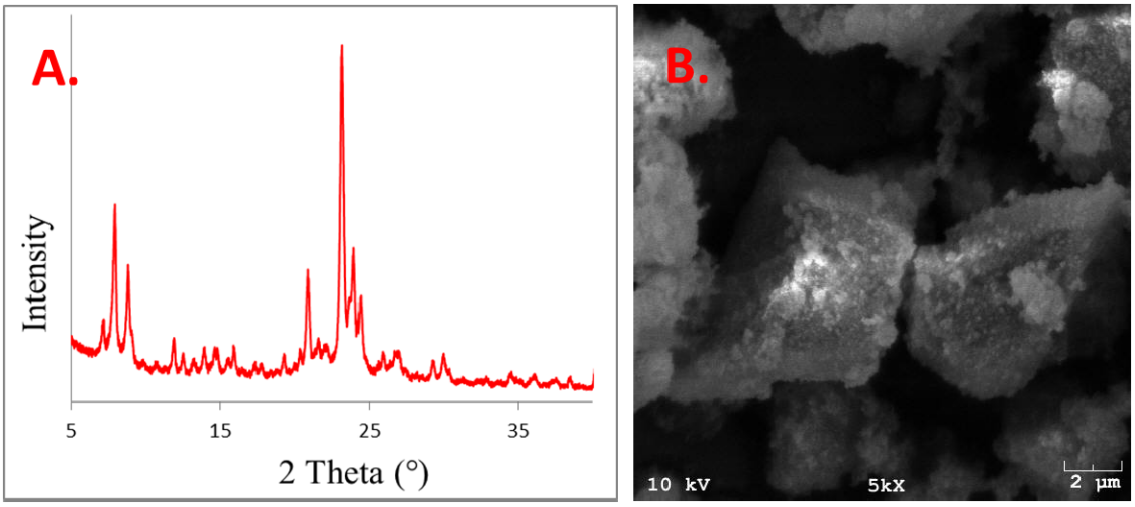

Figure 5.10: (A) X-ray diffraction pattern of lab-synthesized silicalite-1 matched that in literature, (B) SEM imaging of the powder revealed particles larger than suggested by DLS measurements, suggesting a mix of smaller particles along with larger crystals and aggregates.

Dynamic light scattering experiments suggested an average particle size at 130-150 nm with less prominent peaks at 638 nm and 5207 nm. SEM images revealed a mix of particle sizes along with the presence of aggregates and some larger crystals.

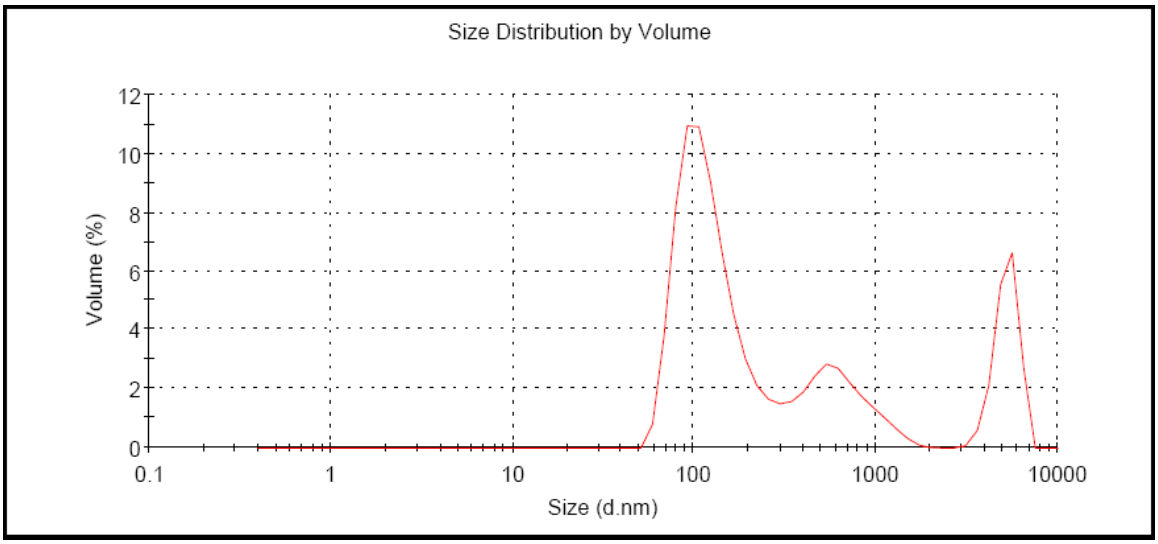

Figure 5.11: Dynamic Light Scattering of lab-synthesized silicalite-1 showing three distinct peaks at 124, 638 and 5208 nm with 62.3 volume % of the sample lying in the 124 nm region.

The major drawback of synthesizing silicalite-1 in the lab was the small batch size. The process would have to be scaled up to a larger glass reactor to be feasible for fiber spinning. However, the size distribution of the silicalite is sensitive to the batch size and it is conceivable that scaling up the reaction size would cause the formation of large crystals. This was resolved when ZSM-5 with very high silica content was provided by our collaborators at Exxonmobil and proved to be an adequate replacement for the pure-silica form. Work was then transitioned to incorporating the ZSM-5 into the hollow fiber platform.

5.7 High-silica ZSM-5 as hydrophobic sorbent

High-silica ZSM-5 samples were obtained from Exxonmobil and screened for suitability for addition to the hollow fiber platform. However, batches were only

chosen if they were sufficiently size-reduced to less than a micron with no aggregates. The following sections discuss the performance of high silica ZSM-5 (≈750 SiO_2/Al_2O_3) with a sub-micron particle size distribution and a very uniform particle size distribution.

5.7.1 ZSM-5 characterization and sample dope preparation

High silica ZSM-5 with a reported SiO_2/Al_2O_3 of 750 was scanned via EDX (Energy-Dispersive X-ray spectroscopy) to verify the SiO_2/Al_2O_3 ratio. However, there was a considerable variance in SiO_2/Al_2O_3 results, at 128.6±22.4. It was realized that the alumina content was too low to be reliably estimated via EDX.

The sorbent was then incorporated into a CA based dope and extruded through a syringe to produce solid fibers of the sort described in Section 3.2.5. An SEM micrograph of fibers thus produced is shown below.

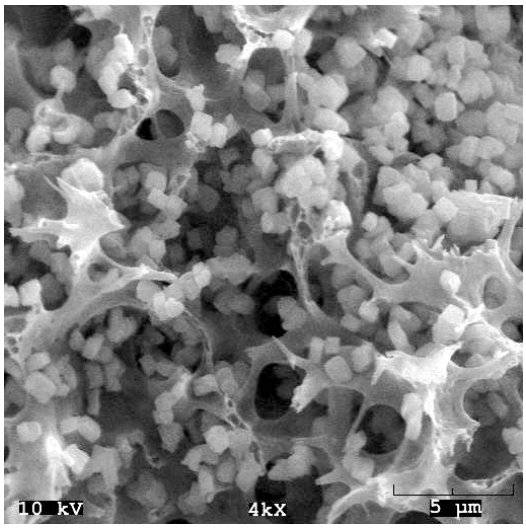

Figure 5.12: High-silica ZSM-5 in CA matrix at 75% mass loading of sorbent.

Mock fiber extrusion was done to establish the feasibility of dope preparation with ZSM-5 and to study the effectiveness of dispersion. It was observed that ZSM-5 could be readily incorporated into the spin dope at high loadings, like 13X zeolite, and formed a similarly open-porous pore network. The crystals also proved to be very monodisperse and showed minimal aggregation in the fiber. Cellulose acetate was eventually replaced with Torlon® but first, sorption characterization of the ZSM-5 powder was undertaken.

5.7.2 ZSM-5 sorption characterization

5.7.2.1 TGA thermal cycling

The CO_2 capacity of ZSM-5 was measured via TGA and packed bed sorption experiments. The sample was loaded into the TGA and thermal cycling was performed as described in Section 3.4.5 under three gas feeds: dry helium, moisture-saturated helium and moisture-saturated 90% He/ 10% CO_2. The dry helium feed showed no significant sorption on cycling, but the wet helium and wet CO_2-He showed evidence of sorption and desorption.

Since water outcompetes CO_2 on other hydrophilic sorbents such as 13X, it was decided that the CO_2 capacity on ZSM-5 would be inferred by subtracting the swing capacity for wet helium from the wet capacity for wet CO_2-He. Such a calculation would be at best a conservative estimate of sorbed CO_2; however, this provided a quick way to determine if the sorbent was viable in a wet feed, since hydrophilic sorbents

subjected to such a treatment generally showed no additional CO_2 sorption in the CO_2 containing feed. In addition, the wet helium sorption was performed first, before performing He-H_2O-CO_2 sorption on the same sample, thereby further ensuring that any CO_2 adsorbing would do so on a sample that already had sorbed moisture. The high-silica ZSM-5 showed increased capacity in the CO_2-containing feed, indicating that it was a viable wet feed sorbent. The plot of the mass change on cycling between 45 °C and 100 °C is provided below, with the initial mass normalized to 100. Since the sorption experiments are performed in series, the initial state for each experiment is slightly different, in spite of the 36-hour drying procedure; hence only the swing capacities are calculated here as they are the effective functional capacities of the sorbent.

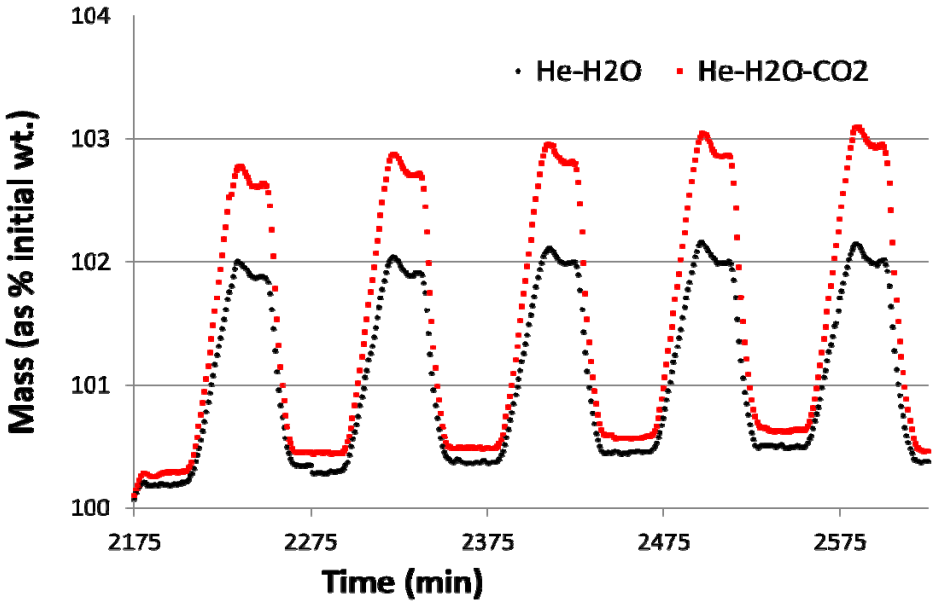

Figure 5.12: TGA thermal cycling data for high-silica ZSM-5 in CA matrix at 75% mass loading of sorbent.

The working capacity (or swing capacity) under mixed CO_2-water feeds was expressed in mass rather than moles because of the inability to differentiate sorbed

CO_2 and H_2O. The difference in capacities yielded a value of 0.81±0.11 g CO_2/100g sorbent, or 0.18±0.02 mmol CO_2/g sorbent.

Table 5.3: Working capacity of high-silica ZSM-5 for different gas feeds.

Gas Feed	Working Capacity (g/100 g)	Working Capacity (mmol/ g)
He-H_2O	1.57±0.04	0.87±0.02
He-CO_2-H_2O	2.38±0.1	---
Residual CO_2 Capacity	0.81±0.11	0.18±0.02

The results above indicated that high-silica ZSM-5 was a viable CO_2 sorbent even in the presence of moisture. Further sorption characterization was performed in a flow system, with a mass spectrometer to determine the exact amount of CO_2 sorbed.

5.7.2.2 ZSM-5 packed bed sorption

The sorbent was then loaded in a cell that allowed the capacity to be measured in a flow system. The cell was simply an in-line filter casing normally used to strain spin dopes, whose ends were plugged with glass wool to hold the sample. The sample was carefully weighed prior to being loaded into the cell. The sample cell was wrapped in heating tape to dry the sample in-situ. The sorption setup and experimental procedure for kinetic sorption experiments have been described in Section 3.4.4. The gas

mixture used was a moisture-saturated 10% He/10% CO_2/80 % N_2 mixture (by volume). Nitrogen acted as the sweep gas and Helium was the inert tracer, with CO_2 and H_2O as the probe gases. Helium was important as a means of gauging the backmixing and axial dispersion in the system [18]. In an ideal system with no adsorption and no backmixing (inviscid flow with flow channels always parallel to each other), both CO_2 and helium would remain in the system only as long as it would take them to traverse the length of the output bed. Hence both the sorption and desorption curves would be sharp step signals that take time $\left(\frac{l}{v}\right)\left(\frac{\tau}{\varepsilon}\right)$ seconds to exit the bed, where l is the bed length (m), v is the local velocity (m/s), τ is the tortuosity and ε is the porosity- this is the residence time of the system. In a real system, backmixing in the flow channels and viscous flow all combine to produce a range of residence times rather than one universal residence time, which manifests itself as a sigmoid output rather than a step output as shown in Figure 5.13.

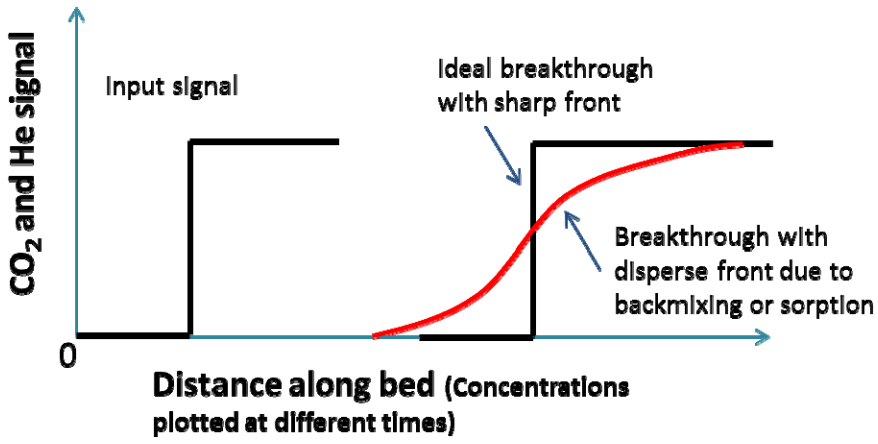

Figure 5.13: Schematic of ideal and real output signals for a packed bed that is subjected to a step change in the gas concentration.

In a non-adsorbing system, this dispersed concentration front is identical for CO_2 and He, and reflects the non-ideality of the flow system: fiber packing, short-circuits in the bed and pore structures that are length-wise discontinuous but still accessible. The degree of spread of the breakthrough curve is thus an indicator of the system design efficacy.

In sorbent bed systems, there is an offset between CO_2 and helium signals due to sorption, since He is essentially non-sorbing. Infinitely fast sorption would simply separate the CO_2 and helium signals without changing the shape of the CO_2 curve. This may be mathematically described as an additional residence time for CO_2 but not helium. However, CO_2 has finite sorption kinetics, which, in addition to thermal effects, causes the CO_2 curve to spread out more than the helium front. For example, fiber sorbents with occluded sorbent particles show a greater CO_2 spread than ones with readily accessible sorbent. Thus, providing an inert tracer like helium allows distinction between system-derived lags and sorption-derived lags. In practice, this means that the CO_2 breakthrough curve can simply be subtracted from the helium curve to eliminate system non-idealities and only study CO_2 sorption. Sorption experiments were performed on the sorbent powder as well as fiber sorbents.

Initially, sorption was performed on a packed bed of high-silica ZSM-5 to study its performance in wet feeds. The probe gas (10% He, 10% CO_2 and rest nitrogen by volume) had already been passed through the water-containing bubbling apparatus till the water signal was constant. This was done to ensure that the water in the bubbler was at equilibrium with the mixed gas feed when it was turned on again. After the bed was

online, it was flushed with nitrogen to remove the last traces of moisture, and the wet feed was turned on. The bed effluent was probed with a mass spectrometer and the breakthrough curves for helium and CO_2 were plotted. It was difficult to control the water vapor concentration even with nitrogen flushing; however, the water concentration remained at 4.64% by vol. during sorption.

The CO_2 and helium breakthrough plots are provided in Figure 5.14. The CO_2 sorption capacity, measured as the difference between the areas under the CO_2 and He breakthrough curves, was found to be 0.462 mmol of CO_2/g sorbent at 35 °C. Thus, the experiment proved that high-silica ZSM-5 readily adsorbed CO_2 even in the presence of moisture. In the packed bed experiment, the CO_2 breakthrough occurred very early and breakthrough capacity was less than 10% of the equilibrium capacity.

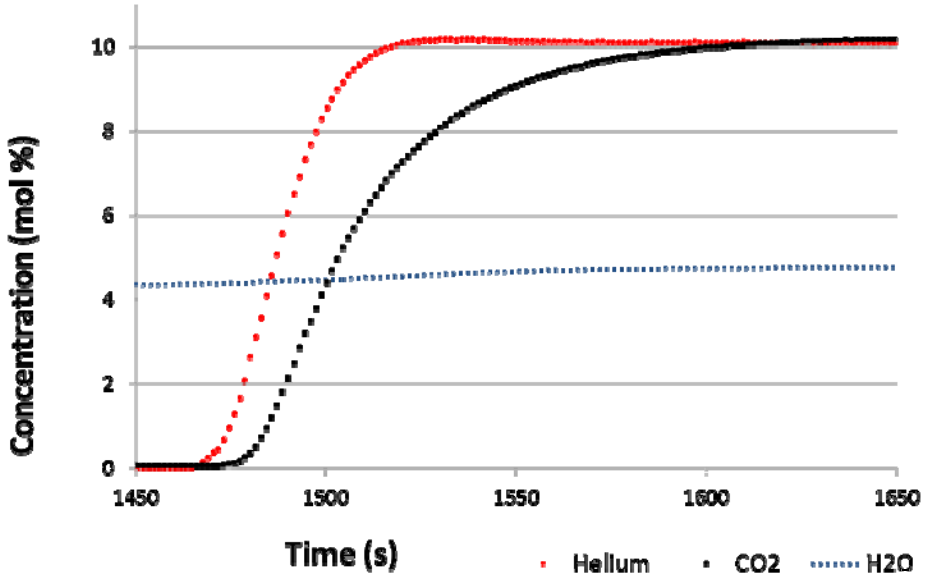

Figure 5.14: Helium and CO_2 breakthrough curves for High-silica ZSM-5 in the presence of moisture.

Having found that high-silica ZSM-5 could effectively sorb CO_2 in wet gas feeds, steps were taken to incorporate this material into Torlon®-based fibers.

5.7.3 Fiber Spinning with ZSM-5

With evidence that ZSM-5 exhibited CO_2 sorption in wet feeds, a spin was planned using this as the sorbent in Torlon® fibers. The dope composition and spin conditions for Torlon® fibers had already been optimized and have been provided in Table 4.4. The spin conditions were as follows.

Table 5.4: Spin conditions for ZSM-5/Torlon® at 75% target loading

Spin Parameters	
Core Flow Rate	800-1000 ml/hr
Bore Flow Rate	300 ml/hr
Bore Composition	20:80 Water: NMP
Operating Temperature	50 °C
Take-up Rate	20 m/min
Air Gap	3 cm

5.7.3.1 Spin Results

The ZSM-5 was readily incorporated into the Torlon® dope at high loading. Large-diameter fibers could be easily spun with no breaks even at elevated spin temperatures (50 °C). The fibers were solvent-exchanged and dried as described

previously; then the fiber dimensions, capacity and permeance were measured. TGA burn off experiments revealed that the fibers contained 71.4% by weight of dry sorbent.

5.7.3.2 SEM Analysis

SEM imaging confirmed that the fibers contained fewer and less prominent macrovoids than in previous spins. The pore structure was examined and found to be porous, with uniform dispersion of the zeolite crystals.

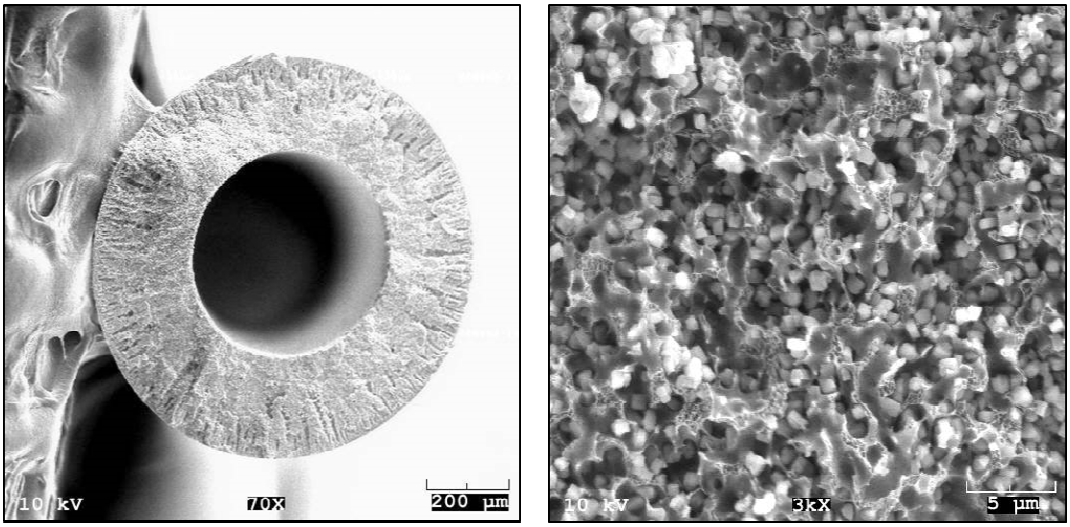

Figure 5.15: Cross-section of fiber sorbents showing (A.) reduced macrovoids and good concentricity, and (B.) fiber pore structure with zeolite crystals well-dispersed in the open polymer matrix.

5.7.3.3 Permeance Measurement and Porosimetry

Nitrogen permeance measurements were performed on fibers with outer diameters 1539 µm (determined from SEM imaging) and the permeance was plotted

against average system pressure to estimate the fiber pore dimensions. The permeance data is shown in the following figure.

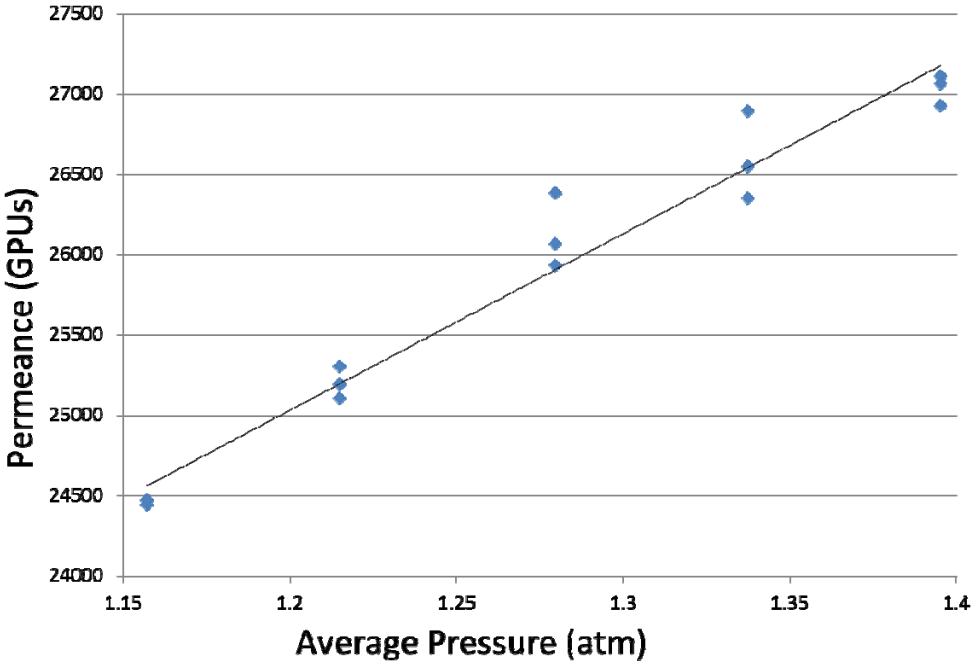

Figure 5.16: Plot of N_2 permeance vs. average system pressure for fiber sorbents spun with high-silica ZSM-5. Fiber O.D was 1539 µm.

The ratio of Knudsen to Poiseuille contributions to gas flux, measured as (Intercept/ (Slope*average p)) (Section 2.2.5) was 17.7, which implies that the Knudsen contribution to flow dominated over Poiseuille contribution at the test conditions. The ratio of slope to the intercept in the permeance vs. pressure curve was used to estimate the average pore diameter based on Knudsen diffusion. For fibers spun as above, the d_{pore} was estimated to be 837 nm. Nitrogen has a mean free path of 74.2 nm at the average test pressure. This implies that the diffusion primarily occurs in the transition region between Knudsen and molecular diffusion.

5.7.3.4 TGA Analysis

Fiber samples from this spin were loaded into the TGA and thermally cycled between 45°C and 100 °C under different gas feeds. As in previous experiments, TGA sorption was performed under He-CO_2-H_2O and He-H_2O mixtures and the difference between the two cycle capacities was deduced to be that of CO_2 in wet feeds. It was mentioned that such a capacity would be a conservative estimate since an implicit assumption there was that the CO_2-H_2O sorption competition was adversely affecting CO_2 sorption but not H_2O sorption. For the Torlon®-ZSM-5 fibers, an additional thermal cycling was performed under dry He-CO_2 mixtures to determine the cycle capacity under dry conditions.

Table 5.5: Working capacity of Torlon®/ ZSM-5 for different gas feeds.

Gas Feed	Working Capacity (g/100 g)	Working Capacity of relevant component (mmol/ g)
He-H_2O	1.21±0.2	0.67±0.11 **(H_2O)**
He-CO_2-H_2O	1.69±0.22	---
Residual CO_2 Capacity	0.48±0.23	0.11±0.05 **(CO_2)**
He-CO_2	1.10±0.10	0.25±0.02 **(CO_2)**

As in the previous case, the sorption capacity under mixed feed was expressed in mass rather than moles because of the inability to differentiate sorbed CO_2

and H_2O. The cycle capacities are shown in Table 5.5. They were found to be close to the values for the ZSM-5 powder samples when the 71.4% mass loading of sorbent in fibers was accounted for.

It was found that the working capacity for the fiber sorbents under dry CO_2 feeds was more than twice that inferred from wet sorption. The actual CO_2 sorption in wet feeds is likely to lie between the values obtained for dry CO_2 sorption and wet sorption assuming preferential water sorption; i.e, between 0.11 and 0.25 mmol CO_2/g fiber.

5.7.3.5 Packed Bed Sorption

Flow sorption experiments were next performed with a module containing Torlon®/ZSM-5 fiber in a similar manner to the packed bed sorption. The module was maintained at 35°C. Desorption was accomplished with a nitrogen sweep. A greater separation (sharper CO_2 breathrough) was observed between the helium and CO_2 curves than for the packed bed samples. The equilibrium and breakthrough capacities were calculated based on the CO_2 and helium concentration fronts.

The capacities were calculated from both sorption and desorption curves and the experiment was repeated and found to be reproducible. The average equilibrium CO_2 capacity was found to be 0.316 mmol CO_2/ g dry sorbent. The breakthrough capacity was lower, at 0.054 mmol CO_2/g. at 17% of the equilibrium capacity; this was still much higher than that of the packed bed experiment. Given that the experiment was carried out

in a single-fiber module with room for CO_2 bypass, closely packed fibers are more likely to capture CO_2 without such an early breakthrough.

Thus ZSM-5 was found to be a good sorbent choice for the fiber sorbent platform owing to its superior adaptability to the fiber spinning process and its retention of CO_2 capacity in wet feeds without the need for chemical functionalization. It was found to be readily processible during dope preparation and produced fibers with good mechanical properties. Furthermore, it is likely to be the most easily available sorbent at the industrial level due to its simple synthesis, and was selected to be the sorbent of choice for further experiments involving barrier layer deposition.

5.8 Conclusions

Zeolitic and siliceous sorbents were studied for adaptation to the hollow fiber RTSA project. Sorbents were both used as-is or chemically and physically modified to better suit the CO_2 capture purpose. Material constraints identified early on were availability at lab scale and endurance through the dope preparation process. Aminated silicas had stability issues during the heavy processing undertaken as part of the fiber production process and could only be loaded at small mass percentages due to their low density. Thermal and hydrolytic degradation of the silica did not bode well for the long-term performance of fiber sorbents based on them.

Zeolites were attractive sorbents in terms of availability and robustness; however their hydrophilicity was a problem. Nitridation of 13X proved to be inadequate as a mechanism to transform 13X into a hydrophobic sorbent. High-silica ZSM-5 was

found to overcome these issues and in addition retained its capacity for CO_2 even in wet feeds and was deemed to be the most robust of the solid sorbent materials. It's relatively low heat of sorption is a huge advantage as well. While its capacity was lower than that of some aminated sorbents reported in literature, it still provides a highly stable and substantial swing capacity and is likely to be the sorbent most suited for processing at an industrial scale.

5.9 References

1. Rege, S.U. and R.T. Yang, *A novel FTIR method for studying mixed gas adsorption at low concentrations: H_2O and CO_2 on NaX zeolite and γ-alumina.* Chemical engineering science, 2001. **56**(12): p. 3781-3796.

2. Auerbach, S.M., K.A. Carrado, and P.K. Dutta, *Handbook of zeolite science and technology*2003: CRC Press.

3. Dunne, J., et al., *Calorimetric heats of adsorption and adsorption isotherms. 1. O_2, N_2, Ar, CO_2, CH_4, C_2H_6, and SF_6 on silicalite.* Langmuir, 1996. **12**(24): p. 5888-5895.

4. Duval, J.-M., et al., *Adsorbent filled membranes for gas separation. Part 1. Improvement of the gas separation properties of polymeric membranes by incorporation of microporous adsorbents.* Journal of membrane science, 1993. **80**(1): p. 189-198.

5. Hammond, K.D. and S.M. Auerbach, *Modeling the structure and spectroscopy of alkaline zeolites.* ChemInform, 2012. **43**(44).

6. Walton, K.S., M.B. Abney, and M. Douglas LeVan, *CO_2 adsorption in Y and X zeolites modified by alkali metal cation exchange.* Microporous and Mesoporous Materials, 2006. **91**(1): p. 78-84.

7. Fink, P. and J. Datka, *Infrared spectroscopic studies of amination of ZSM-5 zeolites.* J. Chem. Soc., Faraday Trans. 1, 1989. **85**(10): p. 3079-3086.

8. Ernst, S., et al., *A novel family of solid basic catalysts obtained by nitridation of crystalline microporous aluminosilicates and aluminophosphates.* Applied Catalysis A: General, 2000. **200**(1): p. 117-123.

9. Dogan, F., et al., *Searching for microporous, strongly basic catalysts: Experimental and calculated 29Si NMR spectra of heavily nitrogen-doped Y zeolites.* Journal of the American Chemical Society, 2009. **131**(31): p. 11062-11079.

10. Hammond, K.D., et al., *Optimizing the Synthesis of Nitrogen-Substituted Zeolites.* Chemistry of materials, 2009. **22**(1): p. 130-142.

11. Narasimharao, K., et al., *Novel solid basic catalysts by nitridation of zeolite beta at low temperature.* Microporous and Mesoporous Materials, 2006. **90**(1): p. 377-383.

12. Anderson, M.W., *Simplified description of MCM-48.* Zeolites, 1997. **19**(4): p. 220-227.

13. Ryoo, R., S.H. Joo, and J.M. Kim, *Energetically favored formation of MCM-48 from cationic-neutral surfactant mixtures.* The Journal of Physical Chemistry B, 1999. **103**(35): p. 7435-7440.

14. Alfredsson, V. and M.W. Anderson, *Structure of MCM-48 revealed by transmission electron microscopy.* Chemistry of materials, 1996. **8**(5): p. 1141-1146.

15. Xu, J., et al., *A reliable synthesis of cubic mesoporous MCM-48 molecular sieve.* Chemistry of materials, 1998. **10**(11): p. 3690-3698.

16. Choi, S., J.H. Drese, and C.W. Jones, *Adsorbent materials for carbon dioxide capture from large anthropogenic point sources.* ChemSusChem, 2009. **2**(9): p. 796-854.

17. Hicks, J.C., et al., *Designing adsorbents for CO_2 capture from flue gas-hyperbranched aminosilicas capable of capturing CO_2 reversibly.* Journal of the American Chemical Society, 2008. **130**(10): p. 2902-2903.

18. Lively, R.P., *Hollow fiber sorbents for post-combustion CO_2 capture, PhD Dissertation*, 2011, Georgia Institute of Technology.

19. Agarwal, V., et al., *Kinetic stability of nitrogen-substituted sites in HY and silicalite from first principles.* Journal of Catalysis, 2010. **270**(2): p. 249-255.

20. Ernst, S., et al., *The influence of water on the activity of nitrided zeolites in base-catalyzed reactions*, in *Studies in Surface Science and Catalysis*, G.G. R. Aiello and F. Testa, Editors. 2002, Elsevier. p. 549-556.

21. Vakili, D., et al., *Synthesis of Hydrophobic Silicalite Adsorbent from Domestic Resources: The Effect of Alkalinity on the Crystal Size and Morphology.* Iran. J. Chem. Chem. Eng. Vol, 2005. **24**(4).

22. Persson, A.E., et al., *The synthesis of discrete colloidal particles of TPA-silicalite-1*. Zeolites, 1994. **14**(7): p. 557-567.

CHAPTER 6

LUMEN-SIDE BARRIER LAYER DEVELOPMENT

6.1 Overview of Barrier Material Selection

The performance of fiber sorbents as *adsorptive heat exchangers* is predicated on the application of a low-permeance barrier on the inner fiber wall. Such a barrier is meant to allow thermal contact between the heat transfer fluid flowing in the bore while precluding physical contact which would manifest itself as water/steam wastage and sorbent blockage. The key challenge in barrier fabrication in this research is the scale of the barrier, which would occur as a hollow cylinder a few microns wide and a few hundred microns in diameter. This immediately disqualifies a number of industrial barriers that can only be fabricated on large scales. Only polymeric and metallic barriers were considered implementable at this scale.

6.1.1 Metallic Barrier Layers

Metallic coatings have the advantage of being extremely impervious, and in some cases, resistant to oxidation. However, they cannot be deposited easily, even if precipitated from solution. Electroplating of metallic barriers is problematic since the application of electric current may degrade the matrix polymer and sorbent and there is no guarantee that the metal will deposit only on the lumen. For this work, a method of chemically depositing a metal layer, called *electroless plating*, was explored. Electroless

plating involves the deposition of a metal, usually nickel, from a salt solution containing a reducing agent [1]. The precipitating metal catalyzes further deposition; hence the process is autocatalytic. However, there is a necessary pre-treatment step often involving acids or strong oxidizers [2], which would attack zeolitic or aminated sorbents. Additionally, the technology is designed for smooth metal or plastic surfaces, and we were unable to find a contractor willing to attempt plating a porous polymer surface.

6.1.2 Polymeric Barrier Layers via Co-extrusion and Post-treatment

Polymeric barriers were considered the most feasible option for the same reason that the fibers themselves were polymeric: processibility and mechanical stability. Prior work on the fiber sorbent platform utilized PVDC and neoprene as barrier materials [3]. PVDC produced extremely low-permeance barriers with effective face-sealing, but degraded at 125 °C [4] and to a lesser extent, even at 90 °C [5]. In both cases, the polymer chain underwent dehydrohalogenation releasing hydrogen chloride, which would damage the sorbent apart from the barrier layer itself. Neoprene is more stable over a wider temperature range especially with crosslinking, but is not as good as a barrier as PVDC or PAN.

6.1.2.1 Barrier Layer deposition via co-extrusion

In this work, a number of other polymer barrier candidates were selected to be cast into barriers. As detailed in Section 2.4 there are two ways that polymers can be cast: co-extrusion during fiber spinning or via post-treatment of spun fibers. The key

restrictions on polymers for co-extrusion are the requirement for some miscibility with Torlon® and solubility in a suitable solvent. The latter condition precluded the selection of good barrier materials like Ryton®- poly(p-phenylene sulfide) or PPS, which is insoluble below 200 °C. Thus Torlon® is the obvious choice for co-extruded barriers

6.1.2.2 Barrier layer deposition via post-treatment

Material selection for post-treatment is somewhat complex. Barriers may be cast from solution or from polymer suspensions (usually aqueous) depending upon which state a particular polymer is obtained. Aforementioned rubbery polymers such as PVDC and Neoprene® are virtually insoluble at room temperature in viable solvents and thus cannot be cast from solution [6]. On the other hand, when cast as latex particles from aqueous suspension, their very low glass transition temperatures means that the particles can be made to interdiffuse with each other and coalesce into a continuous dense barrier. So PVDC and Neoprene® are best cast from latex suspension. Semicrystalline polymers such as PTFE may also be available commercially in latex form. In the case of PTFE, its glass transition temperature is too high (160-240 °C) [7, 8] to allow easy coalescence of the particles. Thus the only viable avenue to form barriers from such polymers is through solution casting.

Solution casting is applicable for any easily soluble polymer that produces low-viscosity solutions. A further caveat is that the solvent should dissolve the barrier polymer but not the matrix polymer (Torlon®). This precondition means that now the material selection process involves the solvent as well. Torlon® is advantageous as a

matrix polymer in this regard because it is only soluble in dipolar aprotic solvents like NMP and DMSO, allowing barrier layer formation from polymers that are soluble in a wider range of less polar solvents. However, it was discovered that PAN was the only polymer that was both soluble and a good barrier, and for this research, it was chosen as the material for solution-cast barriers. O_2 and H_2O permeabilities of the different polymers discussed above are tabulated below.

Table 6.1: O_2 and H_2O permeability and Tg of barrier polymers studied in this work.

Polymer	O_2 Permeability (Barrer)	H_2O Permeability (Barrer)	Glass Transition Temp. (T_g) (°C)
PVDC [9, 10]	0.002	1.4-10	-19
Neoprene® [9, 11]	4.0	914	-50
Torlon® [12, 13]	0.12	4.8	275
PAN [14]	0.0003	40-55 [15]	95
PTFE [7, 14]	4.9	33	160-240

While PAN is available in copolymer form with a number of other monomers [9], the pure form has the least water permeability [16] and was chosen for barrier formation. PAN dissolves in two kinds of solvents: in polar aprotic solvents like ethylene carbonate (EC), propylene carbonate (PC), NMP and DMSO; and in concentrated aqueous solutions of ionic salts such as sodium thiocyanate (NaSCN) and zinc halides. Aqueous salt solutions pose a number of challenges such as extreme toxicity

(sodium thiocyanate) and corrosiveness (zinc chloride). Furthermore, PAN only dissolves at very high salt concentrations: in 53% NaSCN by weight [17] and 65-80% $ZnCl_2$ by weight [18]. Such high salt concentrations are required to disrupt the hydrogen bonding in water to dissolve PAN [19]; however this results in extremely viscous solutions and would produce salt-infused barriers from which the salt would have to be leached out *after* drying. Organic solvents avoid many of the issues mentioned above - they are more environmentally benign and produce lower viscosity solutions that leave no salt residue on drying. Of the solvents mentioned above, the dipolar aprotic solvents such as NMP and DMF were inadmissible since they dissolve the Torlon® that constitutes the fiber matrix. However, EC and PC overcome this problem since they dissolve PAN but not Torlon®.

Table 6.2: Properties of PAN solvents ethylene carbonate and propylene carbonate [20].

Solvent	Molecular Structure	Melting Point (°C)	Boiling Point (°C)
Ethylene Carbonate (EC)	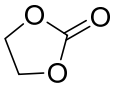	36.4	248
Propylene Carbonate (PC)	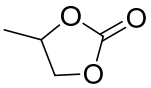	-49.2	241.7

Some batches of PAN obtained from Sigma Aldrich were found to be insoluble in propylene carbonate even though the reported Hildebrand solubility

parameters for EC and PC [21, 22] lie well within the range reported for PAN [23]. However, all PAN batches were soluble in ethylene carbonate, and it came to be preferred eventually in spite of its rather high melting point (Table 6.2).

Barrier fabrication discussed in the following sections mostly focuses on barrier layer co-extrusion using Torlon® as the lumen layer and solvent-casting of PAN lumen barriers via post-treatment. The barrier formation and material selection philosophy is summarized below. The boxes shaded in blue represent examples of barrier materials that were considered or pursued for this work.

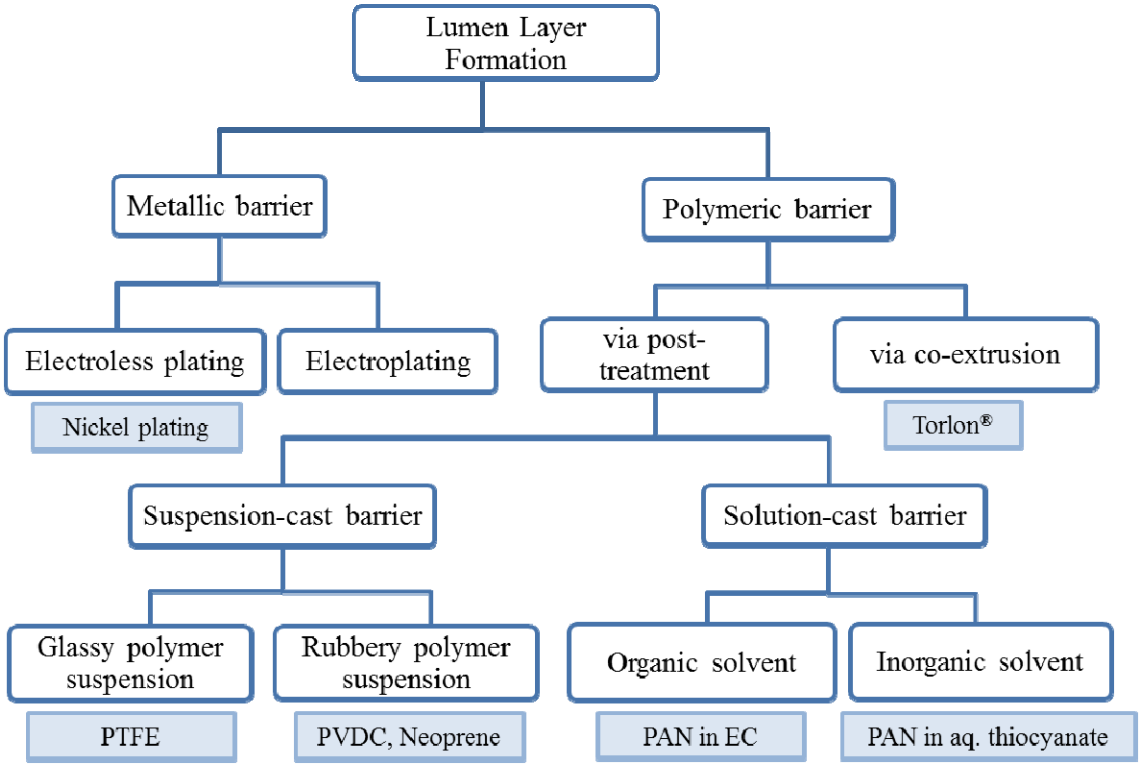

Figure 6.1: Options available to cast barriers on the lumen of hollow fibers. Torlon® co-extrusion and post-treatment using PAN solution were found to be the most feasible barrier deposition methods.

6.2 Internal Barrier Formation via Solvent Extraction

The principles behind co-extruded barriers were discussed in detail in Section 2.4.1. The experimental procedure is essentially the same as that for spinning single-layer fiber sorbents except for the addition of a barrier dope and the complications therein. In essence, solvent extraction, rather than non-solvent intrusion is to be encouraged on the inner wall of the extrudate. In externally-skinned membrane fibers, solvent extraction is accomplished via evaporation when the extrudate passes through the air gap above the quench bath.

6.2.1 Internal barrier via evaporation

Evaporation was initially seen as a possible internal skin formation method, since this is how fibers with external skins have been produced traditionally. A trial spin was undertaken using nitrogen as the bore fluid. A nitrogen cylinder was connected to the bore needle of the spinneret with the idea of establishing a gaseous bore fluid into which the solvent and volatile non-solvent could evaporate. The spin temperature was 50 °C. A solution containing 25% Torlon® by weight with remainder NMP and THF in a 2:3 weight ratio was used as the "core", barrier-forming dope, with THF being the volatile non-solvent. The "sheath" sorbent dope had the composition mentioned in Table 4.2. The experimental setup is pictured in Figure 6.2. However, spinning with nitrogen as bore fluid was difficult to the point of impossibility. Once the core and sheath dopes started flowing, the nitrogen flow was started through the bore needle. The regulator was cracked open to allow a low flow of nitrogen in the bore, and

this caused a pulsed, discontinuous bore rather than a continuous channel. At higher pressures, the nitrogen blew out the bore making fiber collection impossible. At this point, nitrogen was abandoned as a bore fluid on account of the instability it caused during spinning. Instead, it was decided to develop a liquid bore fluid to achieve solvent extraction.

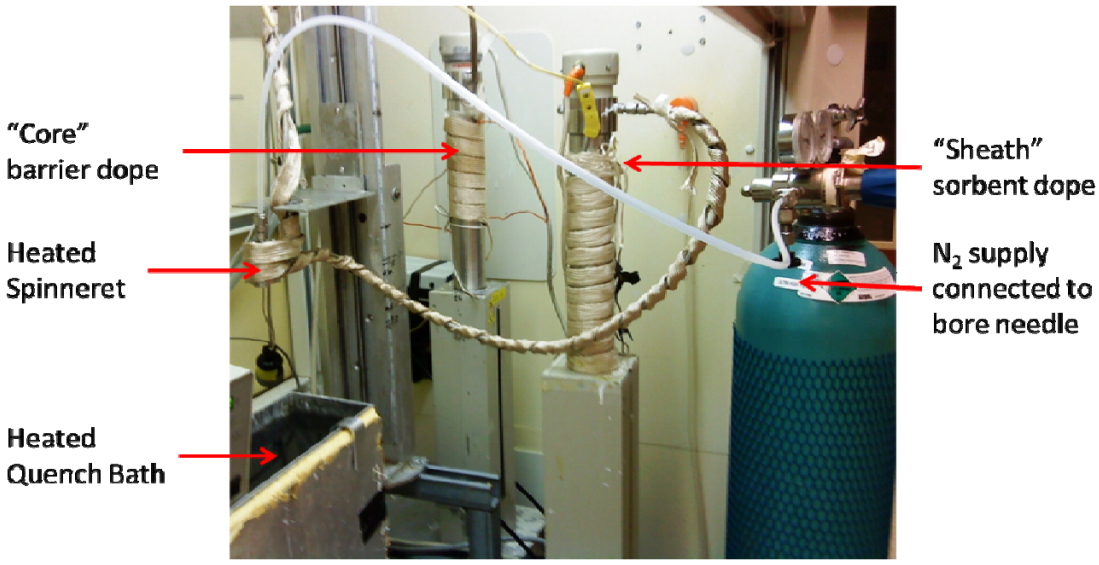

Figure 6.2: Experimental setup to spin dual-layer fiber sorbents using nitrogen or air as the bore fluid. The setup is identical to other dual-layer spins except for the connection of a nitrogen source to the bore needle instead of a syringe pump.

6.2.2 Internal skin formation through liquid bore fluids

Research had been undertaken earlier in the Koros group to produce dense-skinned micropillows from polyamic acid solution [24] using a liquid medium to extract the solvent and non-solvent components from a polymer solution. Drops of the polymer solution were extruded from a triple-orifice, dual-layer spinneret into a bath of poly(propylene glycol) (PPG). Had water been used, as would occur in membrane spins,

there would be diffusion of water into the polymer. PPG on the other hand is minimally invasive on account of its high molecular weight, and so NMP diffused out of the polymer, thereby vitrifying it. It was envisioned that a similar extraction would be achieved on the internal surface of a hollow fiber being spun if the bore fluid had a PPG component.

6.2.3 PEG vs. PPG for solvent extraction

Both PEG and PPG are high-molecular weight liquid polymers and could theoretically be used as the extracting agent. "Drop tests" were performed by releasing droplets of Torlon® dope into vials of PEG and PPG and visually observing the changes to the droplets over a few hours. The dope used here contained 34 wt.% Torlon®, 50.4 wt.% NMP, 12.6 wt. % tetrahydrofuran and 3 wt.% water. This composition had been found to give defect-free, high-performance Torlon® fiber membranes in earlier research in the Koros group [12], and was retained for barrier formation purposes instead of the Torlon®/PVP dope composition developed in Chapter 4. It was reasoned that the PVP-containing dope composition developed in this work should be used for fiber sorbent fabrication whereas the membrane dope composition containing 34% Torlon® should be used for barrier formation wherever possible.

The drop tests revealed that Torlon® droplets in PPG hardened into dark transparent spheres indicating vitrification. PEG accomplished less pronounced vitrification along with some phase separation. Therefore PPG was preferred as the bore fluid component.

6.2.4 Internal Barrier Formation on a Single-Layer Fiber

While forming a barrier by co-extrusion, it would be advantageous to use two dopes during spinning: an inner pure polymer dope that would form the barrier layer and an outer sorbent dope that would contain the dispersed sorbent particles. The alternative, to use only a sorbent dope and attempt to densify part of it into the lumen barrier was considered less efficient because it would render inactive some of the sorbent contained within and there is no guarantee that the sorbent dope composition chosen in this work would also yield good barriers. Hence it was decided to use a dedicated barrier dope flowing concentrically with the sorbent dope. However, to first establish that internal vitrification via spinning would be possible, sorbent-free single-layer fibers were spun and their barrier properties were analyzed before moving on to dual-layer fibers. The dope makeup used for this purpose has already been described in Section 6.2.3.

6.2.4.1 Optimization of PPG-based Bore Fluid

While PPG is an effective solvent extraction agent for micropillow fabrication, spinning single-layer fibers with PPG as the bore fluid proved to be very difficult. The fiber continually broke even at very low draw ratios and take-up proved impossible. It appeared that vitrification was occurring too rapidly to accommodate any tension arising out of drawing out the fiber, resulting in fiber breaks near the spinneret. The air gap was reduced to less than 3 cm to facilitate phase separation from the fiber exterior but even this was insufficient to reduce fiber breakage. As a remedial measure, water and NMP were re-introduced in increments into the bore fluid to bring it closer to

the more familiar and spinnable 80:20 NMP: water composition. The NMP-to-water ratio was maintained at 4:1. It was found that the dope was spinnable with fewer fiber breaks with a bore fluid makeup of 20% PPG, 64% NMP and 16% water by mass. The dope composition and spin conditions are provided below.

Table 6.3: Dope composition and spin conditions for single-layer internally-skinned Torlon® fibers.

Dope Component	Concentration in Dope (%)
Torlon®	34
NMP	50.4
Water	3
THF	12.6

Spin Parameters	
Core Flow Rate	100 ml/hr
Bore Flow Rate	30 ml/hr
Bore Composition	20:64:16 PPG:NMP:Water
Operating Temperature	50 °C
Take-up Rate m/min	13.3 m/min
Air Gap	3 cm

The fibers thus produced were solvent-exchanged and dried in the usual manner described in Chapter 3. The dried fibers were analyzed under SEM and their helium permeance was measured in the constant pressure system described in Chapter 3. The permeance was low enough that it could only be conveniently measured at ≈ 100 psi pressure differential. The fibers yielded a low helium permeance of 0.16 GPUs at 102 psi Δp.

The fibers were found to have a well-defined, 2-3 μm thick internal skin (Figure 6.3). The densifying effect of PPG is observed on comparing with Torlon® fibers spun using 80% NMP/20% water bore fluid (Figure 6.4).

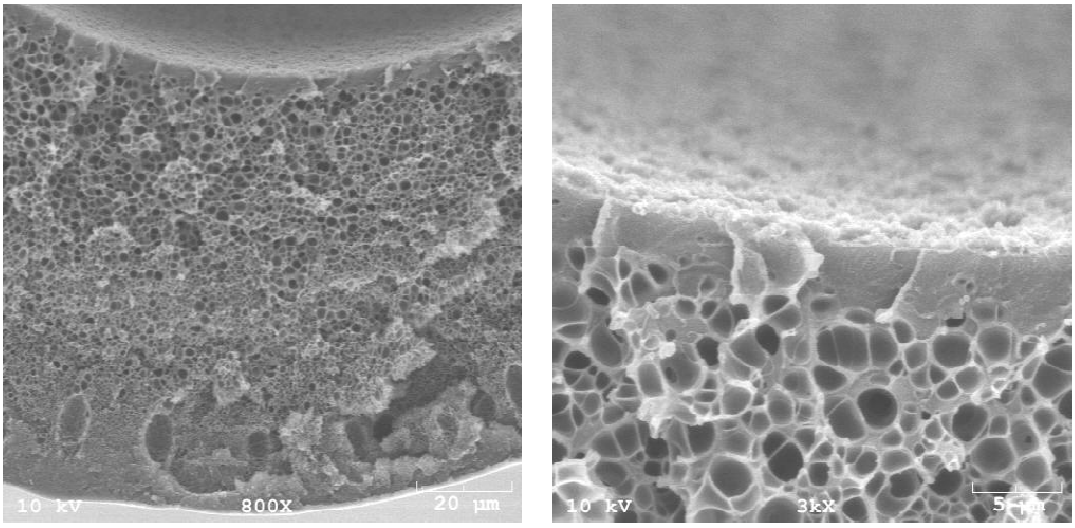

Figure 6.3: Cross-section of internally-skinned Torlon® fibers showing the pore morphology and a close-up view of the internal dense layer.

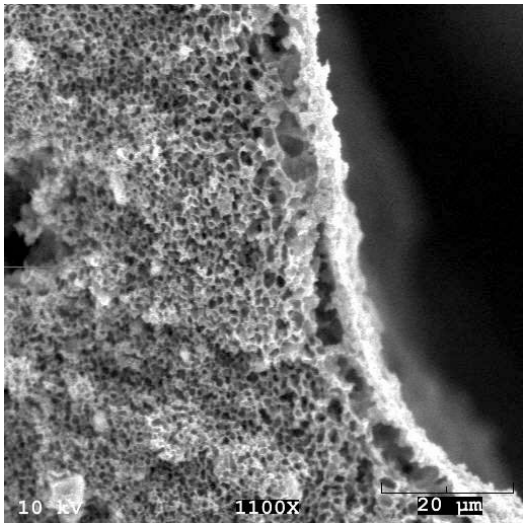

Figure 6.4: Single-layer Torlon® fibers spun with bore fluid containing 80% NMP/20% water by weight show a porous rather than dense internal skin, unlike fibers spun with PPG in the bore fluid.

6.2.4.2 Introduction of PEG into Bore Fluid

Having found that PPG had to be diluted with NMP/water to be usable as a bore fluid, focus was turned to replacing the NMP in the bore fluid with another liquid, thereby enhancing skin formation via increasing the NMP concentration difference between the bore and the dope. PEG was chosen, since as a liquid polymer, it is less likely to diffuse into the extruded fiber and is partially miscible with both water and PPG. A number of PEG-PPG-water mixtures were made in order to identify one that would both maximize PPG content and keep the mixture single-phase. Of the combinations tried, 40 wt.% PPG /52 wt.% PEG/8 wt.% water met this condition and was chosen as the bore fluid for the subsequent spin. Spinning was still troublesome due to occasional fiber breaks, but with a very low take-up rate of 5-10 m/min, fibers were eventually able to be taken up and subsequently processed.

SEM characterization of these fibers revealed a very clearly defined, dense inner skin as shown in Figure 6.5. The internal skin was about 5-10 μ thick. There was significant macrovoid occurrence, which was possibly a result of the very low air gap and thick wall (>200 μm).

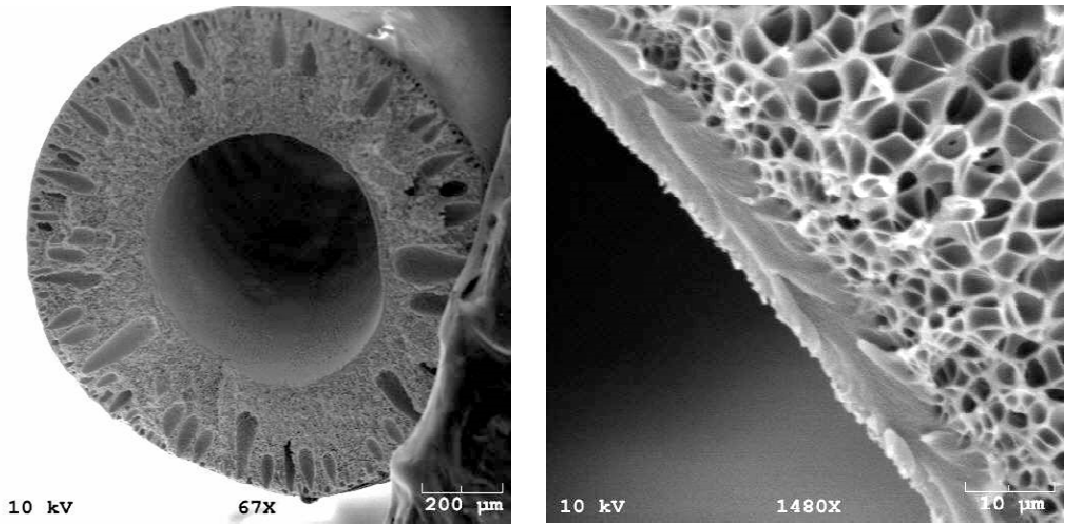

Figure 6.5: Cross-section of internally-skinned Torlon® fiber sorbents produced with a PPG/PEG/water bore fluid. The internal skin was thicker and better-defined than when the bore fluid lacked PEG.

It was also observed that the inner surface of the internal skin was much smoother and showed much less pitting than fibers spun without PEG in the bore fluid.

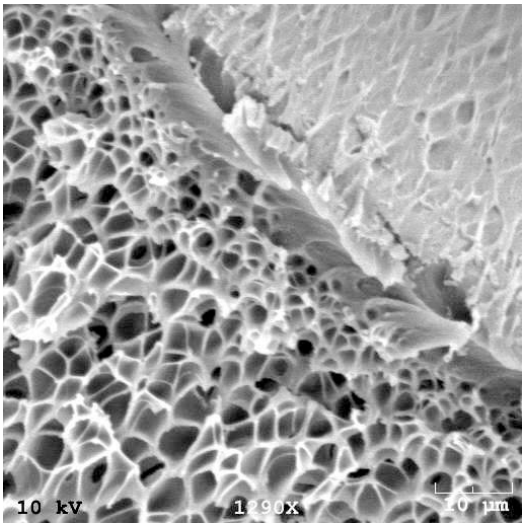

Figure 6.6: View of inner wall showing a smoother surface than for fibers spun without PEG in the bore fluid.

The previous figure also showed that the dense layer was surrounded by a uniform pore structure which appeared to be of *closed cell morphology*. Characterization of these fibers through permeance measurements indicated a very low helium permeance of 0.06-0.08 GPUs at ≈100 psi Δp.

Such a low permeance could only be possible with the absence of any lumen-layer bypass, i.e. gas molecules circumventing the barrier layer by flowing through the face of the fiber and out into the shell side of the module (instead of through the fiber wall). This would indicate that the resistance to barrier layer bypass was provided by the pore structure of the fiber (in addition to the dense skin) lending credence to the idea that the pore structure was closed-cell. This was further corroborated by the fact that the measured permeance of 0.08 GPUs corresponds to 63 μ of dense, defect-free Torlon®, whereas SEM images of the fiber showed a dense layer only between 5-10 μ thick. Thus the remainder of the diffusion resistance came from the closed cell pore structure, which may be imagined as a resistance in series with the inner dense wall. In fact, just a series resistance of closed cell pores about 300 μm thick of 80% porosity (i.e. 20% dense) would explain most of the apparent 63 μm barrier layer.

The closed cell resistance in itself is not detrimental to the barrier performance but is likely to increase the thermal resistance of the barrier. When spun as dual-layer fibers, the core layer needs to have a higher proportion of dense Torlon® to the closed cell Torlon® in order to minimize thermal diffusion resistance in the barrier while retaining barrier properties.

6.2.5 Co-extrusion of Torlon® Barrier: Dual-Layer Spinning

With the feasibility of spinning single-layer fibers with highly impermeable internal skins established, a dual-layer spin was attempted wherein a Torlon®-only dope would be co-extruded with an outer Torlon®/sorbent dope. The core dope was the same as the one used in Section 6.2.3. The sheath dope was the sorbent dope developed in Chapter 4 (Table 4.4). A dual-layer spinneret with a recessed core needle and an enlarged sheath area [24] was used to spin fibers with a constricted barrier layer and a wider sheath layer. Different bore fluid compositions were used; starting with 80/20 wt. % NMP/water bore fluid that had been used for single-layer sorbent spins.

6.2.5.1 Dual-layer Fiber spinning with an NMP-water bore fluid

Initially, 80/20 NMP/water mixture was used as the bore fluid and was found to yield concentric layers as shown in Figure 6.7. This composition is the same used for single-layer fiber spins and was used as a “safe” dope fluid before other less proven bore fluids were used.

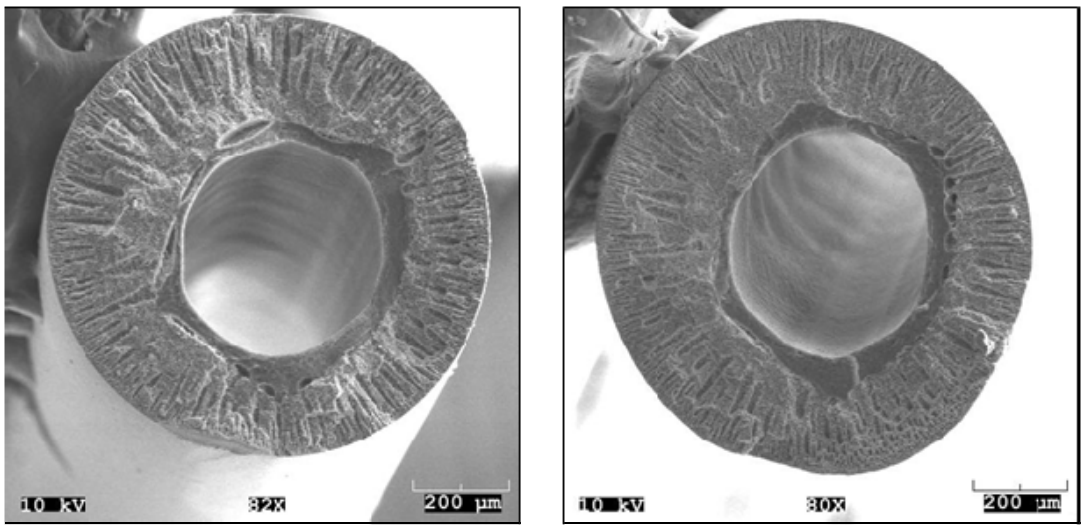

Figure 6.7: Cross-section of dual-layer fiber sorbents spun using NMP-water bore fluid. Warping of the core-sheath boundary can be observed in these images with gaps that appear to be circumferential expansions of macrovoids into the core layer.

The fibers spun had a bore that was concentric with the fiber outer diameter; however, the interface between the two layers was warped. There is evidence of the sheath layer having deformed around the core layer and of macrovoids in the sheath area protruding into the core layer and expanding circumferentially. This was probably the result of stresses accumulating during phase separation that normally do not occur with single fiber spins, where there is reduced resistance to diffusion of water into the fiber and of solvent out of the polymer solution. The inner surface of the core layer had little visible densification and a porous structure was observed throughout the core layer and even close to the inner wall.

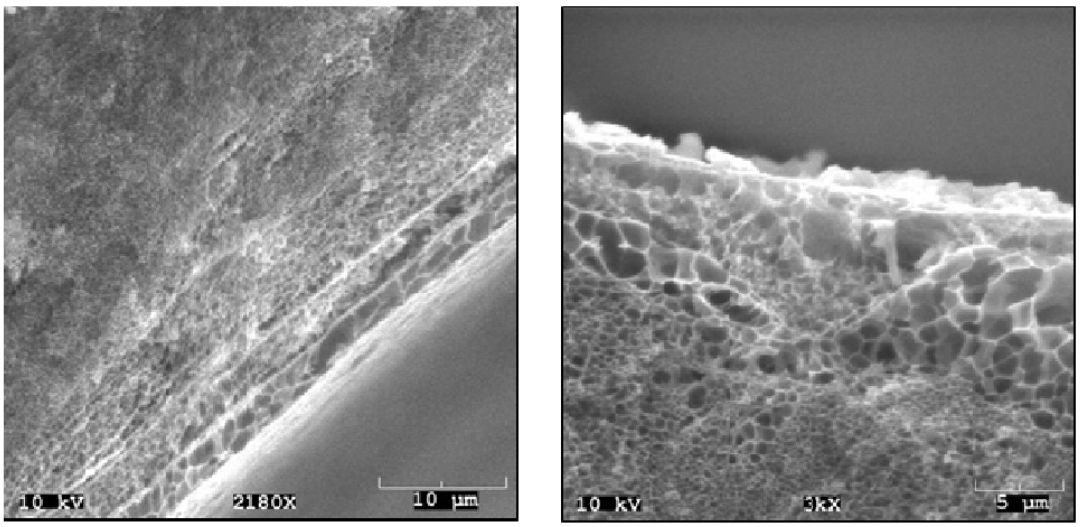

Figure 6.8: Inner wall of fibers spun with only NMP and water in the bore shows little densification and a pore network extended till the surface.

6.2.5.2 Dual-layer Fiber spinning with an extracting bore fluid

To form an internal barrier, the bore fluid was then switched to the PPG-PEG-water mixture given in Section 6.2.4.2. The spin parameters and dope makeup are given in Table 6.4.

Table 6.4: Bore Fluid composition and spin parameters for spinning dual-layer fiber sorbents.

Bore Fluid Component	Concentration (wt. %)
PPG	40
PEG	52
Water	8

Spin Parameters	
Bore Flow Rate	100 ml/hr
Core Flow Rate	100 ml/hr
Sheath Flow Rate	300 ml/hr
Operating Temperature	50 °C
Take-up Rate m/min	13.2 m/min
Air Gap	6 cm

Fiber uptake was somewhat difficult due to fiber breaks, but fibers could still be collected with reasonable predictability once a good take-up rate (13.2 m/min) was established.

The fibers obtained still had a bore that was concentric with the outer fiber wall; however, the core-sheath interface was highly non-circular and riddled with macrovoids. It was discovered that the irregularity of the core layer had worsened as the spin progressed, i.e., the fibers collected later were more irregular than the ones collected earlier, and the irregular core formation could not be identified and reversed during the spin. I hypothesize that the relatively high core flow rate (Table 6.4) was the cause of this irregularity in the core layer dimension, although it had originally been set high to avoid breaks in the core layer. In places, the core layer had extended to the fiber's external surface as shown in Figure 6.9.

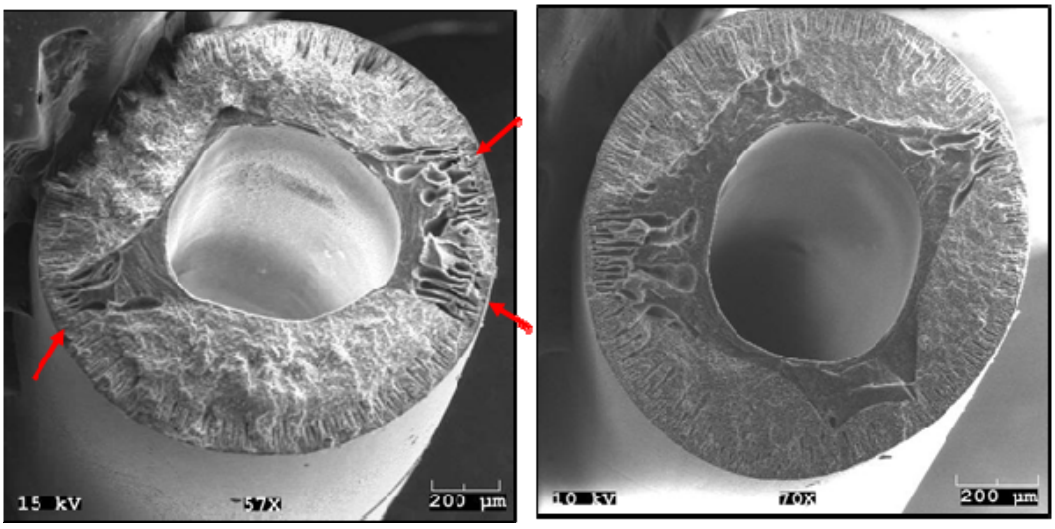

Figure 6.9: Dual layer fibers spun with PEG-PPG-water bore fluid. The core-sheath boundary was very irregular, in places reaching the outer wall (marked with red arrows.)

The inner wall of the core layer indicated the formation of a dense layer and suppressed pore formation as shown in Figure 6.10.

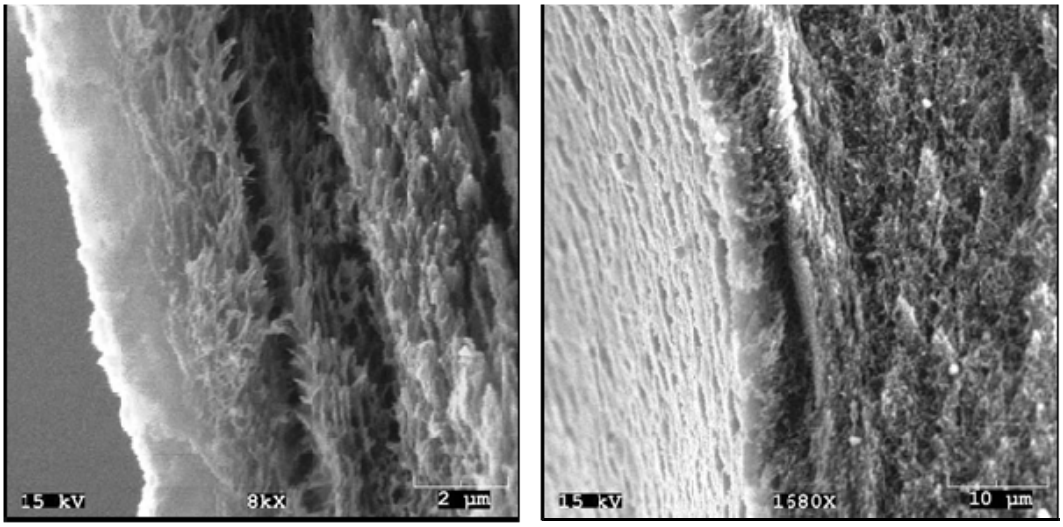

Figure 6.10: Inner wall dual-layer fibers spun using PEG-PPG-water bore fluid. A dense skin can be observed on the inner layer of the fiber.

The permeance of the fibers was found to be 11250 ± 65 GPUs of helium at 10 psi Δp. This is too high a permeance for dense-skinned fibers. Closer examination of the core layer revealed that some of the macrovoids had perforated the inner wall leaving large holes which would explain permeances of this magnitude.

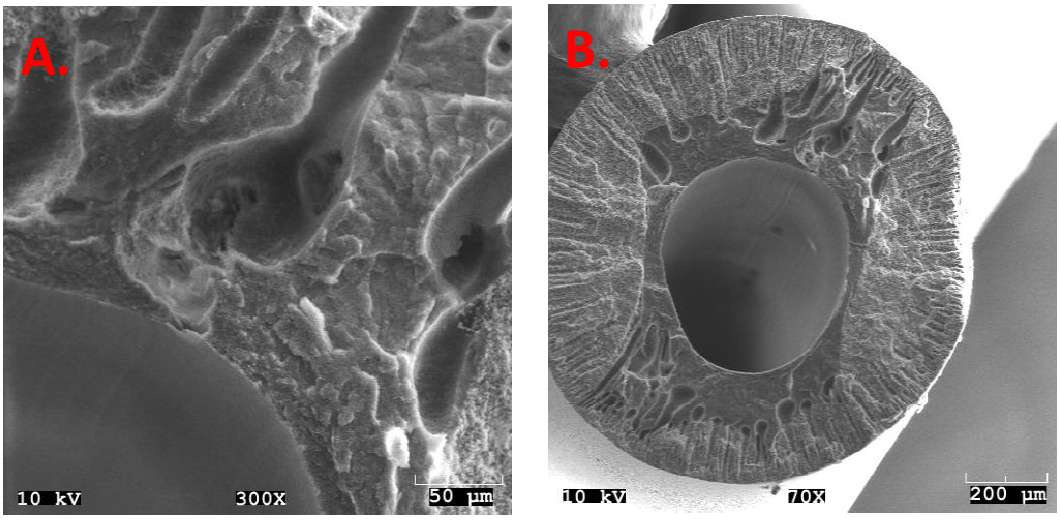

Figure 6.11: SEM micrographs of the dual-layer fiber sorbents showing A. macrovoids extend through the core layer into the lumen, and B. evidence of holes left in the inner wall by the macrovoids.

Thus the chief flaws in the spun dual-layer fibers were the highly non-circular core layer extending to the outer surface in places, and the macrovoids puncturing the lumen wall. The macrovoids could potentially be suppressed by decreasing fiber dimensions but this would call for an increased take-up rate which was difficult to accomplish. Alternatively, they could be reduced by lowering the core-to-sheath flow rate ratio since it appeared that at least some of the macrovoid formation was driven by the diffusion of non-solvent to the core layer. (The non-solvent concentration gradient remains even after fiber formation and for much longer than fibers spun with a neutral bore fluid. The gradient could be dissipated more quickly by having a narrower core layer) It was hypothesized that decreasing the core layer thickness would also prevent it from deforming extensively. More disquieting was the tendency of spin irregularities, like the irregular core layer, to worsen progressively through the spin with no means of controlling them.

6.2.5.3 Dual-layer Fiber spinning with a narrow core layer

Since a major pitfall in spinning dual-layer fibers was the presence of macrovoids perforating the bore, it was resolved to decrease the ratio of core-to-sheath flow rates to produce a thinner and less macrovoid-prone core layer. The core and sheath dope concentrations were the same as in Table 6.4. The bore fluid makeup was to be the same water-PPG-PEG mixture as previously (Section 6.2.5.2); however, the problems encountered with spinning internal barriers (pulsing, fiber breaks) necessitated the incorporation of NMP into the bore fluid during the course of the spin. Finally, some level of control was achieved with the following bore fluid and spin parameters.

Table 6.5: Revised bore fluid composition and spin parameters for narrower core layer.

Bore Fluid Component	Concentration in Dope (%)
PPG	31.5
PEG	45
Water	7
NMP	16.5

Bore Flow Rate	100 ml/hr
Core Flow Rate	50 ml/hr
Sheath Flow Rate	300 ml/hr
Operating Temperature	50 °C
Take-up Rate m/min	15 m/min
Air Gap	3 cm

SEM analysis on the solvent-exchanged fibers revealed that a narrower barrier layer had indeed been achieved and macrovoids were markedly reduced compared to the previous results. The core layer however did not completely surround the lumen, with sections where the outer sheath layer was exposed to the lumen. The part of the

inner wall lacking densification is seen as a dark track on the inner wall (Figure 6.12.A) and the lack of a skin was confirmed by closer SEM examination. Interestingly, this showed that the sorbent dope was unable to undergo densification in the presence of PPG/PEG whereas the pure polymer solution did (Figure 6.12.B), either because of the effect of the PVP pore-former contained in that dope or because of the nucleation-inducing properties of the sorbent properties contained within.

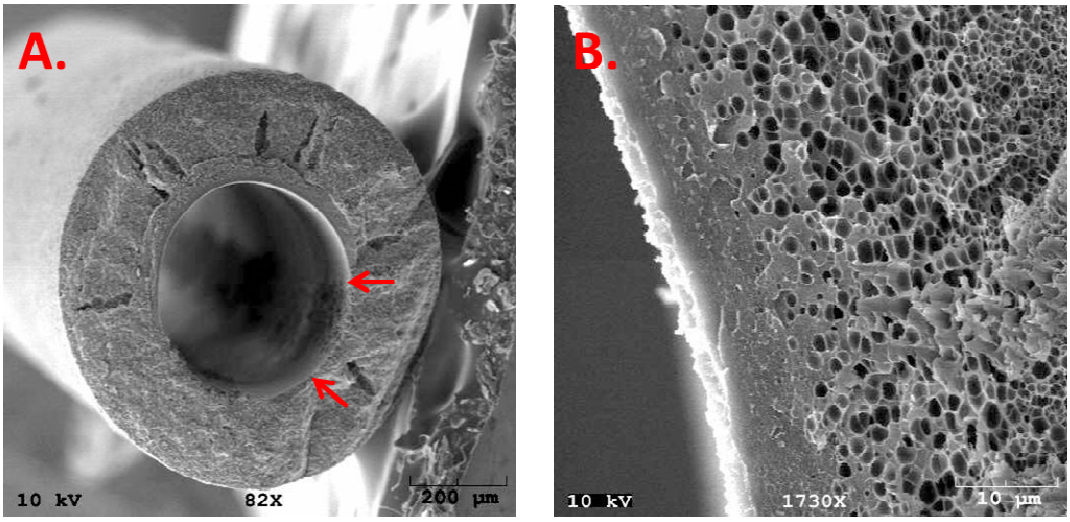

Figure 6.12: SEM micrographs of dual-layer fiber sorbents showing A. incomplete formation of the core barrier layer with the outer sorbent layer partly encountering the fiber bore, and B. evidence of densification where the core layer did occur.

The incompletely formed barrier layer was found in all spin states and was attributed to uncontrolled instability in the spin. It would have been difficult to correct such an error in the spin even if it had been identified since there are no spin conditions that could have been changed to avoid this. The permeance of the fibers was measured nevertheless and found to be 2817±39.5 GPUs at 11.3 psi Δp. This was too high to be

acceptable for a barrier-inlaid fiber sorbent but was not surprising considering the breach in the barrier layer described above.

6.2.6 Conclusions from Dual-Layer Sorbent Spins

This section described the methodical procedure developed to establish fibers with co-spun internal barriers. It was shown that PPG could act as an effective solvent-extraction agent to form an internal dense barrier, as observed in analysis of single-layer Torlon® fibers. Subsequent efforts to translate these results to dual-layer fibers encountered spinnability issues that were dealt with through adjustments to the spin parameters, including changes to the bore-fluid composition mid-spin. Macrovoids produced in initial spins were reduced by decreasing the thickness of the core layer. However, irregular formation of the bore layer was a continuing problem: the core layer was either extremely non-circular or had breaks in continuity. This was reflected in poor barrier performance even though there was visual evidence of dense skin formation on areas that were covered by the core layer. A complete barrier was elusive despite undertaking multiple spin attempts. Hence the research focus was gradually shifted to barrier layer formation using other means: solvent-cast PAN barriers.

The results obtained from barrier co-extrusion are nevertheless extremely promising for single-layer fibers (that might subsequently be impregnated with sorbent material), and potentially for the production of larger fibers where a low take-up rate and a larger spinneret could be used to offset the instabilities encountered in barrier co-extrusion.

6.3 Solvent-cast PAN Barriers

As an alternative to the Torlon® barrier co-extrusion, PAN-based barriers were cast via post-treatment. PAN is an effective gas barrier which, on exposure to air and high temperatures, especially > 180 °C, forms a stable, cross-linked "ladder" polymer. It is not commercially available as a dispersion so it was determined to solution-cast PAN on already spun fiber sorbents. As discussed in Section 6.1.2.2, ethylene carbonate (EC) and propylene carbonate (PC) were chosen as the solvent that would dissolve PAN without attacking the Torlon® fiber matrix. The experimental setup and procedure to coat fibers with PAN is provided in Section 3.3.1. The fibers that were subsequently post-treated to form lumen barriers have already been described in Chapter 4, and have a Helium permeance of over 25,000 GPUs (Section 4.5.2.2).

6.3.1 Preliminary PAN-EC barrier deposition on a horizontally held module

In order to observe if a dense PAN layer could be solution-cast on the fiber sorbent lumen, a preliminary post-treatment experiment was done by pumping a 10% by weight solution of PAN in EC through a single-fiber module. 10 g of the solution was held in a U-tube and forced through the fiber module under 30 psi upstream N_2 pressure. The temperature was maintained at 60 °C by means of heating tape to keep EC from freezing and to hasten the drying process. The module was held horizontally for convenience. Once the EC had flowed out of the fiber and it had been swept clean, the N_2

sweep was maintained overnight at a lowered pressure differential in order to dry the PAN layer.

On testing the dried fiber, it was found that the fiber permeance had been hugely reduced. For these particular fibers, the nitrogen permeance was reduced from about 10,553 ±85 GPUs before post-treatment to 8.3 ±0.12 GPUs at 1.8 atm average pressure. The helium permeance was higher as shown in the Figure 6.13.

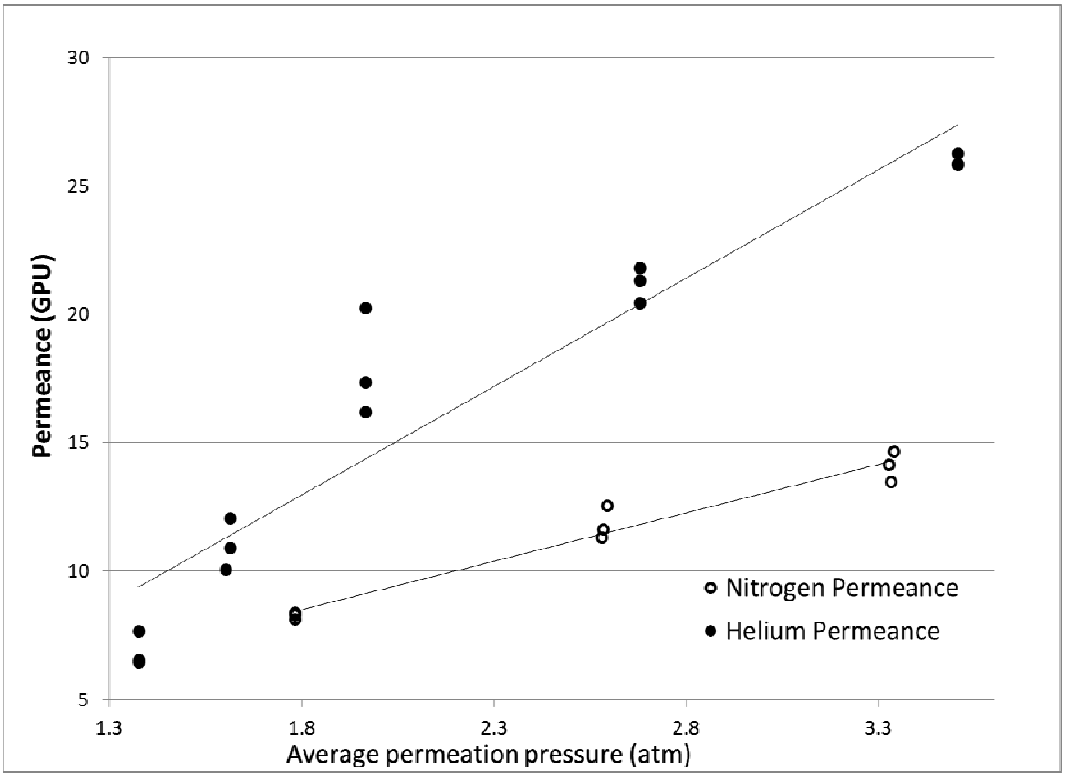

Figure 6.13: N_2 and He permeance plot of single layer Torlon® sorbents post-treated with PAN-EC solution.

It is seen in the graph that the N_2 and He permeances increased with increasing system pressure, indicating that there was some viscous flow resulting from a few macroscopic defects in the barrier layer.

SEM analysis of these treated fibers showed that a dense PAN layer had indeed been deposited on the inner fiber surface as shown in Figure 6.14.

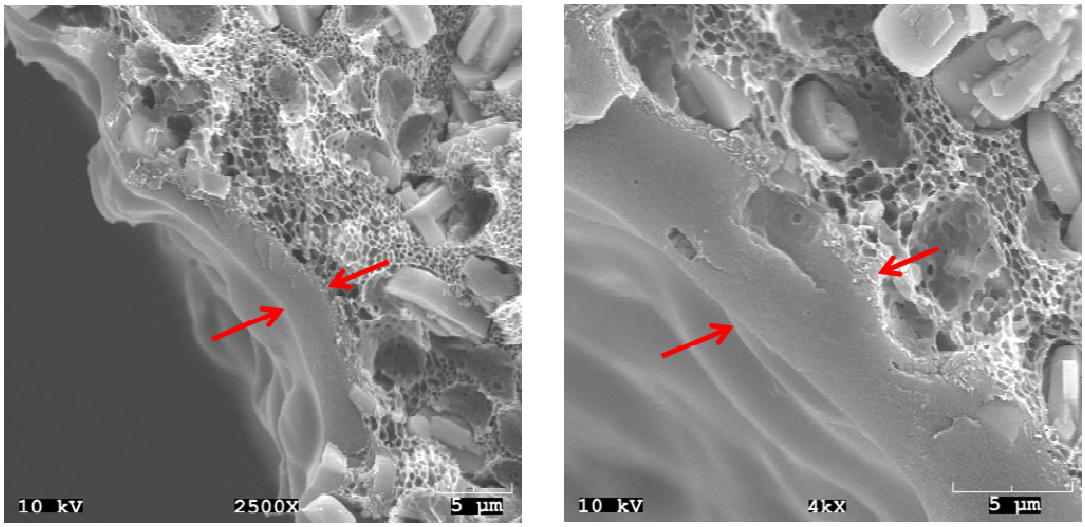

Figure 6.14: SEM images of post-treated fiber sorbents with PAN barrier of approximate thickness 5 µm. The barrier layer is the dense area between the arrow marks.

The barrier layer had a varying thickness along the radius (2-10 µm). This non-uniformity was attributed to the fact that the module was held horizontally during the post-treatment process. Having thus established that a dense PAN layer could be cast on the fiber lumen, subsequent modifications were made to improve the process. These included suspending the module vertically and using a Teledyne ISCO pump to drive the PAN solution through the bore. These changes, along with the optimized drying protocol have been provided in Section 3.3.1.

6.3.1.1 Fiber blockage issues

Frequent fiber blockages were encountered while attempting to post-treat using a 10% PAN-EC solution. This was later discovered to be due to the presence of impurities in the PAN solution that formed visible, gelatinous particulates ("fisheyes") in solution. These particulates could also potentially compromise barrier integrity. Centrifugation was undertaken to remove them but it was difficult to centrifuge the viscous 10% PAN solutions. Diluted 3% PAN solutions could be successfully centrifuged; however it was difficult to reduce the permeance below 20 GPUs of nitrogen (at 1.8 atm) with the resultant solution. Eventually, 8% PAN solution in PC was prepared and centrifuged to remove particulates. The resultant solution was then used for post treatment.

6.3.2 PAN barrier formation on vertically suspended module

Since horizontally supported modules did not form a symmetrical PAN layer, the module was suspended vertically and PAN solution was flowed through it. This time, an 8% solution of PAN in PC was used since there was no heating arrangement set up to enable the use of EC as a solvent; and because PC and EC were assumed to be equivalent in their applicability as solvent. The solution had been centrifuged and the particulates removed prior to use. The ISCO pump and solution feed line were not heated but otherwise the experimental setup and procedure were as described in Section 3.3.1. The fibers were post-treated twice (once from each side). The permeance was measured and found to be very low, about 0.19 ±0.03 at 3.1 atm average pressure (88.3 psia

upstream pressure). The nitrogen and oxygen permeances were too low to be measured with the bubble flow meter and the helium permeance did not show an upward trend as seen in Figure 6.15 below, suggesting the formation of a defect-free dense layer.

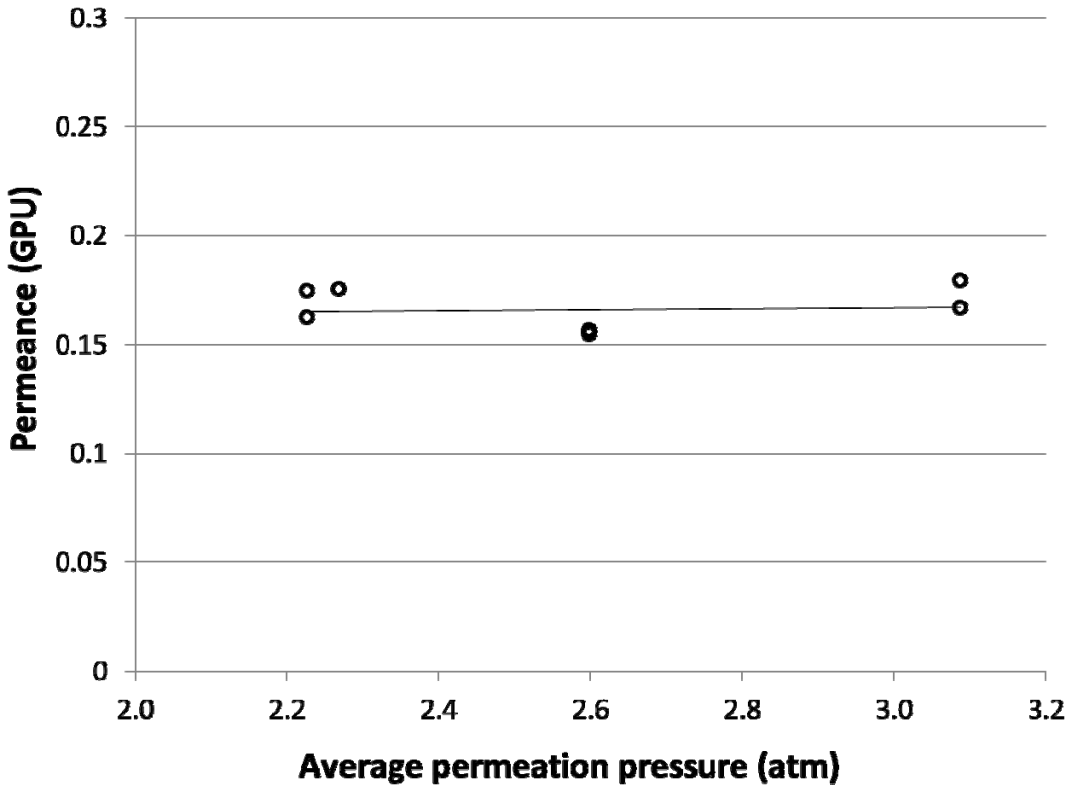

Figure 6.15: He permeance plot of single layer Torlon® sorbents post-treated twice with PAN-PC solution. The He permeance did not vary linearly indicating the absence of bulk-flow defects.

The module was broken and the fibers were imaged with SEM. The images indicated the formation of a dense, unbroken lumen barrier. There was some roughness observed on the inner surface, possibly from the gel particles that had not been removed by centrifugation. However, the barrier itself was essentially dense and there

was no sign that the sorbent layer was in any way compromising barrier integrity (Figure 6.16).

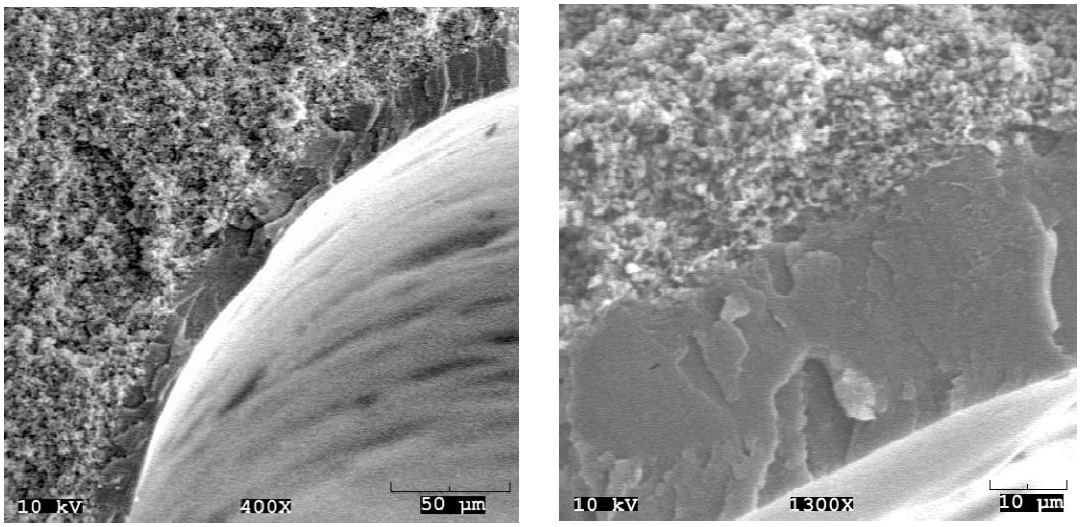

Figure 6.16: SEM images of the dense PAN layer showing some roughness on the internal surface, possibly from remaining particulates in the PAN solution, and a close up view of the barrier showing its dense nature.

Having obtained a dense, low-permeance barrier from PAN in PC solvent, it was decided to avoid the problem of particulate impurities by obtaining a new batch of the same PAN material from Sigma Aldrich. The new PAN did not contain any particulates and provided a clear solution that was much less prone to fiber clogging during post-treatment. The new batch of PAN was also only soluble in EC but not propylene carbonate (PC), and so the experiments were continued with EC as the solvent.

6.3.3 PAN barrier formation from EC solution

Experiments with post-treating Torlon®-based fibers were continued with a 5% PAN solution in Ethylene carbonate (EC). Repeated post-treatment with this solution could be performed without fiber bore blockage, a serious problem with earlier PAN solutions that contained gelatinous particulates. The pressure drop during post-treatment was found to be in the range 100-170 psi for a PAN-EC flow rate of 10 ml/hr. Post-treatment experiments showed decreases in the barrier permeance with each step of post-treatment. After 2-post-treatments, the helium permeance was reduced to less than 0.8 GPUs and O_2 permeance was less than 0.3 GPUs even at about 75 psi Δp. The original permeance of these fibers was over 25,000 GPUs (Section 4.5.2.2).

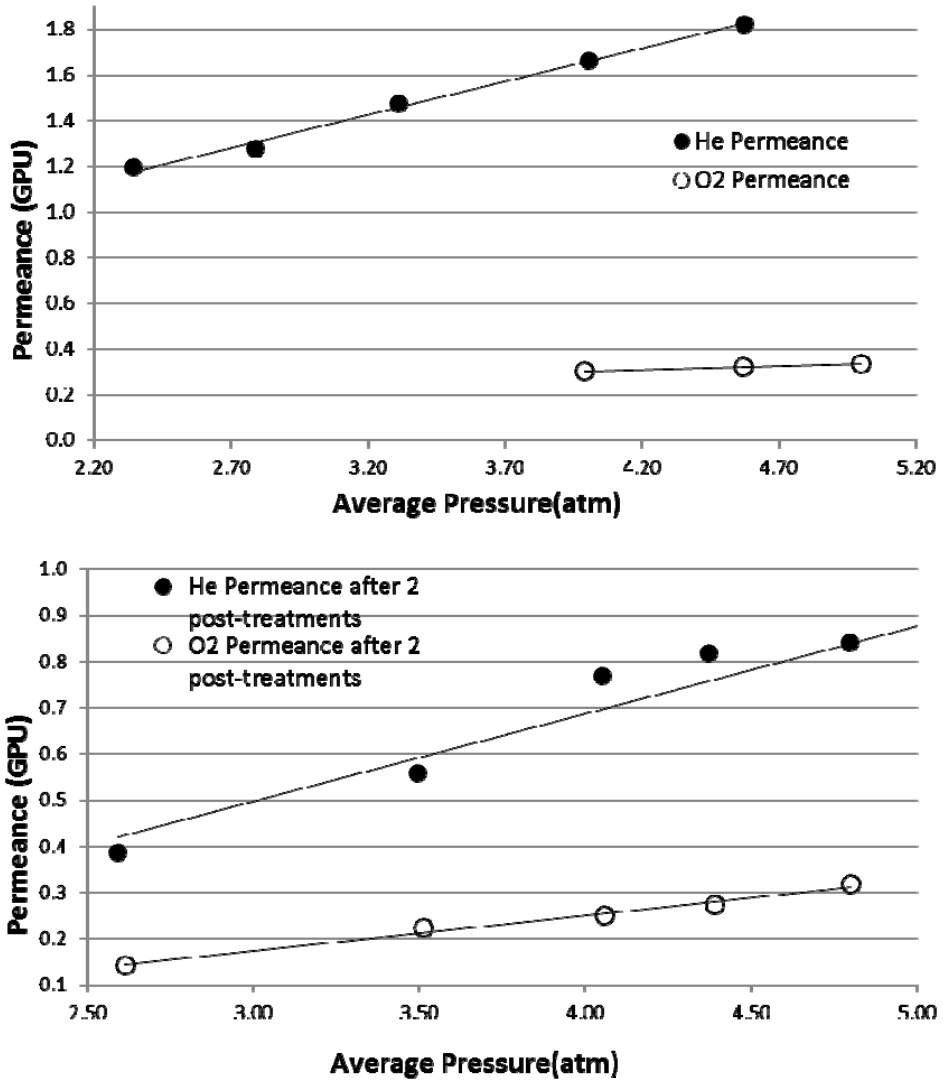

Figure 6.17: Reduction in helium and oxygen permeances on post-treating fiber sorbents with 8% PAN-EC solution twice.

Thermal stabilization was carried out after each post-treatment step as it was seen as an important part of barrier formation. A drawback of solution-cast barriers is that repeated castings do not necessarily provide better barriers because the films cast in the first step may be re-dissolved in subsequent post-treatments. Since PAN stabilization also causes insolubilization, it was seen as a useful way to immobilize the barrier and increase its thickness in each post-treatment step. Literature indicates that

PAN insolubilization can occur when heated to 180 °C in air for 3 hours [25, 26]. This was verified by heating a PAN film in air for 3 hours. The film turned black and was insoluble in NMP even on heating.

In this work, thermal stabilization was performed by flowing oxygen through the fiber bore with the module heated to 190 °C for 1 hour as an approximation of these literature conditions. The thermal soak time was reduced to avoid possible oxidation of the Torlon® itself. Fibers thus treated showed strong coloration of the PAN layer when viewed under the optical microscope which is considered an indicator of insolubilization. Hence it was assumed that the 1-hour treatment was sufficient to cause PAN insolubilization. As further evidence, SEM analysis of fibers stabilized in this manner and post-treated again occasionally shows the presence of two distinct PAN layers (Figure 6.18).

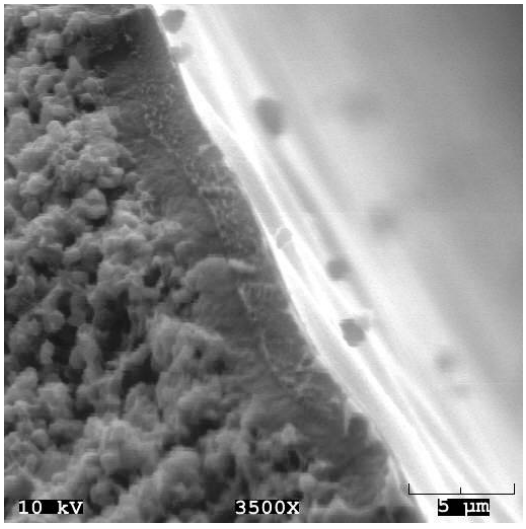

Figure 6.18: The inner surface of a post-treated PAN barrier showing distinct layers obtained by post-treating, then stabilizing the film followed by a second post-treatment.

The particles on the inner wall of the fiber are sorbent particles dislodged by the sample preparation process.

6.3.4 Effect of post-treatment solution concentration on effective barrier formation

The concentration of the PAN solution use for post-treatment presented a trade-off between barrier layer effectiveness and the solution viscosity. Solutions with more than 10% PAN by weight were viscous and prone to fiber clogging with fibers of 530 µm bore diameter. On the other hand, 5% and less PAN produce thinner and comparatively high-permeance barriers that could not always be improved by repeated post-treatment. Sample SEMs are provided for qualitative comparison of barrier layers produced with 3-, 5- and 8 wt. % PAN solutions in EC (Figure 6.19).

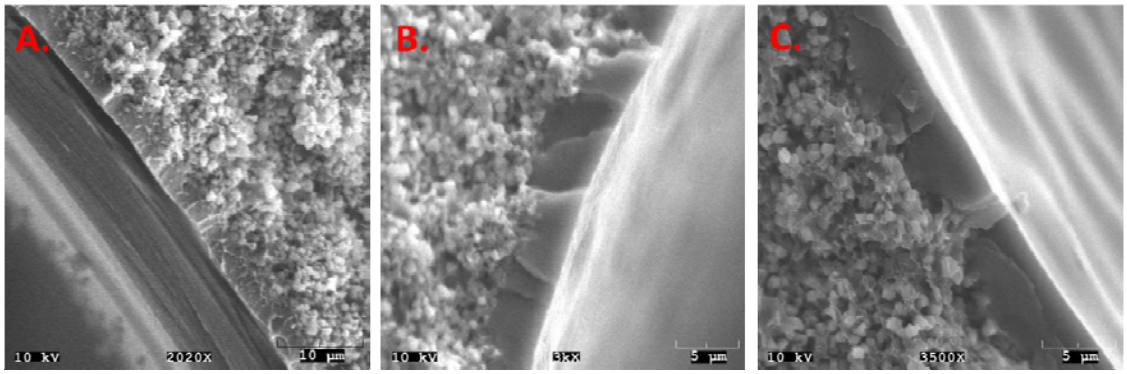

Figure 6.19: Qualitative comparison of PAN barriers cast from A. 3% PAN in EC, B. 5% PAN in EC, and C. 8% PAN in EC. The 8% PAN solution was most effective in producing low-permeance barriers.

6.3.4.1 PAN barrier formation with 8% by wt. PAN solution

It was found that 8% PAN solutions provided moderately viscous solutions that posed a low risk of fiber blockage while showing a significant improvement in the barrier properties. After the first post-treatment step using an 8% PAN solution, the barrier had an oxygen permeance of ≈ 95 GPUs at 15 psi pressure differential, from an original permeance of 25,000 GPUs. On completing the second post-treatment step, the oxygen permeance dropped to an average of 0.25 GPUs at a pressure differential of 100-200 psi.

SEM imaging of the fiber samples treated with 8 wt. % PAN solutions showed the deposition of a dense PAN layer between 3-5 μm thick on the internal walls. The barrier surface was smooth and there were no clumps or irregularities observed. The samples imaged showed no inclusions or breaks in the barrier layer.

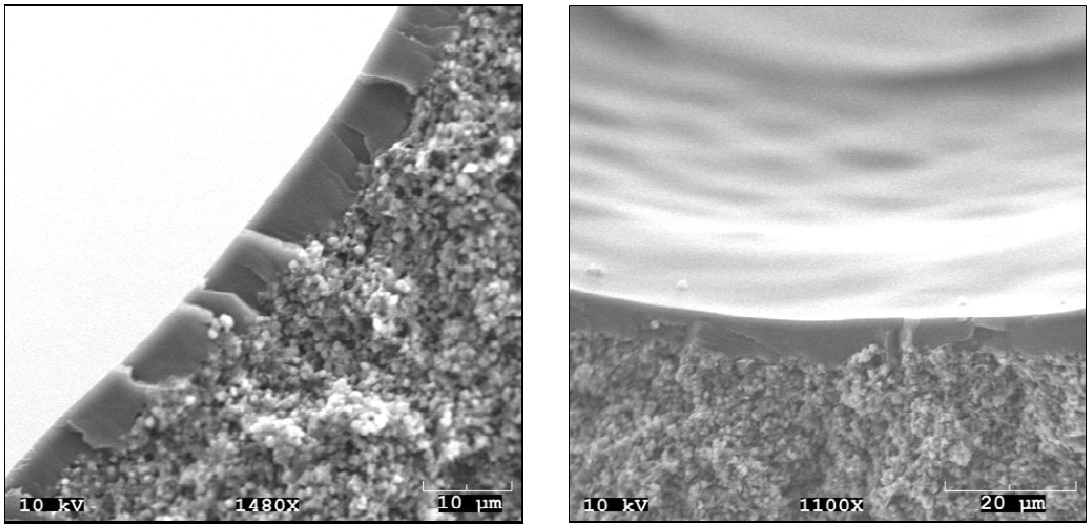

Figure 6.20: PAN barrier cast from 8% solution in EC showing smooth surface and lack of inclusions.

The helium and oxygen permeances after two post-treatment steps were plotted (Figure 6.21) and showed the lowest permeances that had yet been achieved with PAN -EC post-treatment. Oxygen was chosen instead of nitrogen for convenience, since nitrogen permeation was often too slow to measure with the bubble flow meter. It is noted here that prior to each permeance measurement, gas was flowed through the bore to ensure that the low permeance was not just an artifact of a blocked bore, and was truly permeating through the lumen layer.

The helium permeance was 0.35±0.03 GPUs at 4.4 atm average pressure (100 psi Δp). This permeance implies a skin thickness of 1.45 µm of PAN if a permeability of 0.53 Barrers is taken [14]. The average helium/oxygen selectivity was only 1.47 in this experiment whereas the reported He/O_2 selectivities range from 25 to 1770 [14, 27]. The low selectivity could be the result of a few macroscopic defects;

however, no such defects were observed in any SEM images taken. It was decided to test the lumen layer for its functionality as a water barrier.

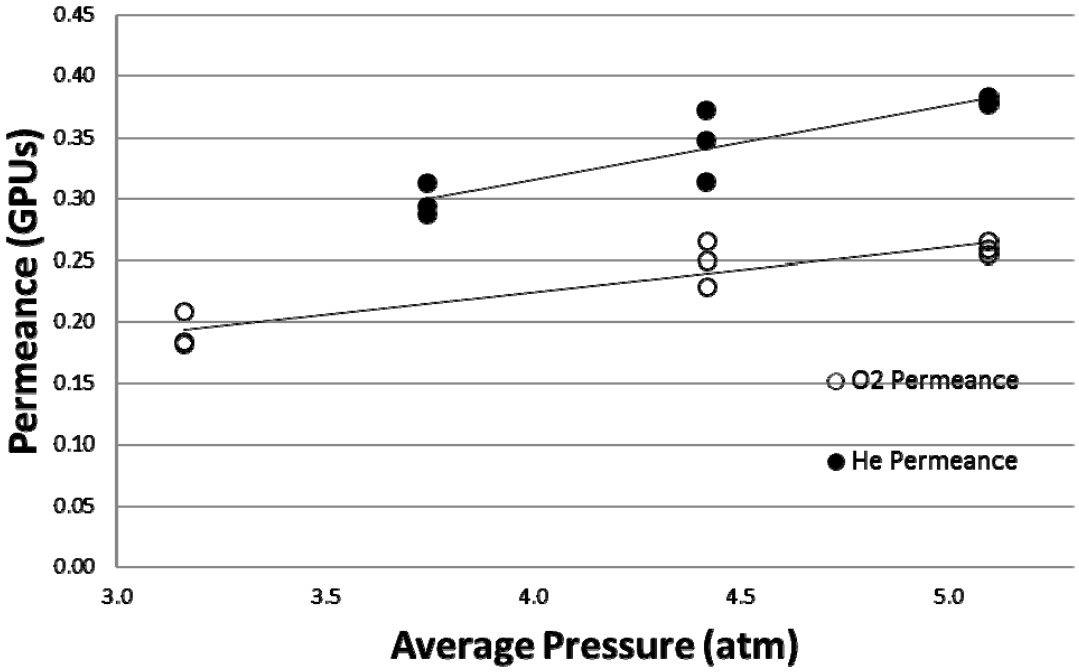

Figure 6.21: He, O_2 permeance vs. average pressure for twice-cast PAN barriers from 8 wt. % PAN solution in EC.

6.3.4.2 Water transmission through fiber bore

The fiber had to be tested to ensure that the barrier could prevent water permeation to a significant level. This was done by holding water in the fiber bore at pressures up to 60 psi, and monitoring the shell side for appearance of water. Water was injected into the fiber bore using a nitrogen line connected to the bore side of the fiber module. Once it was established that water was flowing through the bore with no blocks or obstructions, the downstream bore end was capped and the bore was pressurized at 60 psig. The bore was left pressurized for 24 hours to allow water transport to the (capped)

shell side. After this period, the shell side was opened and visually inspected for the presence of water using a nitrogen flow to sweep out any collected water. The module tested did not indicate the appearance of water over a period of 24 hours as shown by the retention of water in the pressurized bore and its absence on the shell side. This, coupled with the fact that the fibers could maintain a water flow rate effectively without observable leakage to the shell side of the fiber led us to believe that the PAN layer was functional as an isolating barrier.

Furthermore, the PAN barriers had the benefit of providing efficient face sealing, as evinced by the low permeances achieved, which would not have been possible with any lumen layer bypass. This was corroborated through SEM imaging.

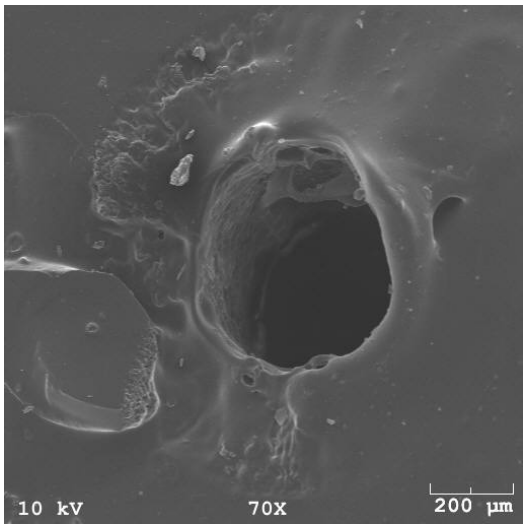

Figure 6.22: Module ends of Torlon® fibers internally coated with PAN barrier, showing effective face-sealing by the post-treatment solution.

Overall, PAN post-treatment was very effective as a barrier formation method due to the low permeances achieved and the obvious presence of a dense,

unbroken PAN layer. PC solvent was found to provide more effective barriers than EC but EC was a more universal solvent and still provided durable, water-tight barriers. The barrier functionality was investigated by flowing water through the bore and by holding water under pressure in the bore.

6.4 Improvements in Barrier Formation

While good barriers could be obtained via post-treatment and, to a lesser extent, co-extrusion, there remain possible methods of improving barrier performances in both cases.

6.4.1 Modifications to produce better fibers with co-extruded barriers

While good internal Torlon® barriers could be produced on single-layer, pure-Torlon® fibers, the transition to dual layer fibers encountered stability and spinnability issues that eventually led to the preference for post-treated barriers. Some of these issues could have been avoided by spinning at very low take-up rates, possibly by allowing extrusion under gravity rather than under tension. Such a setup is likely to produce very thick fibers: something that could be combated by reducing the extrusion rates correspondingly.

Another possible modification is to replace the "inverted" spinneret with a "recessed" spinneret, both being dual-layer spinnerets used in the Koros Group. The inverted and recessed spinnerets are similar in their positioning of the bore and core

needles, but differ in the dimensions of each channel. The inverted spinneret, used in this work for dual layer spins, has a core channel 137.2 μm wide and a sheath channel 614.6 μm wide so as to provide a narrow lumen barrier and a broader sorbent layer [28]. The recessed spinneret has the core and sheath channel dimensions reversed. Since the use of the inverted spinneret sometimes produced fibers with an incomplete barrier, using the recessed spinneret could produce a complete barrier. The core and sheath flow rates could be adjusted to avoid fiber with an excessively thick barrier.

6.4.2 Improvements to PAN post-treatment

While PAN-ethylene carbonate (EC) solutions were shown to produce water-tight barriers, propylene carbonate (PC) was nevertheless more effective for this purpose, producing barriers with helium permeance as low as 0.1 GPUs. PC could not dissolve some batches of PAN, but it is worth investigating grades of PAN (possibly co-polymers) that would be cast from a PC solution, or finding conditions in which pure PAN would dissolve in PC.

A further improvement to solution-cast barriers would be the application of Torlon® films on PAN barriers that had been insolubilized by stabilization. Torlon®-NMP solution would be run through the fiber bore, where an already-cast PAN film would protect the fiber matrix from dissolution. This would combine the low gas permeability of PAN with the low water-permeability of Torlon®, giving an even more effective barrier layer.

6.5 Summary and Conclusions

Different materials were explored as candidates for lumen barrier formation. It was discovered that each material had its advantages and drawbacks and different barrier deposition methods had to be developed for each. Torlon® and PAN were two of the more promising barrier materials studied and they were cast via co-extrusion and post-treatment, respectively. Torlon® was found to provide extremely low-permeance barriers when spun as a single layer fiber, but dual-layer fibers spun had spinning defects such as macrovoids that damaged the barrier properties of the inner layer. Still, a dense skin was observed on the lumen for all the spins undertaken and the poor performance of the dual-layer barriers was attributed to the macroscopic breaks in barrier continuity; a problem that could potentially be remedied at slow spin conditions.

Focus was then moved on the selection of a suitable solvent to cast a PAN film on already-spun fiber sorbents. An 8 wt. % PAN solution in ethylene carbonate was found to produce relatively problem-free low-permeance barriers that retained liquid water in the bores without any leaks, even at high pressure differentials. Water vapour is still likely to permeate through the lumen layer, especially at high temperatures, where steam would be the heat transfer fluid used. However, the flue gas is already anticipated to be saturated with moisture, and the sorbents studied were moisture-tolerant; so such PAN-based barriers were deemed to be functional in a saturated gas feed. PAN samples that could be dissolved in propylene carbonate produced even lower helium permeances, so PAN copolymers that are soluble in propylene carbonate are another possible barrier candidate.

6.6 References

1. Schmeling, E.-L., H. Friebe, and U. Reininghaus, *Electroless metal plating*, US Patent 3934054 A, filed Dec 3, 1973, and issued Jan 20, 1976.

2. Mallory, G.O. and J.B. Hajdu, *Electroless plating: fundamentals and applications*1990: Access Online via Elsevier.

3. Lively, R.P., et al., *Formation of defect-free latex films on porous fiber supports.* ACS applied materials & interfaces, 2011. **3**(9): p. 3568-3582.

4. Piringer, O.G. and A.L. Baner, *Plastic packaging: interactions with food and pharmaceuticals*2008: Wiley. com.

5. Grant, D., *The pyrolysis of poly (vinylidene chloride) in solution.* Polymer, 1970. **11**(11): p. 581-596.

6. Wessling, R.A., *The solubility of poly(vinylidene chloride).* Journal of Applied Polymer Science, 1970. **14**(6): p. 1531-1545.

7. Hougham, G., *Fluoropolymers 2: properties*. Vol. 2. 1999: Springer.

8. Tuminello, W.H. and G.T. Dee, *Thermodynamics of poly (tetrafluoroethylene) solubility.* Macromolecules, 1994. **27**(3): p. 669-676.

9. Sweeting, O.J. and D. Rosato, *The science and technology of polymer films*1968: Interscience Publishers New York.

10. Park, H., et al. *Effect of solvent exchange on the morphology of asymmetric membranes*. in *ACS Symposium Series*. 2000. ACS Publications.

11. Kauffman, G.B., S.W. Mason, and R.B. Seymour, *Happy and unhappy balls: Neoprene and polynorbornene.* Journal of Chemical Education, 1990. **67**(3): p. 198.

12. Kosuri, M.R., *Polymeric membranes for super critical carbon dioxide ($scCO_2$) separations.* 2009.

13. Solvay Specialty Polymers. 2013 [cited 2013 Sep 16]; Available from: http://www.solvayplastics.com/sites/solvayplastics/EN/specialty_polymers/Spire_Ultra_Polymers/Pages/Torlon.aspx.

14. Allen, S., et al., *The barrier properties of polyacrylonitrile.* Journal of membrane science, 1977. **2**: p. 153-163.

15. Stannett, V., et al., *Sorption and transport of water vapor in glassy poly(acrylonitrile).* Polymer Engineering & Science, 1980. **20**(4): p. 300-304.

16. Salame, M. *Transport properties of nitrile polymers*. in *Journal of Polymer Science: Polymer Symposia*. 1973. Wiley Online Library.

17. Iovleva, M., V. Smirnova, and G. Budnitskii, *The Solubility of Polyacrylonitrile.* Fibre Chemistry, 2001. **33**(4): p. 262-264.

18. Edwards, H., et al., *Raman spectroscopic studies of the polyacrylonitrile-zinc complexes in aqueous solutions of zinc chloride and bromide.* Polymer international, 1993. **30**(1): p. 25-32.

19. Hoskins, A., H. Edwards, and A. Johnson, *Vibrational spectroscopic studies of poly (acrylonitrile-co-vinyl acetate) in aqueous solutions containing metal ions: mechanism of the dissolution process.* Polymer communications, 1991. **32**(3): p. 89-93.

20. Peppel, W., *Preparation and properties of the alkylene carbonates.* Industrial & Engineering Chemistry, 1958. **50**(5): p. 767-770.

21. Chernyak, Y., *Dielectric constant, dipole moment, and solubility parameters of some cyclic acid esters.* Journal of Chemical & Engineering Data, 2006. **51**(2): p. 416-418.

22. Abboud, J.-L. and R. Notari, *Critical compilation of scales of solvent parameters. Part I. Pure, non-hydrogen bond donor solvents.* Pure and Applied Chemistry, 1999. **71**(4): p. 645-718.

23. Barton, A.F., *CRC handbook of polymer-liquid interaction parameters and solubility parameters*1990: CRC press.

24. Shan Wickramanayake, W., et al., *Fabrication of hollow, spherical polymeric "micropillows" using a dual layer spinneret.* Journal of Applied Polymer Science, 2011. **121**(5): p. 2835-2842.

25. Prescott, R., Pocess for the Manufacture of Continuous High Modulus Carbon Yarns and Monofilaments, US Patent 3533743 A, filed May 28, 1968, and issued Oct 13, 1970.

26. Dalton, S., F. Heatley, and P.M. Budd, *Thermal stabilization of polyacrylonitrile fibres.* Polymer, 1999. **40**(20): p. 5531-5543.

27. Yasuda, H. and T. Hirotsu, *The effect of glass transition on gas permeabilities.* Journal of Applied Polymer Science, 1977. **21**(1): p. 105-112.

28. Lively, R.P., *Hollow fiber sorbents for post-combustion CO_2 capture, PhD Dissertation*, 2011, Georgia Institute of Technology.

CHAPTER 7

SUMMARY, CONCLUSIONS AND FUTURE DIRECTIONS

7.1 Summary of Results

This work focused on identifying materials for incorporation into the hollow fiber RTSA platform and devising means to fabricate each component with the least effort. Material selection focused on the requirements of a good flue gas sorption system: water-resistant, mechanically robust sorbent, durable matrix polymer and a low-permeance barrier layer. Once the materials were identified, research was performed on forming them into fibers in such a way that their desirable properties would be expressed to the fullest with minimum effort.

Some of the observations from the research bear special mention.

1. Torlon® was found to be a more than adequate replacement for cellulose acetate as the matrix polymer. Dope formulations containing Torlon® with NMP as solvent, water as non-solvent and PVP pore former were found to be readily spinnable and could accommodate high loadings of sorbents, yielding porous, durable fiber sorbents with over 70% sorbent by mass.

2. PVP used as pore-former was instrumental in reducing the occurrence of macrovoids in the fibers, and in increasing the dope viscosity even at a relatively

low Torlon® concentration. A spin dope that has relatively less Torlon® yet still has a high viscosity opens the path to even higher sorbent loadings.

3. Development of the ternary phase diagram via the cloud point experiment for each polymer-pore former combination considered was found to be essential in order to streamline the dope selection process and insert some measure of predictability into dope spinning performance.

4. High-silica ZSM-5 was found to be a workable, water-resistant sorbent that retained its capacity for CO_2 in humid feeds even without any chemical modification process. It is seen as a water-resistant sorbent readily available at commercial scales of production: an important necessity for sorbents aimed at power plant CO_2 capture.

5. Different materials were explored for laying an internal fiber barrier and the different barrier deposition techniques suited to each material were explored. A constant challenge in this area was the tradeoff between a material's barrier nature and its processibility into a film.

6. Of the different barrier layer deposition methods explored, two were pursued in depth: dual-layer co-extrusion of a Torlon® barrier for a Torlon® fiber sorbent; and PAN barrier layer via solution-casting. While co-extrusion was found to produce good single-layer barriers, it fell short when attempted as a dual-layer spin, with an outer, porous sorbent layer, and an inner barrier layer. On the other

hand, PAN post-treatment provided an effective barrier that could be improved by heat-stabilizing and re-casting.

The use of Torlon® as the matrix polymer does increase material cost to the system; Torlon® has an order of magnitude higher price than cellulose acetate as quoted by our suppliers Solvay Advanced Polymers. In addition, the PAN solution coating process is also likely to have a higher material and process cost than processes using PVDC latex, owing to both the higher viscosity of the PAN-EC solution and the Cost of the materials themselves vis-à-vis PVDC latex preparations. However, these concerns are somewhat offset by the fact the cellulose acetate as the matrix polymer and PVDC as the barrier polymer are simply unfeasible for the platform owing to their thermal instability. In this situation, Torlon® and PAN become the cheapest option that fulfils the RTSA goals. In addition, the sorbent materials are more likely to control the overall material costs since many of them are still not available at industrial production levels. In such a situation, Torlon® and PAN basically form the base of a platform in which novel and promising sorbent materials may be inserted in order to produce a fiber sorbent with good capture characteristics and focus may then be turned on reducing material costs, either due to economies of scale or through further exploration of related , cheaper materials.

7.1.1 Matrix polymer selection

Torlon® was chosen to replace cellulose acetate as a robust, high-T_g polymer to constitute the matrix. It was found to perform well in this function and could incorporate 3 times its weight in zeolite and still maintain structural integrity. It also

provided an open matrix structure with the help of pore former (PVP) that yielded high gas permeances comparable to cellulose acetate. It was the polymer of choice for this work and has been pursued in other research for membrane and sorbent development.

7.1.1 Sorbent selection

Initially, having used 13X as a base-case sorbent, focus was moved to more water resistant sorbents such as aminated silicas and MFI zeolites. Stability issues were encountered with amine-functionalized silicas and chemically modified zeolites. In previous research, pure silica ZSM-5, also called silicalite-1, had been found to retain its sorption capacity in the presence of moisture and was viewed as a possible sorbent for this research. Silicalite-1 had not previously been incorporated into the sorbent structure and posed some challenges in large-scale synthesis. Alternatives to silicalite-1 were sought, and high-silica ZSM-5 was considered for this purpose. It was found that ZSM-5 retained its capacity in the presence of moisture and could be loaded into the fibers at high mass fractions. Readily available, mechanically and chemically robust with no additional modification needed to retain its CO_2 capacity in the presence of moisture, high-silica ZSM-5 was found to be a prime candidate for incorporation into the hollow fiber RTSA platform.

7.1.2 Barrier Formation

While several materials were probed as candidates for barrier layer formation, two paths were investigated in particular: Torlon® via co-extrusion and PAN

via post-treatment. These two materials were found to contain the right mix of barrier properties and processibility. While Torlon® did have the potential to produce low-permeance barriers; dual-layer fiber spinning was found to be a delicate and unpredictable experience. Several spins were undertaken but ultimately foiled due to spin irregularities and fiber breaks. PAN was ultimately more effective in producing a dense layer on the fiber that could be stabilized and then enhanced by repetition of the post-treatment process. PAN barriers were found to yield a very low gas permeance and remained water-tight even after extended periods of time under pressurized water held in the fiber bore.

7.2 Future Directions

In this work, significant progress was made in integrating more reliable and better-performing materials and in developing an overall philosophy of material selection and processing for the RTSA platform. This also helped identify some future areas of enquiry that either complement or advance the hollow fiber RTSA platform. These are listed below, grouped into sorbent, matrix and barrier polymer materials.

7.2.1 Further improvements in sorbent materials

While high-silica ZSM-5 was found to be a robust, hydrophobic zeolite, a major concern through this research was the unavailability of higher capacity sorbents in larger, spin-scale quantities. Sorbent performance in dry and wet CO_2 feeds did not necessarily translate into better applicability for the RTSA platform. As an example, aminated silicas had an order of magnitude larger capacity in wet feeds compared to

ZSM-5, but could not be incorporated at high loading into the fiber. Furthermore, they were found to lose capacity and structural integrity on being subjected to the dope preparation process. Work in this area must focus on developing sorbents that can withstand oxidative and hydrolytic environments.

Alternatively, since the hollow fiber formation itself is a mechanically taxing process to many sorbents, methods need to be developed to allow functionalization of the fibers after fabrication. This could also extend to development of a process where degraded fiber sorbents are able to be removed from service and chemically processed so that they regain their CO_2 sorption capacity and can be reused. This is likely to be a necessity for sorbents that owe their activity to amine-functionalization since even solid amines appear to be prone to thermal and hydrolytic degradation.

7.2.2 Better Fiber Matrices

Torlon® has been found to be an ideal candidate for the polymer matrix. In this work, dope optimization was performed until there was evidence of good pore structure, but there are always avenues to improve the fiber diffusion kinetics. Potential areas of research include further investigating the role of PVP as a pore former and inclusion of high-molecular weight PVP (M_w 1.3 million) into the dope preparation process.

High-molecular weight PVP provides an intriguing option wherein the dope viscosity can be increased without increasing the amount of Torlon® in the dope.

This would allow increasing the amount of sorbent in the dope without increasing the Torlon® content, thereby providing fibers with even higher sorbent loadings. This could also potentially be a path to incorporating aminated silica, which was found to be difficult to blend into the dopes on account of its low density. Using high molecular weight PVP would thus allow increasing the amount of silica that can be incorporated into the sorbents beyond the 30 wt. % that was possible in the work.

7.2.3 Improvements to barrier layer formation

Different materials were sought for fabrication and the results of this survey were summarized in Chapter 6. In this work, PAN was found to give the most promising water and gas barrier. While Torlon® appeared to be more suitable as a barrier material for single layer fibers, dual-layer fibers with a Torlon® inner barrier and a Torlon®-sorbent outer layer were difficult to fabricate. Based on the work done here, some of the possible directions in barrier deposition are:

1. Perfecting the spinning of single-layer Torlon® fibers that have a porous wall with a dense, low-permeance inner wall. This would allow the functionalization of the fiber itself with a suitable amine source to act as a CO_2 sorbent. Currently, fibers have been obtained with a dense inner wall, but the outer cellular layer was found to be closed-cell in morphology, which would be detrimental to gas diffusion. Addition of PVP to the polymer dope would allow the formation of an open-celled outer layer that would allow rapid gas interchange. Such single-layer fibers are not however expected to be

possible with dispersed solid sorbents in them, which perforate the inner dense layer and render it permeable to gas diffusion.

2. Dual-layer PAN/Torlon® barriers made via post-treatment would further reduce the water permeance of PAN barriers [1]. Torlon® barriers cannot normally be solution-cast, because any Torlon® solution would dissolve the underlying fiber wall, also composed of Torlon®. However, if a PAN film were already cast and thermally stabilized [2], this would enable the casting of a Torlon® film on the PAN layer, which in turn would protect the fiber underneath.

3. 1,8-Diazabicyclo[5.4.0]undec-7-ene, also called DBU is a basic compound used in the Koros group to aid ionic liquid functionalization of Torlon® fibers [3]. It was found to produce some densification of the Torlon® itself, as measured by a lowered permeance. DBU and other possible candidates that cause Torlon® pore collapse could be explored to cause selective densification of the inner wall, resulting in a barrier layer. Owing to the lower viscosity of DBU solutions and the low boiling point of its solvent (hexane), this process would be easier to accomplish than PAN barrier formation while retaining many of its advantages such as single-step face sealing.

Polyamic acid-based barriers: Polyamic acid has been used as a low permeance material to produce inflated polymer micropillows that were designed to retain their shape and internal pressure by limiting diffusion across their skin [4]. This material has not been tested as a barrier for the hollow fiber RTSA project but could

potentially provide a candidate for barrier layer formation either via post-treatment or dual-layer spinning.

7.2.4 Fiber Characterization via thermal cycling in flow system

While the sorbent crystals have been tested in the flow sorption system and the water-tightness of the PAN-treated fibers have been studied separately, complete characterization of the fiber sorbent with both water-resistant sorbent and a low-permeance barrier layer is yet to be performed. Testing of such fibers under a water-moderated thermal cycling process will help to validate both the sorbent and barrier performance and will be done in future work, along with methods to further scale up the PAN barrier deposition.

7.3 References

1. Sumitomo, H. and K. Hashimoto, *Polyamides as barrier materials*, in *Polymer Membranes*, M. Gordon, Editor 1985, Springer Berlin Heidelberg. p. 63-91.

2. Dalton, S., F. Heatley, and P.M. Budd, *Thermal stabilization of polyacrylonitrile fibres.* Polymer, 1999. **40**(20): p. 5531-5543.

3. Lee, J.S., et al., *Ionic liquid-functionalized mesoporous sorbents and their use in the capture of polluting gases*, 2013, US Patent App. 13/868,600.

4. Shan Wickramanayake, W., et al., *Fabrication of hollow, spherical polymeric "micropillows" using a dual layer spinneret.* Journal of Applied Polymer Science, 2011. **121**(5): p. 2835-2842.